The use of liquid crystal adaptive optics devices in astronomy

Love, Gordon D.

The Use of Liquid Crystal Adaptive Optics Devices in Astronomy

by
Gordon D. Love B.Sc (Dunelm)

A Thesis
Submitted to the University of Durham
for the Degree of
Doctor of Philosophy.

October 1991

Abstract

Images obtained from large astronomical telescopes are distorted and blurred by the effects of the atmosphere. In order to compensate for this, an adaptive optics system can be incorporated downstream from the telescope focus. Conventional technology uses small piezo-driven mirrors to deviate the wavefronts through angles of the order of tens of arcseconds. This thesis is concerned with the possible replacement of these mirrors with liquid crystal phase control devices, in particular, small-angle prisms. The thesis considers the following fundamental optical properties of liquid crystals relevant to astronomy; dispersion, optical quality, dynamic range, and response times. Results of a novel approach to electrically addressing liquid crystals by a ramp voltage are given.

"The living being is stable. It must be so in order not to be destroyed, dissolved or disintegrated by the colossal forces, often adverse, which surround it. By an apparent contradiction it maintains its stability only if it is excitable and capable of modifying itself according to external stimuli and adjusting its response to the stimulation. In a sense it is stable because it is modifiable – the slight instability is the necessary condition for the true stability of the organism."

Charles Richet (1900)

"...I have suggested a special designation for these states, *homeostasis*. The word does not imply something set and immobile, a stagnation. It means a condition – a condition which may vary, but which is relatively constant."

Walter B. Cannon (1932)

Preface

No part of the above thesis has been submitted previously for a degree to Durham or any other University. The work described is the author's own apart from where otherwise indicated. The MARTINI instrument described is an existing prototype device and no part of this is the author's work.

Some of the work contained in this thesis has been published in the following.

- G D Love and J V Major, The Measurement of Optical Thickness and Dispersion in Liquid Crystal Prisms. In *Applied Optics Digest.* Editor. J.C. Dainty, p.123 IOP Publishing Co. 1990.
- G D Love and J V Major, The Application of Edser-Butler Fringes to the Measurement of Optical Structure of Liquid Crystal Prisms and the Determination of Dispersion Characteristics and Thickness. *Journal of Physics D: Applied Physics.* 24(10):1708 1991.

Some work concerning the use of the Jamin interferometer, but not directly contained in this thesis is contained in,

- N J Powell, R W Kelsall, G D Love, and A Purvis. An Investigation of Fringing Fields in Liquid Crystal Diffraction Gratings, in *SPIE Conference on Active and Adaptive Optical Systems.* July 1991.

In astronomy the words ADAPTIVE OPTICS and ACTIVE OPTICS have two distinct definitions. Adaptive optics refers to image correction with a bandwidth of at least several Hertz. Hence it is primarily concerned with correcting image degradation caused by atmospheric seeing.
Active optics involves image correction over longer time scales. It is therefore, for example, concerned with correcting image degradation caused by optical misalignment of the telescope under its own stress as the telescope is pointed and guided.
This convention is adhered to in this thesis.

Contents

Chapter 1

Introduction

This thesis combines two areas of research both of which are expanding fields of current interest. Firstly advances in astronomical instrumentation have made possible the construction of several new superlative telescopes in the last decade, notably the William Herschel Telescope in the Canary Islands and the New Technology Telescope in Chile. If the full potential of these instruments is even to be approached, then it is imperative that they incorporate an adaptive optics system in order to correct for the effects of atmospheric turbulence (known as *seeing*). For example, a 4m telescope has a theoretical diffraction limit of 25 milliarcseconds at visible wavelengths, however seeing limits this image size to typically 1 arcsecond at an average observing site. The seeing is a mixture of two effects; atmospheric seeing and dome seeing; i.e. degradation caused by the passage of light through the atmosphere, and degradation due to turbulence within the telescope dome. These can be improved by choosing a good telescope site and by careful dome ventilation however an adaptive optics system is still necessary. Recent work in adaptive optics has increased the resolution by a factor of ~ 3 but there is still potential for much greater improvement. Image sharpening is of importance for two main reasons. The obvious advantage is that previously undefineable objects may be resolved and the second is that the signal-to-noise ratio is improved. Although this work concentrates on the astronomical applications of an adaptive optics system, such devices are of current interest in other fields. For example, military applications such as surveillance and laser weapons involve the same basic problem of propagation of light through the turbulent atmosphere. The possibility of adaptive optics systems has only become possible relatively recently with the development of new materials, such as

piezo-electric devices and liquid crystals, and the rapid advances in computer speed.

The second topic is liquid crystal technology. This is another area that has seen a resurgence in the last twenty years due to the realisation of the full potential of these devices, along with advances in chemical synthesis of suitable tailor-made molecules. The application of liquid crystals to display technology is well established, however more recently their use as optical control elements is being investigated.

The broader field of applied optics has recently risen to the forefront of technological science.

In particular this thesis considers how a ramped voltage may be applied to a parallel-sided liquid crystal cell to produce a phase wedge in order to simulate the action of a small-angled prism. This follows from some earlier provisional work in Durham by MARGETTS [41].

The liquid crystal, described in detail later, is birefringent. In its normal state, light polarised parallel to a characteristic direction of the crystal (parallel to the polar molecules) will experience the extraordinary refractive index. When a voltage is applied across the thickness of the liquid crystal cell then the molecules rotate and the birefringence approaches zero and the light now experiences the ordinary index (see figure 1.1a.). So now if a ramp voltage is applied, for example 4V at one end of the cell, falling linearly to to zero at the other (figure 1.1b.), then the index falls approximately linearly and the optical thickness will be as shown in figure 1.1c. Consequently a wavefront incident on this modified optical medium will be deflected through angles which are typically around 30 arcseconds. This is the range of angles required in adaptive optics. These prisms may be used to replace the small moving mirrors, driven by piezo-electric actuators, used in traditional adaptive optics systems. They have the potential of being low-cost, of having low power consumption (and hence low heat dissipation), and of being reliable, with a possible very large number of correcting elements.

Some work has been carried out on using liquid crystals as adaptive optics elements (VORONTSOV et al. [62] or BONACCINI et al. [8]). This is, however, still a new application of liquid crystals. This thesis attempts to bring together the two relevant fields. It discusses what the required specification of liquid crystals must

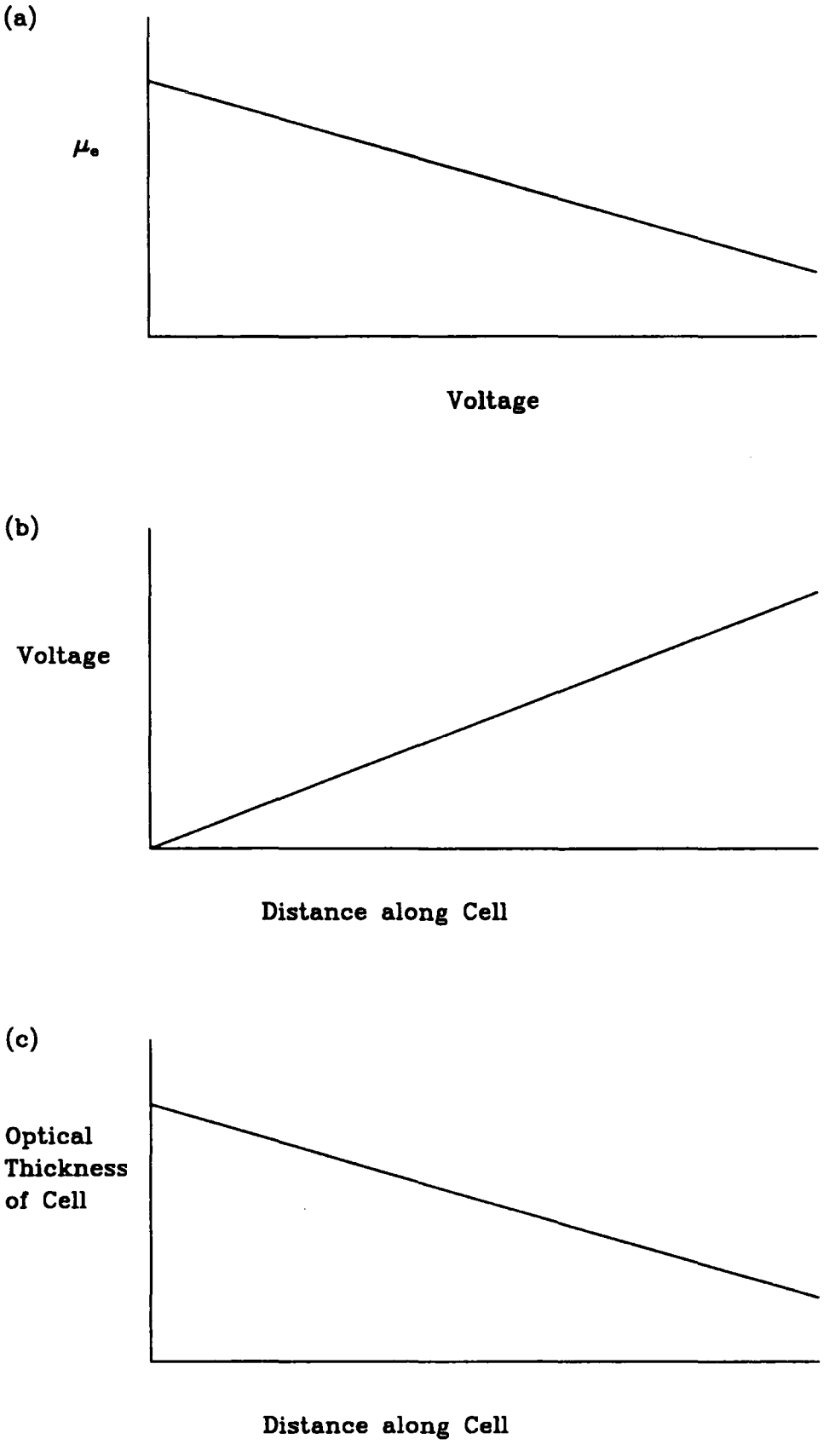

Figure 1.1: Design Concept behind a liquid crystal prism. (a)LC extraordinary index versus voltage. (b) Voltage applied across cell versus distance along cell (c) phase of emergent light from a prism.

be if they are to be of use, what properties of liquid crystals are attractive and what are the problems. This means the properties of liquid crystals are looked on from a slightly alternative viewpoint than the conventional literature on liquid crystals which is generally concerned with display devices.

The structure of the thesis is as follows.

- Chapter Two describes the structure of liquid crystals and how this is affected by the application of an electric field. It gives a brief survey of the applications of liquid crystals, both as display and as control devices.
- Chapter Three discusses the theoretical basis of atmospheric turbulence and how this may be minimised. An example of a working prototype adaptive optics system (The MARTINI System) is described, and how small-angled liquid crystal prisms may be used to replace the piezo-driven mirrors. The relevance of liquid crystals to other astronomical applications, is considered.
- Chapter Four explains the design aspects of a liquid crystal prism, in particular what are the required stroke and response times. The construction of the prisms in a micro-electronics clean room by the author is described.
- Chapter Five describes the testing of the fundamental physical properties of a liquid crystal cell. These are cell thickness, wavelength dispersion, and variation of birefringence with applied voltage. These were measured by a new technique utilising Edser-Butler fringes. The optical quality of a liquid crystal cell is then discussed, measurements of transmission and modulation transfer function were made.
- Chapter Six describes how a liquid crystal cell may be controlled to produce a prism. Methods used to measure a small prism angle are explained, and the results of a prism whose angle may be slowly varied are given.
- Chapter Seven discusses the factors influencing the response time of a liquid crystal cell. Methods of improving this in order to produce a prism with switching times suitable for adaptive optics are considered, using the transient nematic effect and the bias effect.

- Chapter Eight summarises and concludes the work, and in the light of the results, it discusses the future possibilities of adaptive optics in astronomy.

This thesis is, in effect, a design study for the possible use of liquid crystals in astronomy. This work addresses and answers some basic questions and points the way forward to the eventual use of a potentially new application of liquid crystal technology.

Chapter 2

Liquid Crystal Theory

2.1 Introduction

The three common states or phases of matter arise from the different degrees of order in each state. The phase transitions of water as it is heated from a solid, below 0°C, to a liquid, and then to a gas above 100°C, are a familiar sequence. In the solid state the molecules are constrained in a fixed position, and in the case of a crystalline solid, in a fixed pattern or orientation too. In the liquid state there is neither positional nor orientational order, however there remain inter-molecular forces which hold the substance in a dense state. Correspondingly, in the gaseous state the molecules are free to move around and spread evenly throughout its container, as the kinetic energy of the molecules is very large compared to the effect of the force potential between the molecules.

Liquid Crystals (sometimes known as mesogens) are chemical compounds which exhibit some of the properties of both the liquid phase and the solid crystalline phase. When a frozen liquid crystalline material is heated to the liquid crystal phase, the molecules lose their positional order; however they retain some degree of orientational order. This is reflected in the fact that a mesogen will flow and take the shape of its container, yet it is milky in appearance indicating that the substance differs in some way from a normal liquid. When the material is heated even further it undergoes a transition to the isotropic liquid phase, and becomes clear. This series of phase transitions is shown in figure 2.1

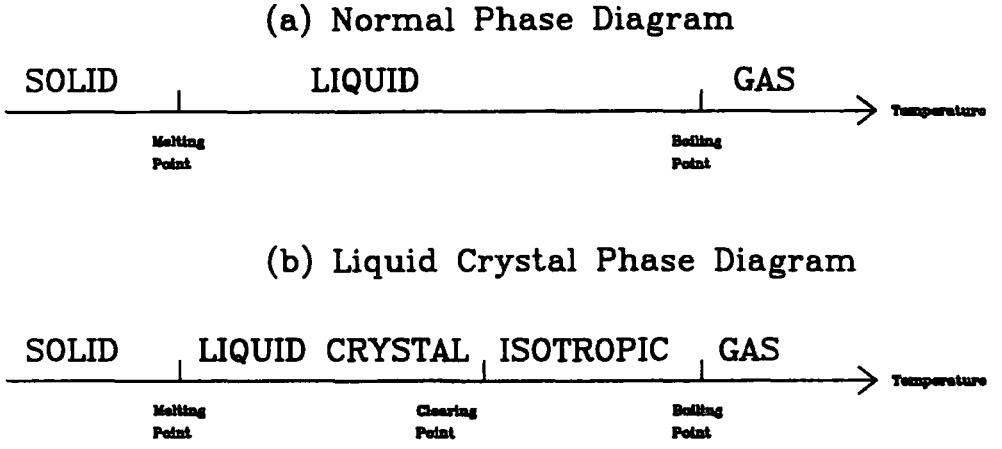

Figure 2.1: Series of phase transitions. (a) undergone by a normal material (b) undergone by a liquid crystal material upon heating

A pre-requisite for mesomorphic behaviour is that the molecules must be highly geometrically anisotropic, usually long in relation to their width (see section 2.3.1). In order to describe the behaviour of liquid crystalline phases it is useful to define a unit vector, co-linear with the long molecular axis, known as the director, $\underline{n}$. Thus in a liquid crystal, there is orientational order so the directors arrange themselves in some ordered fashion. Of the liquid crystals produced by elongated molecules there are three types, nematic, cholesteric, and smectic, each of which is described below and shown in figure 2.2

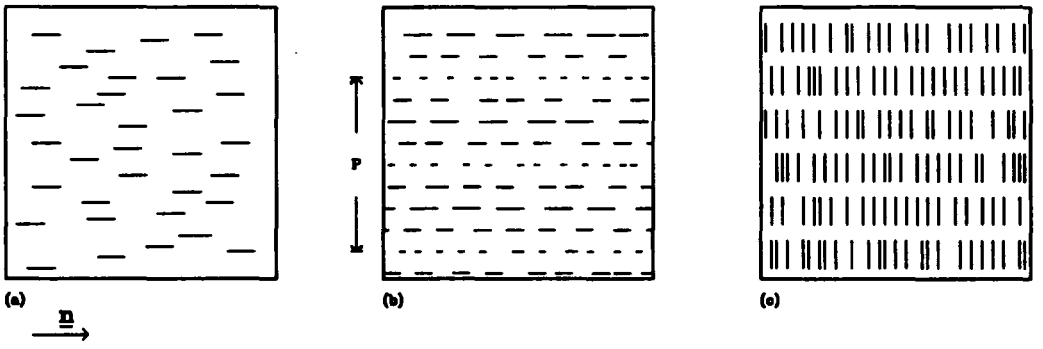

Figure 2.2: Molecular order in thermotropic liquid crystals. (a) Nematic phase. (b) Cholesteric phase. (c) Smectic A phase.

In a nematic type (nematic is derived from the Greek word for thread) the molecules have random positions but the directors are aligned. In practice, thermal

motions of individual molecules cause deviations from the ideal case of parallel alignment, but the average bulk director remains constant.

The cholesteric phase (sometimes known as the chiral nematic phase) is again characterised by random molecular positions, and parallel director alignment within layers, however the director rotates from layer to layer, giving a spiral structure. The *pitch* (P) of a cholesteric liquid crystal is defined as the distance over which the director rotates through 360°. Thus the plane of polarisation of light is rotated as the light is transmitted through the chiral structure.

There are various subsets of the smectic phase (from the Greek for soap), however they are all characterised by molecular positional order as well as director order. For example, smectic A mesophases have molecules formed in layers with the director parallel to the layer normal; in the smectic C phase the molecular directors are tilted at a constant angle to the layer normal.

It should be noted that a liquid crystal can either be nematic or cholesteric, but not both. However smectic mesophases can occur with either the nematic or cholesteric phases. For example when such a substance is heated it goes from solid, to smectic, then to nematic, and then to the isotropic phase.

The most common and well-known mesogens are formed by rod-like molecules, however in 1977 it was discovered that disk-like molecules can also form a liquid crystal phase in which the director is the vector perpendicular to the plane of the molecule. They are known as *discotic* liquid crystals.

So far the discussion has been purely about *thermotropic* liquid crystals, that is, liquid crystals where transitions to and from the mesophase occur only by temperature changes. This thesis is concerned with the electro-optical uses of liquid crystals where thermotropic mesogens are of importance and so concentrates on this class of material.

Another type of liquid crystal where transitions occur by the addition of suitable solvents, are called *lyotropic* liquid crystals. One of the most common of these is soap in water whereby the soap molecules order themselves so that the hydroscopic ends of the molecules attach themselves to the water molecules and the hydrophobic ends to each other. A further example, of great biological importance, are the

phospholipids. They enable cell structures to retain a degree of rigidity despite the fact that biological organisms are about 90% water.

This thesis concentrates on the use of nematic liquid crystals.

2.2 A Brief History of Liquid Crystals

Although observations of the liquid crystal phase had been unwittingly made earlier, the discovery of the mesophase is generally attributed to an Austrian botanist, Friedrich Reinitzer (REINITZER [49]). He observed the unusual phase transitions of an organic cholesterol in 1888. Work on liquid crystals progressed slowly, and indeed in the 1940's they were thought of as little more than a curiosity. Interest was regenerated in the 1960s and a theory describing LC behaviour was formulated. Interest rapidly grew when it was realised that liquid crystals had the potential to respond to very small changes in temperature, mechanical stress, electromagnetic effects and chemical environment. The breakthrough in making liquid crystals that are stable and have phase transitions at suitable temperatures was made by a team of chemists at Hull (NASH et al. [45]). The chemicals they made which are now most widely used in the display industry are characterised by a cyanobiphenyl structure.

By the late 1970s the first liquid crystal displays (LCDs) had been made and the 1980s saw liquid crystals revolutionise any product that had some kind of display. It is interesting to note from the history of liquid crystals that the field has been multidisciplinary, bringing together chemists, physicists, life scientists, and engineers (and now astronomers).

2.3 Operation of Liquid Crystals

This section deals with the structure of liquid crystals, how this is affected by the application of an electric field and what is the result on light incident on the liquid crystal.

2.3.1 Molecular Structure

After much experience of synthesising LC molecules, organic chemists have been able to characterise the type of molecule that will exhibit the liquid crystal phase. Firstly, as mentioned in section 2.1, the molecules must be elongated, secondly the centre of the molecule must have some rigidity, otherwise alignment cannot occur. The third requirement is that the ends of the molecules must be flexible allowing the molecules to position themselves more easily as they move due to thermal motions.

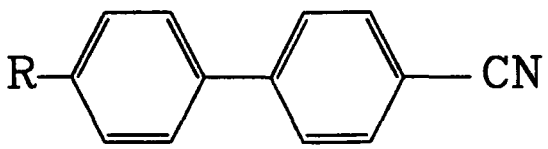

Figure 2.3: Molecular Structure of a Cyanobiphenyl Liquid Crystal Molecule. The 'R' indicates an alkyl group.

Figure 2.3 shows the generic molecular structure of the cyanobiphenyl molecules as developed by Nash and his colleagues. It can be seen that the molecule is elongated in shape. The benzene rings provide rigidity in the central regions, and the single bonds to the cyanide and alkyl groups provide flexible ends. In addition, in this case, the cyano group acts as an electron acceptor and so gives the molecule a permanent electric dipole moment.

As explained in section 2.1 liquid crystals possess molecular order, yet if one considers a small bottle containing a liquid crystal it is obviously unreasonable to expect the director of the molecules at the bottom of the bottle to be pointing in the same direction as the molecules at the top, when they are millions of molecules distant. What is true is that there are areas of alignment over a smaller scale. If a sample of nematic liquid crystal material is viewed under a microscope and between crossed polarisers a series of dark and light areas are seen. The dark areas are where the director is aligned along one of the polaroid axes, and the light areas are where the director is at an intermediate value and so elliptically polarised light is produced. The lines where the director changes abruptly are called *disclinations*. These lead to the scattering of light and give bulk liquid crystal materials a milky appearance.

2.3.2 The Effect of an Electric Field on Molecular Order

For liquid crystals to be of electro-optical use the material is sandwiched between glass to form a thin layer, typically 1μm to 30μm thick. In order to facilitate the application of a voltage across the liquid crystal the glass is coated in a thin layer of conducting, transparent material which is usually a mixture of indium oxide and tin oxide known as ITO.

The effect of an electromagnetic field on a liquid crystal is discussed at length in BLINOV [7] or CHANDRASEKHAR [11] but the treatment is somewhat lengthy and unnecessarily detailed for the present purpose. The following is a simplified description of the basic action of a nematic liquid crystal when subjected to an electric field. As described in the section 2.3.1 molecular order is only uniform over small scales ($\sim$ 10μm) so some way of aligning the molecules over the very large ($\sim$ 1cm) cell area must be made. This is achieved simply by rubbing either the glass or a coating on the glass with a cloth or tissue in one direction. The exact mechanism is not well understood (e.g. CHEN at al. [12]) but it is thought that the rubbing somehow produces micro-grooves which force the molecules in contact with the grooves to all align in the same direction along the rubbing direction and suppresses the formation of disclinations. The molecules actually align so that there is a small angle between the molecules and the glass, known as the *pretilt* angle. Inter-molecular forces promote this alignment and it is then energetically favourable for all the molecules in the layer to be similarly aligned. This type of alignment is called *homogenous* alignment. This is a simplification since alignment can also be induced whereby the molecule directors are ordered perpendicular to the glass (called *homeotropic* alignment) or alignment can be made to occur perpendicular to the rubbing direction. The construction of liquid crystal cells is discussed in greater detail in section 4.4.

The effect of an electric field on a liquid crystal is essentially that of a dipole in an electric field. Consider figure 2.4 which shows the forces on a molecule which has a dipole either along the director (the long axis) or perpendicular to it (i.e. whether the molecule has positive or negative dielectric anisotropy). Even though there is no net force on the molecule there is a resultant couple and the molecules rotate. The couple is obviously much greater when the dipole is along the molecule,

as in diagram (a), and it is this case that is relevant to cyanobiphenyls. Thus when an electric field is applied the molecules are forced to rotate and align with the field. There is another couple on the molecules due to the alignment layer which causes the molecule to be aligned in the orthogonal direction. This can be thought of as a simple elastic force whereby the couple on the molecule is proportional to the amount of twist[1]. The molecule therefore reorientates itself so that the couple due to the applied voltage balances that of the inter-molecular forces and alignment layer. The greater the applied voltage, the greater the rotation of the molecule up to a saturation point when the molecule has rotated through 90°.

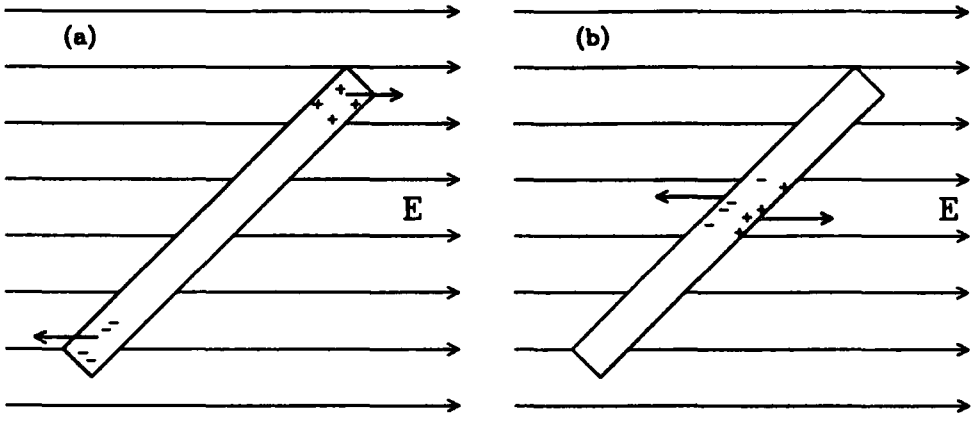

Figure 2.4: Forces on a Molecular Dipole in an Electric Field. (a) Dipole parallel to director. (b) Dipole perpendicular to director.

When a D.C. electric field is applied the liquid crystal material will degrade electro-chemically. To avoid this an AC field must be used to drive the LC cell. At first sight it would appear that the direction of the couple on the molecule due an AC voltage would keep reversing, having a time averaged value of zero. This apparent contradiction is explained when one considers that the primary interaction of the electric field is with the induced dipole moment. The torque, $\underline{\mathbf{T}}$, on a dipole in an electric field,$\underline{\mathbf{E}}$, is given by (e.g. GRANT AND PHILIPS [29])

$$\underline{\mathbf{T}} = \underline{\mathbf{P}} \times \underline{\mathbf{E}} \tag{2.1}$$

where $\underline{\mathbf{P}}$ is the dipole moment. The molecular dipole moment is given by the sum

[1]In Blinov [7] *twist* refers to a specific form of molecular deformation (the others being *splay* and *bend*), but here it is used to refer to any kind of deformation away from that preferred by the inter-molecular forces.

of the permanent and induced dipole moments and although the permanent dipole moment is fixed, the induced dipole moment can flip at the same frequency as the applied AC voltage ($\sim$ 1KHz), because of electron mobility within the molecule. Conversely, due to viscosity, the whole molecule cannot rotate at a frequency of 1KHz, so the torque due to the permanent dipole is averaged to zero. The resultant dipole moment will be given by $\underline{\mathbf{P}}_\mathbf{p} \pm \underline{\mathbf{P}}_\mathbf{i}$ where $\underline{\mathbf{P}}_\mathbf{p}$ is the permanent dipole moment and $\underline{\mathbf{P}}_\mathbf{i}$ is the induced dipole moment and the $\pm$ is governed by the direction of the applied AC field. Assuming then, that the time for molecular rotation is large, and that the time for electron mobility within the molecules is small compared to the frequency of the applied field then the time-averaged torque on the molecule is then given by

$$\langle \underline{\mathbf{T}} \rangle = \frac{1}{2}\left[(\underline{\mathbf{P}}_\mathbf{p} + \underline{\mathbf{P}}_\mathbf{i}) \times \underline{\mathbf{E}}) - (\underline{\mathbf{P}}_\mathbf{p} - \underline{\mathbf{P}}_\mathbf{i}) \times \underline{\mathbf{E}})\right] \tag{2.2}$$

or

$$\langle \underline{\mathbf{T}} \rangle = \underline{\mathbf{P}}_\mathbf{i} \times \underline{\mathbf{E}}. \tag{2.3}$$

which is non-zero. Therefore an AC field can have a net non-zero rotational effect on molecules. This breaks down if the frequency of the field is too great ($\sim$ 1MHz). The induced dipole moment cannot switch fast enough and the LC fails to respond. At the other end of the frequency spectrum, if a very low frequency ($\sim$ few Hz) is applied then the molecules have time to rotate and the cell is seen to partly switch on and off at the same frequency as the applied voltage.

It is interesting to note that these effects can also potentially occur in both liquids and solids, however in liquids with long polar molecules the random, disordered, thermal motion dominates and no bulk effect is seen. In solids the inter-molecular forces dominate and prevent any external field effects. Thus there is nothing intrinsically special in the way liquid crystals react to electric fields, it is just that the material is in a mesophase that allows these effects to manifest themselves.

2.3.3 The Effect of Molecular Order on Light

Ordered elongated molecules, in bulk, have a different dielectric constant for each axis, and correspondingly a different refractive index. If these molecules are unordered then the material will appear optically isotropic, however in the liquid crystal phase the refractive index will depend on whether the polarisation of the light

is parallel to the average director. This manifests itself as *birefringence* whereby incident unpolarised light is split into two orthogonal polarisations travelling at different velocities. The wave which is governed by the 'long' molecular axis (refractive index, μ_e) is known as the *extraordinary ray*, and the other (refractive index, μ_o) is called the *ordinary ray*. However, as explained in the previous section, the molecules can be rotated by the application of an electric field so that the refractive index that a polarised light wave experiences, depends on the angle made with the director. As an example consider the operation of a twisted nematic cell, which is the type of device used for most simple display purposes.

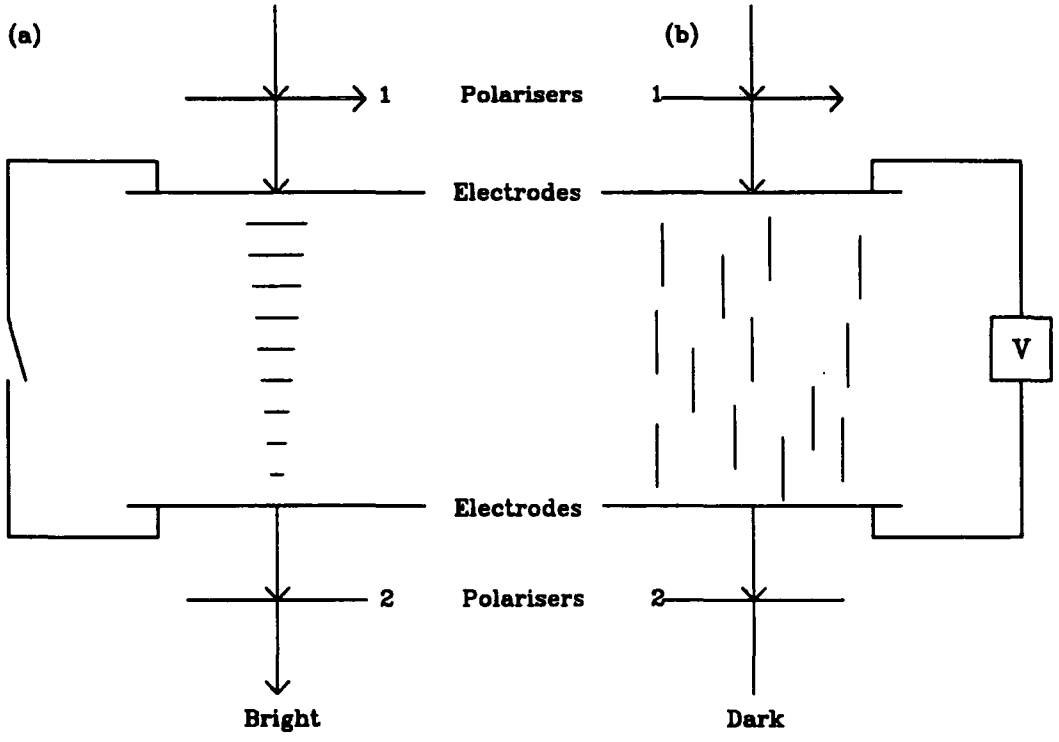

Figure 2.5: Operation of a Twisted Nematic Cell. (a) Voltage Off. (b) Voltage On

A twisted nematic cell is made by sandwiching liquid crystal between two homogenously aligned glasses placed together so that the two rubbing directions are mutually perpendicular. This means that the directors align parallel to each glass, with a gradual rotation of 90° between them as shown in figure 2.5(a). The first polariser is orientated so that its axis is parallel to the extraordinary axis of the liquid crystal at that interface. As the light propagates the twisted structure rotates the plane of polarisation of light so that it emerges in the orthogonal polarisation state and is transmitted by a polariser placed at 90° to the first. It is of interest to briefly compare this effect with that of optical activity. A material which dis-

plays optical activity, e.g. quartz, is composed of helical molecules which interact with the incident light in such a way as to propagate light with the polarisation state rotated. As explained in section 2.1 the cholesteric liquid crystal phase is also characterised by a twisted structure whose pitch is of the order of the wavelength of light. This explains the very large optical activity displayed by these crystals. A full explanation involves the quantum mechanical nature of light and the molecules, but the important difference between the twisted nematic effect and optical activity is that optical activity is strongly wavelength dependent, and the effect occurs whatever the direction of the incident polarisation. A twisted nematic cell only rotates the light in a simple fashion if the light is polarised along either of the crystal axes of the surface layer of molecules and this rotation is wavelength independent (see e.g. HARTSHORNE AND STUART [31]). When an AC voltage is applied to the cell, as in figure 2.5(b), the molecules rotate as described in section 2.3.2 so that the cell no longer appears to be optically active, and the light is blocked by the second polariser. The diagram is simplified, it is only the molecules in the center of the cell that are free to rotate but the effect is the same. The twisted nematic cell is generally used as a binary device, either to produce a light or dark state. In this thesis it is modulation of refractive index that is regarded as important so that a slightly different type of cell is used, although the basic principle is the same as the twisted nematic cell.

There are two other configurations for making a nematic cell; the *anti-parallel cell* and the *parallel* or *pi-cell* (see BOS et al. [9]) They are both made in the same way as the twisted nematic cell except for the rubbing directions. In the anti-parallel cell the glasses are rubbed so that the rubbing directions on each glass are in opposite directions, and accordingly in the same direction for the pi-cell. As mentioned earlier, there is a small angle between the director and glass and it is this that causes the difference between the way the molecules align themselves. The differences are shown in figure 2.6.

The application of an AC voltage across the cell rotates the molecules in both types of cell in the same way as the twisted nematic cell so that the extraordinary ray experiences a refractive index varying from μ_e when no voltage is applied, down to μ_o when the saturation voltage has been applied and the molecules have rotated through 90° and are perpendicular to the cell. The birefringence can therefore

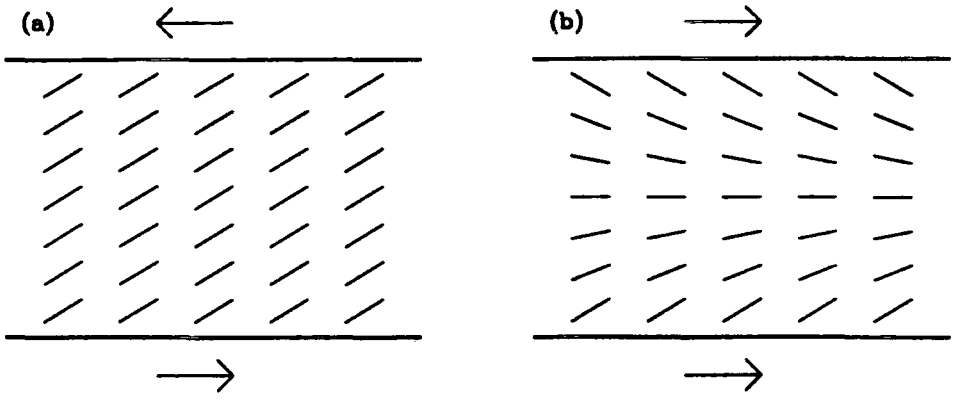

Figure 2.6: Two Homogenous Alignment Configurations. (a) The anti-parallel aligned cell. (b) the Pi-cell or parallel aligned cell. The arrows show the rubbing directions and the pretilt angles are exaggerated. Both cells are shown in the 'Off-State', i.e. no applied field.

be controlled, or if polarised light is used, the refractive index can be electrically 'tuned' between two values. Normally incident unpolarised light passing through the birefringent cell emerges with a phase difference, δ, between the two orthogonally polarised beams, with one plane of polarisation along the director, given by

$$\delta = \frac{2\pi d\Delta\mu}{\lambda}\sin^2\theta \tag{2.4}$$

where λ is the wavelength, d is the LC thickness, $\Delta\mu$ is the birefringence, and θ is the angle between the pretilt direction of the molecules and the propagation direction. The pretilt direction is usually small so equation 2.4 reduces to

$$\delta = \frac{2\pi d\Delta\mu}{\lambda}. \tag{2.5}$$

For example, with typical parameters of $d = 10\mu$m, $\Delta\mu = 0.25$ and $\lambda = 0.5\mu$m, then $\delta = 10\pi$.

Both cell configurations modulate phase in the same way. The pi-cell can operate slightly faster but it is prone to areas of misalignment when the directors relax to their off-position. This causes a patchy appearance when viewed between crossed polaroids. In view of this the cells used in this thesis were all anti-parallel aligned.

When an anti-parallel rubbed cell is placed between crossed polarisers with the cell extraordinary axis parallel to the first polariser then no light is transmitted by

the analyser (second polariser) since the LC cell simply phase retards the light, but does not rotate the plane of polarisation. If the cell is placed at an arbitrary angle between the crossed polarisers, then it acts as a phase plate, and in general, converts plane polarised light to elliptically polarised light. This effect is explained in greater detail in chapter 6.

2.4 Applications of Liquid Crystals

2.4.1 Liquid Crystal Displays

The development of the twisted nematic cell in the late 1970s provided the ideal cheap and low power device for the display industry; which has therefore been the main driving force behind research into LC materials. This section gives the background to liquid crystals by describing some of these devices. For example watches, calculators, telephones, and cameras incorporate LCDs in, what is now, a familiar way. Even the display timetables at some of the London railway stations are huge liquid crystal arrays.

There are other display applications that are not as widely available yet. For example, a variation on the twisted nematic is called a *super twisted nematic.* The principle of operation is similar to the twisted nematic except that a rotation of 270° is induced in the molecules instead of 90°. Its advantages are that it can be viewed from greater angles and it lends itself to a multiplexed device more easily, since it is more responsive to a small change in voltage.

Further twisted nematics can be coloured by the use of coloured polarisers. A coloured polaroid only polarises light of a particular colour, the other wavelengths are left unpolarised, so by using two differently coloured polarisers a two colour display maybe made. An alternative method of making a coloured display is to dissolve a *dichroic dye* in the LC. The dye preferentially absorbs light that is polarised in a particular direction and so by using the ability of a liquid crystal to change the polarisation a coloured display may be used. They have the advantage that only one polariser needs to be used. A variation using chiral nematics means that no polarisers need to be used meaning a very wide viewing angle and a very bright

display.

Another use of chiral nematic liquid crystals is to make a display that has a 'memory', thus the display will remain switched on even after the voltage has been removed. A higher reversed voltage can be used to switch the cell off.

Smectic liquid crystals do not respond to voltages as easily as nematics. However the alignment strongly depends on whether it cooled to form the smectic phase in the presence of an electric field. This is therefore another way of producing a display with a memory. The display may be activated by either using a voltage that causes local heating or by heating with a scanning laser beam. These displays obviously consume considerably more power and are not cheap. However they can have a very large data content and are therefore suitable for large information displays.

One of the important parameters in all LC cells is the cell thickness and very large cells become difficult to make with a constant thickness. A solution to this is to use a *Polymer Dispersed Liquid Crystal Display* (PDLC) whereby the liquid crystal is held as droplets embedded in a solid polymer. The refractive index of either of the LC indices is made to be the same as the polymer, thus in this case the cell is transparent. When the refractive index is switched to the other value the sudden change in index scatters the light and so the display becomes opaque. This is another display that requires no polarisers. Large-scale displays can be fabricated that may be used as switchable windows in buildings and cars, or switchable partitions etc.

One of the most recent developments in display technology is the *active matrix display* where semiconductor devices are incorporated into a display in order to optimise the display characteristics. For example a matrix element in a display may be combined with a miniature thin film transistor. The transistor acts like a switch, the application of a small voltage allows a larger voltage to be controlled and hence operate the liquid crystal. Using this technique the brightness of every element in a very large array may be controlled in an independent way.

By combining some of the advances mentioned the liquid crystal is becoming a serious competitor for the cathode ray tube (CRT). By combining coloured dyes with a very large number of pixels in an active matrix display, colour television displays can be made. At the present only small screens ($\sim$ few inches) can be made

but by the turn of the century the familiar CRT television should be replaced by a flat LC screen.

2.4.2 LC Optical Control Elements

Liquid crystals provide a very attractive way of controlling light both in amplitude and in phase. One of the simplest devices is an fast liquid crystal shutter, based on a ferroelectric LC. The film behaves as a half wave plate between crossed polaroids to act as a voltage switchable shutter [2] which can have switching speeds as fast as 10μs.

The ability to control phase means liquid crystals make an obvious choice for a tunable retardation plate. The cell can be tuned to any retardation (typically between 0 and 10 visible wavelengths for a 10μm thick cell), or alternatively the cell can be used to give a fixed retardation (e.g. $\frac{\pi}{2}$ to convert plane polarised light to circularly polarised light) to light of different wavelengths (e.g. WU [64]).

A novel use of liquid crystals has been to construct a circular liquid crystal switchable structure in such a way as to make a Fresnel zone plate (WILLIAMS et al. [63]). This is a series of transparent and opaque annuli which has the effect of focussing light, the device then operates as a lens which may be switched on or off.

Many optical control devices are based upon a *Liquid Crystal Light Valve* (LCLV) which is shown schematically in figure 2.7. The liquid crystal layer is placed in series with a photoconductive layer whose resistance varies with the amount of light falling on it. If a constant voltage is then applied across the electrodes, the voltage across any particular area of the LC is dependent upon the light incident on the photoconductor. An incident image is then transferred to the output light beam in real time and without any scanning. The light valve is one of various devices known as *Spatial Light Modulators* (SLMs), i.e. any device that has the capability of changing the light beam from place to place. A LCLV can be used, for example, to convert an infrared image to a visible image (WU et al. [67]) if the photoconductor is made sensitive to infra-red.

LCLVs are of increasing importance in the rapidly expanding field of optical

[2] Ealing Electro-Optics PLC, Greycaine Road, Watford, WD2 4PW. U.K.

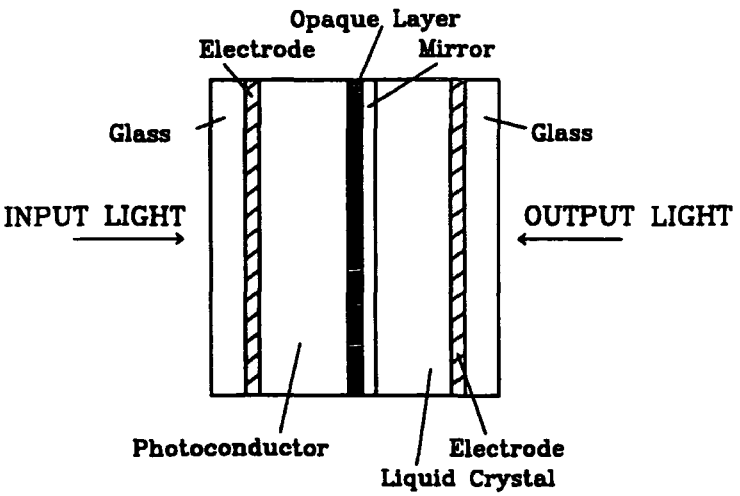

Figure 2.7: Liquid Crystal Light Valve: Image Transfer Device

computing. Although advances in digital computing continue, there are inherent limitations on the speed of an electronic computer. If light is used instead, then not only does the speed increase, but also the ease of creating parallel optical channels. In such technology the SLM performs the same function as the electronic switch in a traditional computer (e.g. COLLINGS et al. [14]).

An example of a different kind of SLM is explained in VASIL'EV et al. [61]. Here light in a Twyman-Green Interferometer is distorted by a small deformable mirror, and the light is corrected by a SLM in the form of an array of variable retardation plates.

2.4.3 Other Uses

Chiral nematic liquid crystals reflect light with a wavelength equal to its pitch, which is in turn sensitive to temperature. Such liquid crystal thermometers have been available for several years now, however their great advantage over traditional measurement devices is that the exact operation temperatures may be finely tuned so that the colour changes occur over a very small temperature range. This can be used, for example, in medicine to show minute differences in skin temperature which can indicate the presence of a tumour.

Development is in progress to utilise the ability of a chiral nematic to respond to

pressure changes to act as a pressure indicator. The mechanical properties of liquid crystals are also being explored, for example the viscosity of certain LC phases is much greater than that of the isotropic phase. In the future clutches or brakes could be made whose hydraulic elements could change their response depending on the pressure or temperature.

In all these examples of the many uses of liquid crystals it is really the same fundamental property that is being exploited, that is, the liquid crystal phase is a very delicate phase and so large changes in its characteristics can be made by small changes to its physical and chemical environment.

Chapter 3

Atmospheric Seeing and Adaptive Optics

3.1 Atmospheric Seeing

The distortion introduced into a stellar image by the atmosphere is caused by very small spatial and temporal differences in the atmospheric refractive index. These are due to small temperature fluctuations in a wind induced turbulent flow. Local temperature variations vary from a few hundredths of a degree in the upper atmosphere, to a few tenths of a degree near to the uneven ground level temperature. The effect of these temperature variations is to set up eddies of size L_o (where L_0 is the outer scale of turbulence, $\sim$ few metres), which in turn produce eddies of smaller and smaller scale until l_0 (the inner scale of turbulence, $\sim$ few millimetres). Consequently the temperature varies on scales ranging between L_0 and l_0. Similarly the refractive index varies on these scales. So when a wavefront of light is propagated through the turbulent atmosphere then variations in phase across the wavefront occur on the same scales.

Similarly KOLMOGOROV [38] has shown that the refractive index structure function, $D_N(\rho)$, which is the mean square difference of refractive index between points separated by a distance, ρ, is given by

$$D_N(\rho) = \langle |\mu_1 - \mu_2|^2 \rangle = C_N^2 \rho^{\frac{2}{3}}, \tag{3.1}$$

where μ_1 and μ_2 are the refractive indices and C_N^2 is termed the refractive index structure constant. C_N^2 is a measure of the strength of the refractive index variations

and hence the turbulence. It can be seen that the change in refractive index between two points increases as the separation, ρ, increases. The atmosphere can be thought of as a complex interaction of many turbulent 'eddies', the strength of which is proportional to the size. C_N^2 varies with height in a non-uniform way; the turbulence occurs in many layers of a few metres depth. The effect of the whole atmosphere is a summation of these layers. A term that is often used to characterise the seeing conditions is the coherence (or seeing parameter), r_0. This is directly related to the sum of the structure constant throughout the atmosphere and is given by

$$r_0 = \left[0.423\left(\frac{\lambda}{2\pi}\right)^2 \sec\theta \int_0^H C_N^2(h)dh\right]^{\frac{3}{5}} \tag{3.2}$$

where θ is the zenith angle and H is the thickness of the atmosphere that contributes to seeing (~20km). Typically at a site of good astronomical seeing the value of r_0 is between 10 and 20cm. A convenient way of visualising the meaning of r_0 is that it is the size of a telescope aperture that would give the same sized diffraction limited image in the absence of any turbulence as that produced by the seeing limited image in a larger aperture telescope.

The effect of the refractive index variations on the image formed depends on the size of the index variations and the size of the aperture used to form the image. With a small telescope, only the small scale eddies are seen, therefore the refractive index variations in total path length are small compared to the wavelength of light and thus the wavefront distortion is small. However the wavefront across the whole telescope will also be part of a larger scale fluctuation, and hence the whole wavefront may be tilted. A large telescope aperture will have greater wavefront distortion because it can sample larger eddies. These larger refractive index variations cause the image to break up into smaller sub-images known as *speckles*. However the wavefront tilt across the whole aperture will be less because some of the fluctuations that added to tilt in the small aperture, now just add to distortion. These effects can be seen in figure 3.1. The other effect on image quality is diffraction, which is inversely proportional to aperture size. Taking diffraction and seeing together, there is then an *optimum aperture* size. Below this the image quality is dominated by diffraction, and above this size the seeing distortion increases. This of course assumes that the seeing remains stationary. This is the *Taylor Hypothesis* which assumes that refractive index variations can be regarded as 'frozen' into the atmosphere relative to the timescales of seeing. Winds in the atmosphere blow these index variations

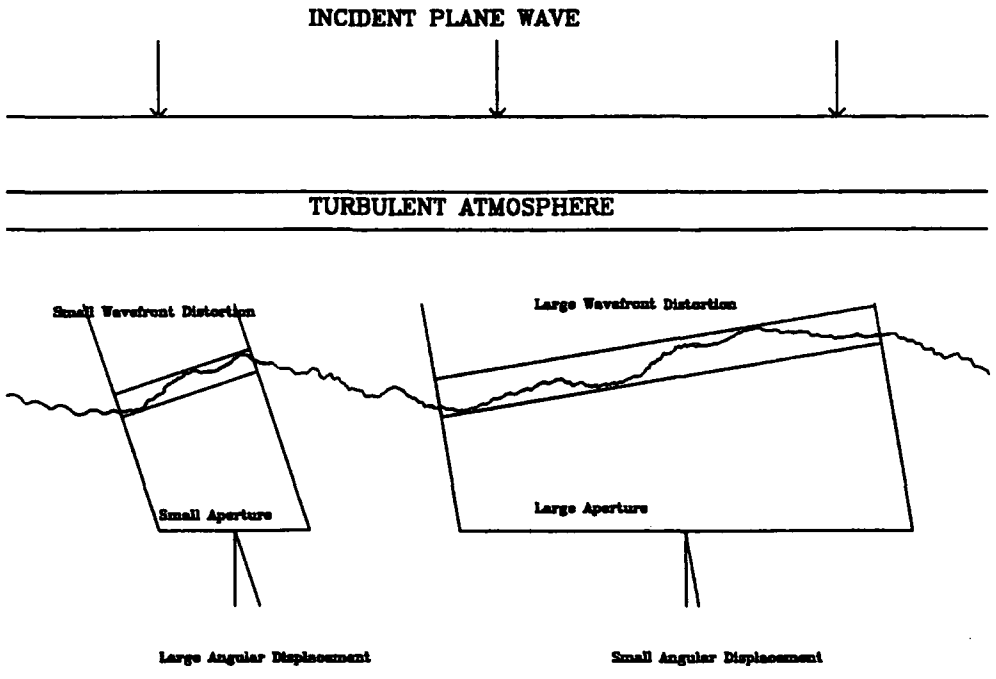

Figure 3.1: Seeing Effects on Different Sized Apertures.

across the telescope aperture and it is the effects of these which give rise to the seeing variations causing the wavefront shape to vary. In the case of a small aperture the distortions remain relatively small, but the tilt in the wavefront varies causes the image to move about in the focal plane. These variations are of the order of the time it takes for wind to move air across the telescope aperture, i.e. fractions of a second, so in a long exposure a blurred image is built up by the (near) superposition of many sharp short exposure images. The large aperture suffers less from image motion, but the wavefront is more corrugated and the image breaks up into speckle. In order to take advantage of the optimum aperture, then *short exposures* ($\sim$ 10ms) must be taken. This is of course impractical in conventional astronomy, but it is the idea upon which the theory of image sharpening is based. If the movement of the image from an optimum aperture can be corrected for, the resulting image should be 2 to 3 times smaller than the equivalent long exposure image (FRIED [27]). An example of image motion from an optimum aperture is shown in chapter 4, figure 4.1.

3.2 Methods of Reducing Seeing Effects

As previously mentioned, much of the seeing arises from temperature fluctuations near the ground and dome seeing. This is minimized by ensuring the telescope dome is as free as possible from heat sources such as electrical equipment, or people. Similarly the dome should be opened for an hour or so prior to observing so that the temperatures can equalise. The landscape around the telescope should be smooth and uniform to avoid turbulence. For example the WHT (William Herschel Telescope) is on top of a volcanic island, some 2400m above the relatively flat sea.

Even after careful selection of conditions and geographical location the image quality is far from optimum so some kind of image correction is necessary of which there are two basic techniques. The first is *post exposure sharpening* whereby all the data is collected without any processing and then processed afterwards to enhance detail. The second is *real time* sharpening whereby an adaptive optics system is employed to enhance the image quality. There are a number of advantages to real time sharpening. Firstly the improvement in signal-to-noise[1], therefore fainter (and more distant) objects may be observed. Secondly the light may be then directed to a second instrument, for example a spectrograph. The third point is that a CCD is much more efficient than time-resolvable instruments needed for post-exposure sharpening.

3.2.1 MARTINI: An Example of an Adaptive Optics System

The MARTINI (Multiple Aperture Real Time Image Normalisation Instrument) device, being developed at Durham, is a prototype adaptive optics system designed to operate on the GHRIL (Ground-based High Resolution Imaging Laboratory) platform at the Nasmyth focus of the WHT (see DOEL et al. [16, 17, 18, 19] or BROWN et al. [10]). The system uses piezo-electrically driven mirrors to remove the atmospherically induced tilt of a wavefront across a telescope aperture (effectively removing the seeing motion of the image). As explained in the previous section, there is an optimum aperture size for tilt correction, this being between 40 and

[1]The improvement in the S/N ratio assumes full aperture coverage. The MARTINI device does not actually improve the S/N because much of the collected light is wasted.

80cm. Therefore the full 4.2m WHT aperture must be split up into a number of sub-apertures. In MARTINI there are six such apertures, the size of which can be varied to match the seeing conditions prevalent at the time of observing.

Figure 3.2 shows the optical layout of MARTINI. Light from the WHT enters the system through an aperture in the centre of the toroidal mirror placed at the Nasmyth focal plane. The divergent beam of light from the focus is then incident on an aperture mask positioned 60cm downstream from the focal plane (conjugate to a height of 3.6km in the atmosphere). This aperture mask consists of a set of six identical circular sub-apertures. Immediately behind each sub-aperture is a piezo-electrically driven plane mirror which reflects the light back onto the toroidal mirror. This mirror is aspherical in shape in order to compensate for astigmatism caused by off-axis imaging. The light is then refocused to a secondary focus where a beam splitter divides it into two. One beam is arranged so that the reference star (a star in the field of view bright enough to produce enough signal for the instrument to work) is imaged onto the photocathode of an Imaging Photon Detector (IPD) via a split-lens system. This split lens consists of an achromatic doublet that has been cut into six pie-shaped segments. The width of the cuts have been chosen such that when the segments were re-assembled they no longer have a common optical axis and thus the focal points of the segments are separated. The cone of light from each sub-aperture is focused by a different segment of the lens onto the IPD, and so six images of the reference star are formed corresponding to the 6 mirrors and the positions of these images are then used in a servo-loop to control the tilt compensating mirrors in such a way as to remove the images' seeing motions.

The other beam of light from the beam splitter is focused onto the CCD via the atmospheric dispersion corrector. This is the 'sharpened output' of the system. The total magnification of the system is designed to be of the order of one, so that the image scale on the CCD (not on the IPD where it has to be quite large in order to avoid saturation of the IPD) is approximately the same as at the true Nasmyth focus (4.46 arcsecs mm^{-1}). An example of some results obtained with MARTINI are shown in figure 3.3 (some results have been published in TANVIR et al. [55] [53][56]). Notice that not only is the resolution improved, but also the peak intensity.

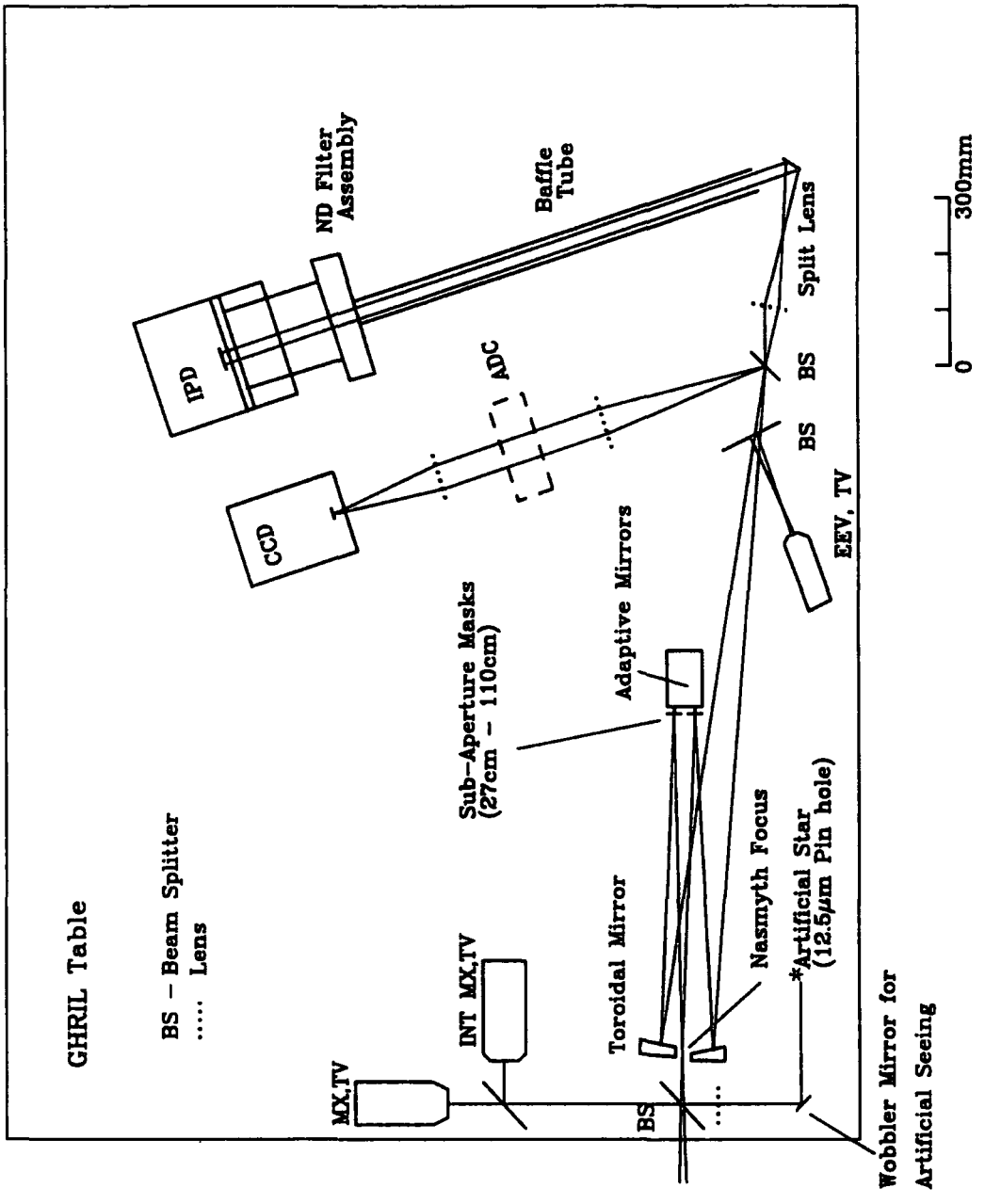

Figure 3.2: The MARTINI Optical Layout. ADC–Atmospheric Dispersion Corrector

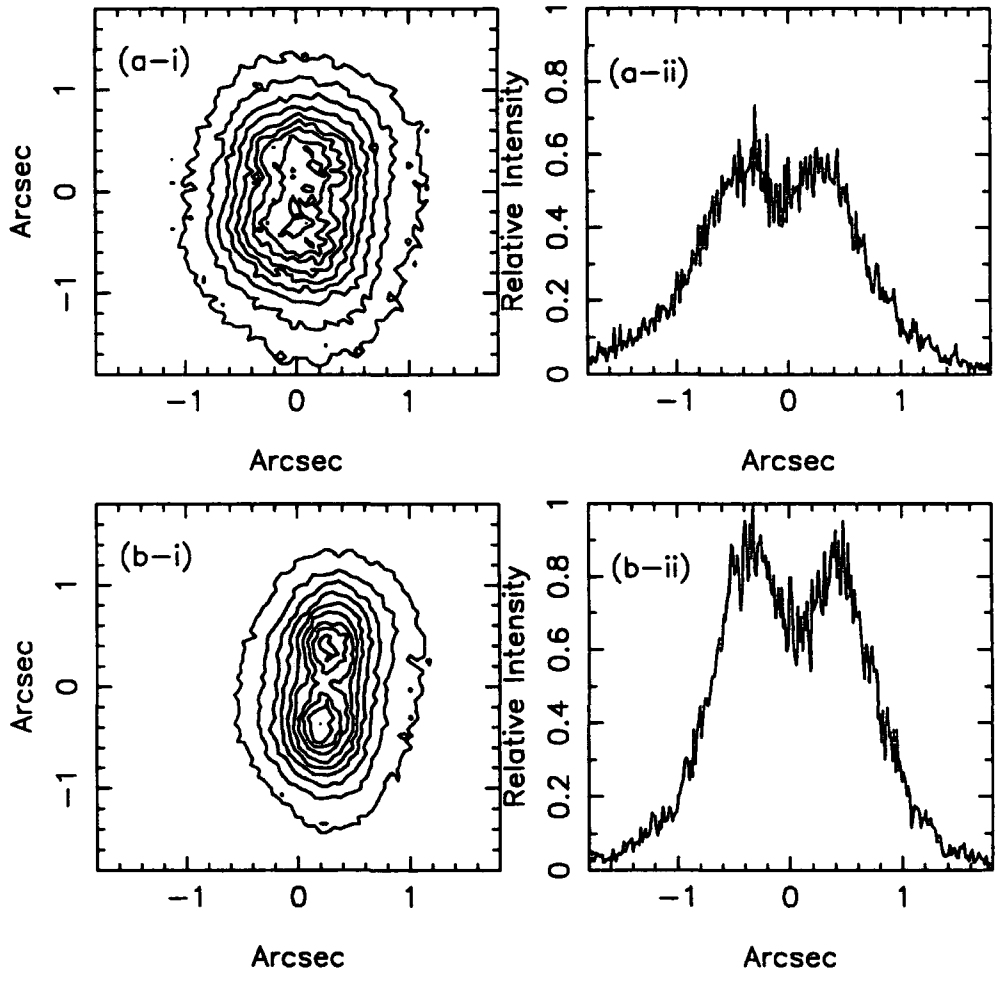

Figure 3.3: Some results from MARTINI. Star *Zeta Boo*. (a) without MARTINI (b)with MARTINI (i) contour plan (ii) cross section.

3.2.2 Other Image Sharpening Devices

Other astronomical adaptive optics devices have been designed and tested. They all utilise piezo-driven mirrors. For example ISIS (THOMPSON AND RYERSON [58]) (Image Stabilisation Instrument System) has been in operation at the 2.24m University of Hawaii telescope since 1984. It uses only one mirror to track the image motion over the whole aperture. The COME-ON project (MERKLE et al. [36]) is part of ESO's developments for the 3.6m telescope at La Silla in Chile. It utilises a two-stage process whereby the overall wavefront tilt is removed by a single active plane mirror. The smaller-scale corrugations are removed by a thin flexible mirror. The device is particularly interesting because the wavefront distortion is sensed at optical wavelengths whilst the final corrected image is recorded in the near infra-red. There is the possibility of using liquid crystals at these infra-red wavelengths as well as in the optical (e.g. WU AND COX [65]).

3.2.3 Adaptive Mirror Technology

The present time is rather an unusual one in the development of astronomical adaptive optics. Up to now research has taken place within university environments, however parallel research has also occurred, primarily in the United States, into the military applications of adaptive optics. Their interest lies in two areas. Firstly surveillance, which is essentially the same problem of observing through the atmosphere, and secondly laser beam transmission for communication and directed energy weapons systems. Their requirements are not exactly the same as those in astronomy, however the funding has been orders of magnitude greater than that in astronomy and so the devices are much more advanced. Recently this technology has been declassified and so the astronomical adaptive optics community is in the position of having a large field of advanced potential technology at its disposal. The following is a brief survey of devices.

The technologies can be divided two categories. Firstly there is *conventional mirror technology.* These can be sub-divided into *segmented mirrors* and *continuous phase sheets*, or *deformable mirrors.* As their name suggests, segmented mirrors consist of discrete mirror elements used to correct different parts of the wavefront.

The mirrors used in MARTINI are an obvious example. The group is considering replacing these six mirrors with a segmented mirror made by THERMO-ELECTRON TECHNOLOGIES CORPORATION[51][34]. This consists of an array of 68 mirrors, each of which has 3 degrees of freedom (tip, tilt and piston). There is a trade-off between dynamic range and response times, but typical figures are 2μm at 10KHz or 8μm at 2.5KHz. Two examples of continuous phase sheets are LITON-ITEK and UNITED TECHNOLOGIES OPTICAL SYSTEMS[22][30]. These devices consist of one large, but flexible mirror, which is deformed by actuator elements behind the mirror. They have the advantage of providing continuity of correction, however there is more potential for cross-talk between actuators. The Liton-Itek device has 241 PMN (Lead Magnesium Niobate) electrostrictive actuators, which have a 6μm stroke at 1KHz.

The second category is *exotic technologies*. These are devices employing new techniques that provide future potential but are not yet ready for astronomical use. For example TEXAS INSTRUMENT'S DMD[25] (Deformable Mirror Device). This is a chip mounted device, constructed by depositing a mirrored layer onto an electrostatically operated layer. This layer is etched so as to leave control points which control the mirror. The stroke is however small, $< 1\mu$m. Another kind of device designed by OPTRON SYSTEMS INC.[52] uses an electron-beam to address an anode grid and a thin layer of $LiNbO_3$ electro-optic crystal, coated with a dielectric mirror. The electron-beam gun scans the device, like a CRT, to change the reflective properties of the mirror. However, the response time is slow, $\sim$ 2Hz.

3.3 Liquid Crystals as Adaptive Optics Devices

Figure 3.4 shows the array of six adaptive mirrors, each controlled by three piezo-electric actuators. The construction is as compact as possible, reducing the possibility of adding more sub-apertures (or mirrors) to increase the aperture coverage. In addition the six amplifiers that control each mirror are large and generate considerable heat in the GHRIL room. These factors, along with cost, are the main reasons for investigating the replacement of these mirrors with liquid crystal prisms to deflect the seeing-distorted light beams.

Figure 3.4: The MARTINI Adaptive Mirror Array, also showing the piezo-electric actuators

The concept behind a LC prism was described in chapter 1 but it is described in greater detail here. The extraordinary refractive index of a liquid crystal cell is electrically controllable[2] By applying a voltage ramp along the length of a liquid crystal cell and keeping the other plate at ground, the voltage across the cell will vary from a maximum at one end down to zero at the other. Hence the optical thickness of a parallel sided liquid crystal prism, of thickness t, will vary from one end to the other. The maximum optical thickness is given by $\mu_e t$ and this occurs at the end of the cell with no voltage across the LC. The minimum optical thickness is given by $\mu_o t$, where μ_o is the ordinary index. This occurs at the end of the cell

[2]The actual graph of μ_e versus voltage is not linear, as described in chapter 5.

where the voltage is at a maximum. The effect of this variation in optical thickness along the cell is to produce a phase wedge, which can deflect light through small angles in a way that is electrically controllable by the applied voltages.

A typical liquid crystal material, with $\mu_e = 1.8$, $\mu_o = 1.5$, in a cell of thickness 10μm, and length 1cm, would give a variation in optical thickness of 18μm to 15μm. Hence the light should be deviated at an angle given by the variation in optical thickness divided by the length of the cell, in this case about 1 arcminute. The exact formula for the deviation of light by a LC prism is derived in the next chapter. It is important to clarify the terminology here. In this thesis, the angle of a LC prism is defined as above, that is, it is the angle through which light is deviated after transmission through such a cell. However, when considering a real prism, the prism angle is usually defined to be the physical angle of the prism, which is not the angle through which light is deviated. It is the former definition that is of relevance here.

3.3.1 Very Long Base Line Interferometry

This is a technique where there is a possibility of using liquid crystal adaptive optics in a relatively simple fashion to combat the effects of seeing. The method is based upon Michelson's Stellar Interferometer (MICHELSON [44]), which is described briefly below. A modern device based on the same physical principle is being constructed and tested at Cambridge called COAST (Cambridge Optical Aperture Synthesis Telescope. [4]).

Figure 3.5 shows the basic apparatus. The outer pair of mirrors, M_1 and M_4 act as 'receivers' and are in general many metres apart. This separation, D, is the baseline and is variable. Light is channeled to the fixed secondary mirrors, M_2 and M_3 which direct the light through two slits into a focussing system to bring the light beams to interfere at a common focus. The spacing of the fringes is determined by the (fixed) spacing of the slits, however the *fringe visibility* is determined by the brightness distribution of the source. In order to extract this brightness distribution, methods of fourier optics are used in a way that is exactly the reverse procedure to that described in section 5.3.2. In this way sub-milliarcsecond measurements may be made. Once again, though, the results are plagued by the

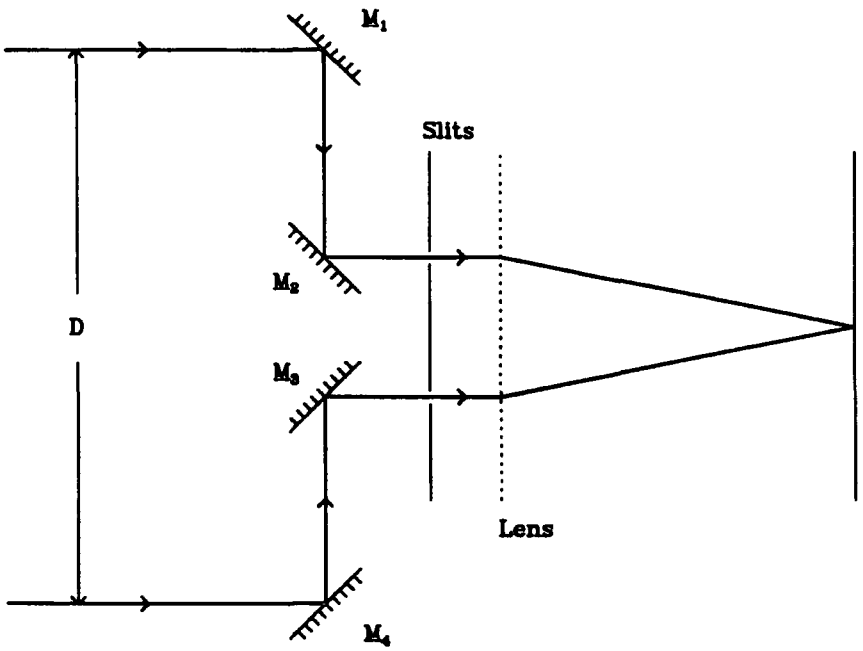

Figure 3.5: Schematic of Michelson's Stellar Interferometer

effects of atmospheric turbulence. The individual apertures used are small enough so that the distortion is small and also that speckle does not occur. There is, however, a phase difference between the two apertures which causes the fringes to oscillate and makes measurements difficult. A simple liquid crystal phase retarder could be placed in one of the light beam paths to correct for the seeing. An adaptive feedback circuit would be needed whereby the position of a fringe is detected on an IPD (or similar device) and any movement is fed back to the liquid crystal. The amount of correction needed is the total phase difference modulo 2π, and is therefore very small, hence only very thin cells are needed. This type of adaptive optics would be simpler than that described in the MARTINI, or similar, system and could therefore be perhaps used as a test ground for liquid crystals in adaptive astronomical optics.

There is a potential use for liquid crystals where ever the need to control phases over a few visible wavelengths is desired.

Chapter 4

Basic Design and Construction of LC Prisms

4.1 Introduction

This chapter deals with the factors that influence the design and construction of a LC prism, in particular the size and speed of prism required. Then the type of electrode structure in order to apply the voltages are considered. These are then followed by details of the construction of the prism.

4.2 Required Prism Parameters

4.2.1 The Angular Size of Prism

FRIED [26] has shown that the mean square wavefront phase error, $\langle|\Delta\phi|^2\rangle$, for an atmospherically distorted wavefront across a circular aperture of diameter D is[1]

$$\langle|\Delta\phi|^2\rangle = 1.013\left(\frac{D}{r_0}\right)^{\frac{5}{3}}. \tag{4.1}$$

From equation 3.2 it can be seen that

$$r_0 = C_N\lambda^{\frac{6}{5}}, \tag{4.2}$$

[1]This equation gives another physical interpretation to r_0. It is the size of an aperture where the r.m.s wavefront error is $\simeq$ 1radian.

r_0	D	$\overline{\Delta z}$	$\overline{\theta}$
15cm	4.2m (full ap.)	1.29μm	4.9″
	60cm ($4r_0$)	0.25μm	6.7″
	15cm (r_0)	0.08μm	8.4″
10cm	4.2m (full ap.)	1.81μm	6.8″
	40cm ($4r_0$)	0.25μm	10.1″
	10cm (r_0)	0.08μm	12.7″

Table 4.1: R.M.S. Correction Parameters ($\lambda = 500$nm).

where C_N is a constant ($\simeq 5.5 \times 10^6$ for $r_0 = 15$cm). If the amount that a wavefront corrector needs to move by is Δz, to correct a phase error of $\Delta\phi$, then

$$\Delta z = \frac{\Delta\phi\lambda}{2\pi}. \tag{4.3}$$

Combining equations 4.1, 4.2, and 4.3 gives the r.m.s correction as

$$\sqrt{\langle|\Delta z|^2\rangle} = KD^{5/6} \tag{4.4}$$

where $K = \sqrt{1.013}/(2\pi C_N^{\frac{5}{6}})$. This is an important result because it shows that the amount of correction needed is wavelength independent. The required r.m.s. correction angle is then

$$\overline{\theta} = \frac{\sqrt{\langle|\Delta z|^2\rangle}}{D} \tag{4.5}$$

However any correction device must be placed at conjugate plane to the average height of seeing so the demagnification of the telescope must be accounted for. The magnification of the WHT for an image at the conjugate focus is $\times 77$, but is different for different telescopes. See appendix A for greater discussion. Therefore

$$\overline{\theta} = \frac{77K}{d^{\frac{1}{6}}} \tag{4.6}$$

where d is the physical size of the correction element ($d = D/77$). The correction angle is then very weakly dependent on the diameter, although the 'throw', $\Delta z \propto D^{\frac{5}{6}}$. Using equations 4.4 and 4.6 some typical figures for the required correction are shown in table 4.1.

Real data collected[2] at the WHT by MARTINI was analysed and compared with the theoretical results. The raw data consisted of xyt positions (i.e. coordinates and time) of individual photons from a 'seeing' affected image collected on the IPD without the MARTINI adaptive optics activated, that is with no sharpening. The positions were grouped into time intervals of 1.5ms in which about 20 photons were collected and the mean position of the photons was calculated to provide a data stream of centroids of image motion. The motion of an image is shown over 6 seconds of time in figure 4.1. (N.B. the IPDs X and Y axes do not correspond to any particular telescope axes.) The image scale (calculated by measuring the spacing of a known binary star) was 0.003 arcsecs/pixel. The deflections by a LC prism needed to correct the centroid motion can be calculated[3]. These are shown in table 4.2. A

Star	Mean X Dev'n	Mean Y Dev'n	Mean Total Dev'n	Max X Dev'n	Max Y Dev'n	Max Total Dev'n
α-Aries	11.1″	10.9″	15.6″	49.3″	55.7″	74.4″
Rigel	10.5″	10.7″	15.0″	38.0″	47.6″	60.9″
Polaris	9.9″	11.7″	15.3″	43.3″	42.5″	60.7″
40cm Aperture 1.5ms Centroid Time						

Table 4.2: Angular Deviations by a LC prism needed to correct image motion calculated from experimental data.

histogram of the required correction is shown in figure 4.2. It can be seen that the theoretical r.m.s values are comparable[4] to the actual data. Therefore the average correction angle is $\sim$ 15 arcseconds. Assuming the fluctuations are gaussian then the 3σ (corresponding to 99.7% of cases) deviation corresponds to $\sim$ 45 arcseconds. (In the case of the example shown in figure 4.2 then 98.4% of cases fall within the 3σ level of variation. Thus the largest prism angles required to cover most eventual

[2]By the MARTINI Group, but analysed by the author.

[3]If the x-deviation is θ_x and the y-deviation is θ_y then the total deviation, θ_{xy} is given by $\cos\theta_{xy} = \cos\theta_x \cos\theta_y$. For small angles this can be approximated by $\theta_{xy}^2 = \theta_x^2 + \theta_y^2$. See appendix E for the full calculation.

[4]It is difficult to make exact comparisons because the value of r_0 is uncertain for the experimental data.

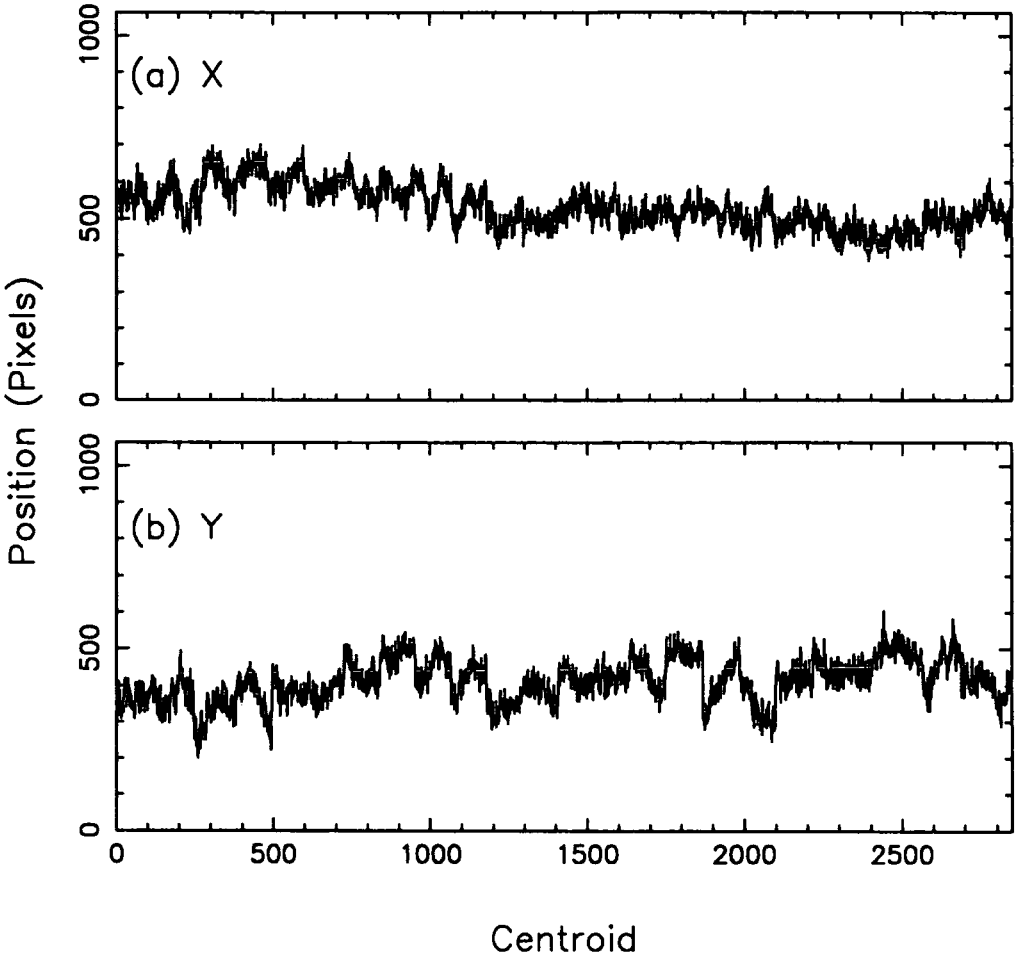

Figure 4.1: Motion of Stellar Image (α-Aries) on the IPD caused by Atmospheric Turbulence (a) X-axis (b) Y-axis

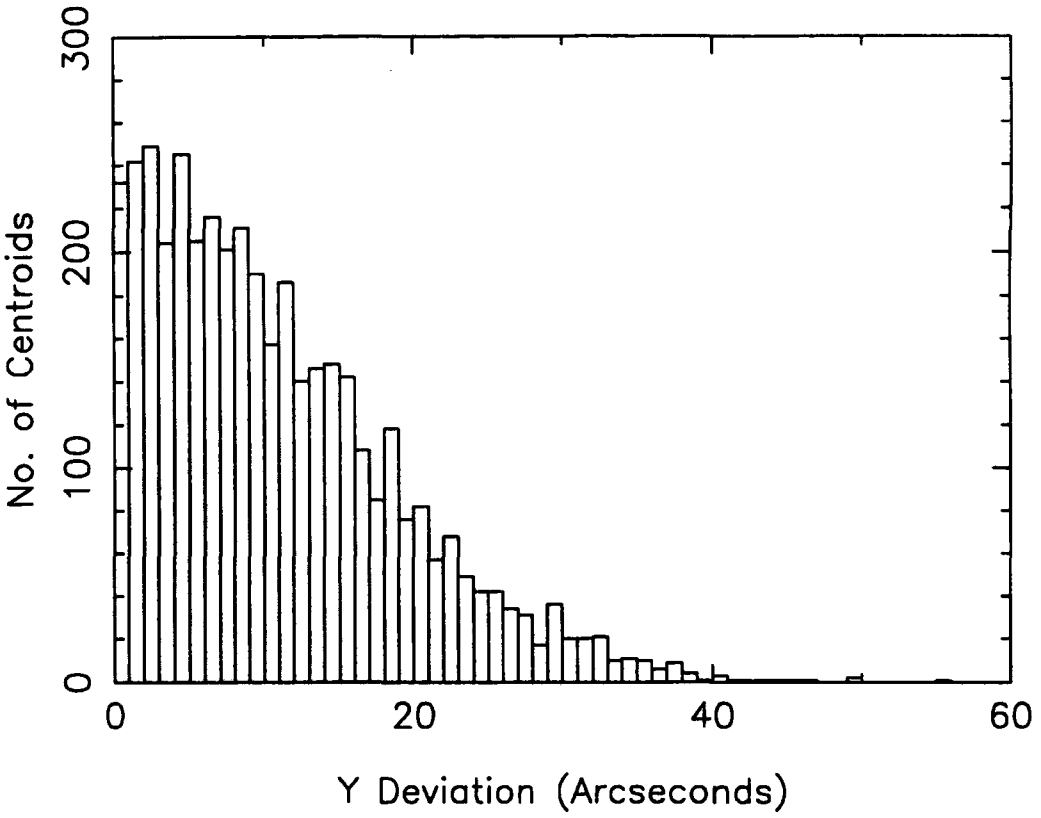

Figure 4.2: Required prism angles to correct for image motions. α-Aries, 40cm aperture, 1.5ms centroid time.

cases, including poorer seeing, is $\sim$ 1arcminute, although the vast majority of seeing effects can be corrected by prism angles half that size.

4.2.2 Higher Orders of Correction

In the previous sub-section the removal of wavefront tilt was considered. However there exists a spectrum of errors, which are given by the traditional Seidal aberrations. In the context of atmospheric turbulence they are more conveniently represented by Zernike Polynomials (see NOLL [46]). The wavefront residual errors after each term (and the previous terms) have been corrected for is shown in table 4.3. It can be seen that most of the wavefront degradation is contained in image tilt. The removal of wavefront tilt is the very important first step in image sharpening.

Zernike Term	Residual Wavefront Error	Description
1	$1.013\left(\frac{D}{r_0}\right)^{\frac{5}{3}}$	No correction
2	$0.134\left(\frac{D}{r_0}\right)^{\frac{5}{3}}$	Tilt Removed (2-d)
3	$0.111\left(\frac{D}{r_0}\right)^{\frac{5}{3}}$	Focus
4	$0.088\left(\frac{D}{r_0}\right)^{\frac{5}{3}}$	Coma
5	$0.065\left(\frac{D}{r_0}\right)^{\frac{5}{3}}$	Astigmatism

Table 4.3: Residual wavefront error after the first few zernike terms have been corrected for.

4.2.3 Response Time Needed in an Adaptive Prism

For turbulence compensation, the correction must be at least as fast as atmospheric changes. To calculate this the Taylor Hypothesis is adopted, as described in section 3.1. If the mean wind velocity across the telescope aperture is V_{cw} then the atmosphere remains static for timescales, τ give by (MARTIN[42])

$$\tau \simeq \frac{D}{V_{cw}}. \tag{4.7}$$

Using typical parameters for a 60cm sub-aperture gives $\tau \sim 40$ms. This figure is an approximation and is obviously (via r_0) wavelength dependent. For example in the infrared the atmosphere remains static over time periods of tenths of seconds.

4.3 Type of Prism

Two alternative approaches to constructing a LC prism were considered. The first is to construct a device with a number of electrode strips. These would be addressed with an increasing series of voltages so as to modulate the refractive index in such a fashion as to form a phase wedge. The second approach is to use a monolithic electrode with a voltage ramp applied along the electrode to modulate the index. Each of these has advantages and disadvantages.

4.3.1 A multi-electrode prism

The primary question is how many electrodes must a prism have in order to simulate a continuous phase wedge? The properties of such a prism were simulated by assuming a simple model for the phase distribution along the cell, and then applying the Huygens-Fresnel principle to investigate the transmitted light intensity distribution. The refractive index was assumed to vary in a step-like fashion as shown in Fig. 4.3. The lowest index is defined to be μ_1 and this is incremented in equal steps up to the

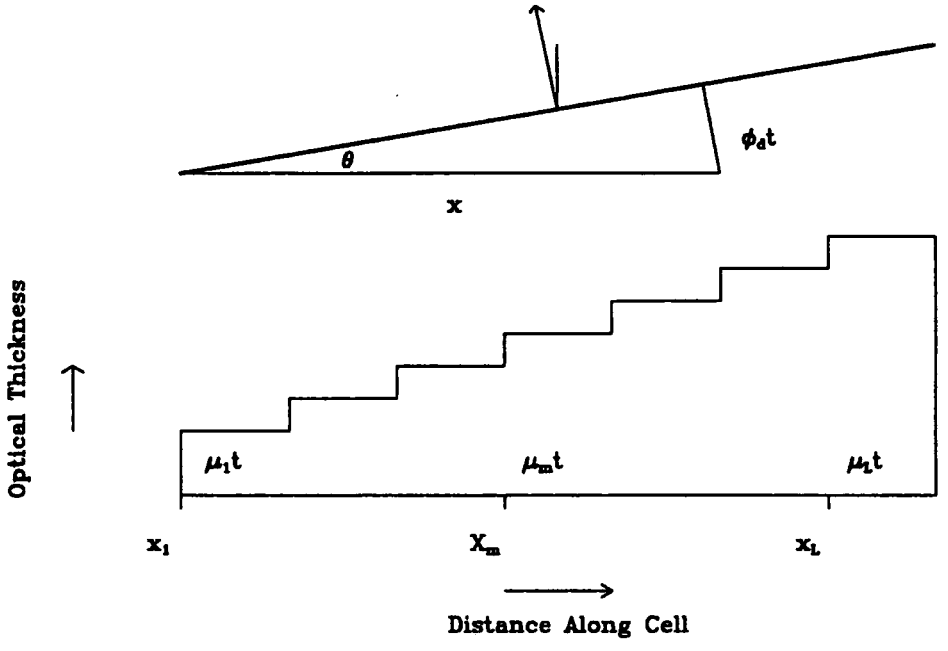

Figure 4.3: Optical thickness of a simulated prism with a multi-electrode structure

maximum index of μ_L, there being L steps in total, each of width d. This assumes that there are no edge effects between step boundaries. The distance along the cell is given by the coordinate x, and the values of the step boundaries are given by x_m where $1 \leq m \leq L$. Since the index varies from μ_1 to μ_m the cell will behave as a prism. Consider a wave incident normally on the cell, and transmitted at an angle[5]

[5]The plane wave, at an angle θ, shown in the diagram is an arbitrary wave. No assumptions are made about the emergent angle, nor about the wave being corrugated. The actual wave transmitted by such a stepped structure would be tilted in the other direction, and also stepped in a similar fashion to the cell optical thickness.

θ. There will be a phase factor due to the wave being tilted given by (see Fig. 4.3)

$$\phi_d = \frac{2\pi}{\lambda} x \sin\theta. \tag{4.8}$$

There will be another phase factor due to the index variations along the cell given by

$$\phi_m = \frac{2\pi}{\lambda}(\mu_m - \mu_1)t, \tag{4.9}$$

where t is the cell thickness. Note that ϕ_m is normalised to be zero for m=1. Combining both the phase factors and summing over the length of the cell gives an expression for the resultant amplitude distribution. However the index is not a continuous function of x therefore the integral must be split into an integral and a summation. Hence the amplitude, A, is

$$A = A_0 \sum_{m=1}^{L} \int_{x_m}^{x_m+d} \exp\left[\frac{2\pi i}{\lambda} x \sin\theta\right] \exp\left[\frac{2\pi i}{\lambda}(\mu_m - \mu_1)t\right] dx \tag{4.10}$$

where A_o is the incident amplitude. Simplifying gives

$$A = A_0 \sum_{m=1}^{L} \int_{x_m}^{x_m+d} \exp\left[\frac{2\pi i}{\lambda}\left(x \sin\theta + (\mu_m - \mu_1)t\right)\right] dx. \tag{4.11}$$

The intensity distribution, assuming equal step widths and equal step increments is given by AA^* as

$$AA^* = A_0^2 d^2 \mathrm{sinc}^2\left(\frac{\pi d \sin\theta}{\lambda}\right) \frac{\sin^2\left[\frac{\pi L}{\lambda}\left(\frac{\Delta\mu t}{L} + d\sin\theta\right)\right]}{\sin^2\left[\frac{\pi}{\lambda}\left(\frac{\Delta\mu t}{L} + d\sin\theta\right)\right]}, \tag{4.12}$$

where $\Delta\mu = \mu_L - \mu_1$. This is a product of the diffraction pattern of a single slit modulated by a pattern due to their spacing. The latter is at a maximum when

$$\frac{\Delta\mu t}{L} + d\sin\theta = 0. \tag{4.13}$$

If the total cell width is W, then $W = Ld$ and

$$\sin\theta = -\frac{\Delta\mu t}{W} \tag{4.14}$$

$\Delta\mu$ is the birefringence. The minus sign indicates that the light is emitted to the opposite side of the normal than shown in Fig. 4.3 (i.e. the $-\theta$ direction). This is to be expected considering that the light from a real prism is emitted towards the thicker end of the wedge. Ignoring the minus sign and using the small angled approximation the light is then deviated by an angle given by

$$\theta = \frac{\Delta\mu t}{W}. \tag{4.15}$$

Some results of this are shown in Fig. 4.4. The x-axis shows the angle θ plotted as a function of the deviation away from the theoretical angle of transmission given by equation 4.11. The y-axes show the normalised intensity. The dashed line shows the diffraction pattern from a rectangular aperture the size of a single electrode width, given by the sinc function, with its maximum in the forward direction given by

$$I = I_0 \left(\frac{\sin\left(\frac{\pi d \sin\theta}{\lambda}\right)}{\left(\frac{\pi d \sin\theta}{\lambda}\right)} \right)^2 , \tag{4.16}$$

where I is the intensity. The solid line shows the intensity distribution of the stepped prism given by the square of equation 4.11. The result is analogous with that of Fraunhofer diffraction from a series of L slits (see e.g. Hecht and Zajac [32]). There is an 'interference term' arising from the interference between the individual steps (however the central maximum is shifted from zero), which is then modulated by an envelope caused by the diffraction pattern from the single step. The total width of the cell is kept fixed, so as the number of electrodes, L, increases, the electrode width, d, decreases and the electrode spacing also decreases. This broadens both the sinc function and the spacing between interference maxima. As can be seen from fig. 4.4, when there are very few electrodes the sinc function envelope is very narrow and the light will not be significantly deviated. As the number of electrodes is increased then the envelope broadens allowing light to propagate at the desired angle. It can be seen that greater than about 30 electrodes are needed in order that the intensity distribution is similar to that of a continuous phase wedge.

The disadvantages of using a multi-electrode structure is that an electrical connection is needed for each electrode. In any astronomical adaptive optics device using many prisms of this sort, then the addressing of each electrode would become very complex. Another problem is that the device can deflect light in one direction only. Another prism with an orthogonal electrode structure would be needed to provide two dimensional deflections. The electrode structure itself will also have a diffraction pattern, so this will also have an effect, albeit small, on the transmitted light. The advantage of a multi-electrode prism is that the precise voltage to apply to each electrode can be calculated by an on-line computer in order to utilise the full birefringence of the liquid crystal. When a monolithic electrode is used only the quasi-linear part of the birefringence versus voltage graph may be utilised in order to make a linear phase wedge.

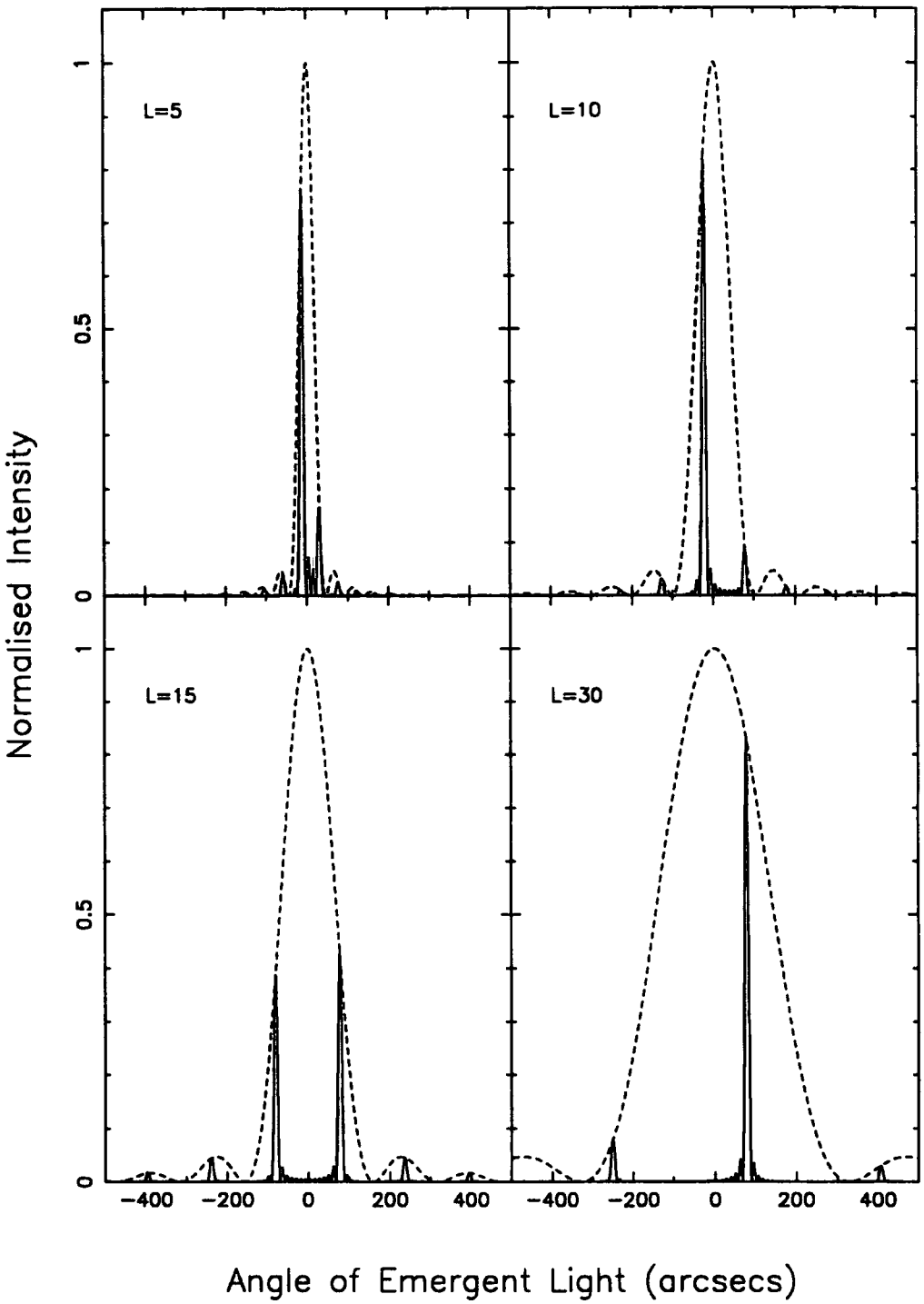

Figure 4.4: Simulated intensity distribution from a prism with a multi-electrode structure with L electrodes. Dashed line — envelope from diffraction pattern from a single electrode. Solid line — Simulated intensity distribution

4.3.2 A monolithic electrode prism

In order to calculate the intensity distribution from a prism with a single continuous electrode a similar calculation to the last section is made. As before consider a wave propagating at an arbitrary angle θ. The phase factor due to the wave being tilted (equation 4.8) remains the same, however the phase factor due to index variations along the cell is now a continuous function of x given by

$$\phi_x = \frac{2\pi}{\lambda}\frac{\Delta\mu t x}{W}. \tag{4.17}$$

Summing over the whole length of the cell gives

$$A = A_0 \int_0^W \exp\left[\frac{2\pi i x}{\lambda}\left(\sin\theta + \frac{\Delta\mu t}{W}\right)\right] dx. \tag{4.18}$$

This expression can be easily integrated and squared to give the intensity-

$$I = I_0 \mathrm{sinc}^2\left[\frac{\pi W}{\lambda}\left(\frac{\Delta\mu t}{W} + \sin\theta\right)\right]. \tag{4.19}$$

The result is the usual sinc function describing the intensity distribution from a rectangular aperture that has been shifted through the the required angle. The maximum propagation angle is given, as before, by equation 4.14.

The disadvantage of using a monolithic-electrode prism, as mentioned before, is that in order to form a linear phase wedge the full birefringence available cannot be used since LC birefringence is not linear with voltage. The advantages are its simplicity, both of construction and of electrical control, and the possibility of deflecting light in 2 directions.

It was decided that due to their simplicity that prisms with a single electrode structure should be investigated

4.3.3 Choice of Liquid Crystal Material

The small angle approximation of the deviation obtained by a LC prism is given by equation 4.15;

$$\theta = \frac{\Delta\mu t}{W}.$$

It can be seen that the angle of deviation is proportional to the birefringence so the liquid crystal chosen was BDH–E44 (Merck Chemicals[6]) on merit of its high birefringence of 0.26.

From the above it can be seen that the cell dimensions also affect the prismatic angle. For example a 10μm thick cell, 1cm in length gives a prism angle of 53″ when a birefringence of 0.26 is used. For maximum angle of deviation the prisms need to be as thick as possible and as short, in length, as possible. However, at first, prisms were made of a convenient size, governed by the physical properties of the available material. The cell length is discussed in more detail in chapter 6 and the cell thickness is discussed in chapter 7.

4.4 Liquid Crystal Cell Construction

The LC cells used to make the phase wedges were built by the author in the microelectronics clean room in the School of Engineering and Applied Science. The broad techniques of industrial cell construction were used along with fine details developed by the author. A clean room, as its name suggests, is a controlled working environment relatively free of air-born dust particles. The microelectronics clean room is a class 10000 clean room with a class 1000 inner room. The 'class' of a clean room refers to the number of air-borne particles in it. Thus a room of class 1000 has < 1000 particles ft^{-3} of size $\geq 0.5\mu$m. The clean room is entered via a lobby in which the user changes into protective clothing to try and minimize dust entering the room. The use of this clean room facilitated the use of suitable equipment and meant that optically flat cells could be made with minimal contamination. Table 4.4 shows the materials used in the construction of LC cells. The glasses used (purchased already coated in ITO) to make the cell need to be clean in order that the PVA layer will bond sufficiently. The glasses are first wiped to remove any large dust particles before they are brought into the clean room. They are then placed in a jig in the selectpure cleaner for 30 minutes in an ultrasonic bath. From this stage on the glasses are held with tweezers to prevent a coating layer of grease from the hands (even though gloves are worn). The glasses are rinsed in deionized water before a final bath in propan-2-ol. After being dried by a hot air blower, they are

[6]Merck Chemicals (formally BDH), Broom Road, Poole, Dorset, U.K.

Components	Auxiliary Materials
Indium-tin-oxide (ITO) coated glass[1] Polyvinyl alcohol (PVA)[2] Liquid Crystal[2] BDH-E44 +1% C15 Powdered spacers[4] Epoxy resin	Disposable syringes MOS selectpure[3] Paper tissues Capillary tubes Propan-2-ol De-ionized water Conductive paint[5]

1. EEV, Waterhouse Lane, Chelmsford, Essex CM1 2QU
2. Merck (formally BDH) Chemicals, Poole, Dorset BH12 4NN
3. Merck Chemicals, Darmstadt, Germany
4. Nippon Electric Glass, Osaka, Japan
5. RS Components Ltd, Corby, NN17 9RS

Table 4.4: Materials used in cell construction

ready for use.

The glasses are first coated with PVA to provide the surface to which the molecules will bond. A solution is made by dissolving the PVA crystals (5g in 800mls deionized water) over a hot plate. This takes several hours so the water level needs to be checked to avoid loss by evaporation. The PVA is applied by a spin coater, a device which rapidly spins a sample with a liquid to be coated so that a very thin surface layer is formed by centrifugal force. The glasses are held onto the spin coater by vacuum pressure so they are given a final check for any dust that could break the seal and then placed onto the coater with the ITO side facing up. It is very important to place the glasses centrally otherwise they spin off and smash. A few drops of the PVA solution are placed onto the glasses (any excess is simply spun off) and the device is run for 30s at 4000rpm. They can then be dried, again with the hot air blower. If optical quality glass is being used, in which case it is too heavy to be held by the spin coater, then they must be treated by simply dipping the glass in a solution of PVA and allowing to drain before drying. A lesser concentration of PVA solution (2g in 800mls water) is used since a thicker layer is

produced when the solution is allowed to drain instead of being spun.

If the glasses have been successfully coated they appear to be slightly coloured due to thin film interference. The micro-grooves in the cell can then be formed by rubbing the cell with a paper tissue in one direction with what is best described as 'firm pressure'. The direction of rubbing is noted for future reference. The glasses can then be assembled.

Assembly of the 2 glasses is carried out in a laminar flow cabinet. This is a workbench with clean air being blown across it which converts the cabinet into a class 100 working area. The glasses need to be separated by $\sim 10\mu$m. For this a suspension of powder spacers is made by mixing $\sim$ 250mg in $\sim$ 5mls of propanol. The spacers are short lengths ($\sim$ 0.1mm) of cylindrical fibres with a cross section of 10μm. The spacers settle out very quickly so the suspension must always be shaken before use. Strips of this are painted onto one of the glasses along two of the edges with a fine brush. The propanol is left to evaporate leaving the spacers lying on the glasses.

The second glass can then be placed on the first and held down with a small brass weight. Careful note of the orientation of the rubbing direction must be made. For example, if a twisted nematic cell is being built the second glass is placed so that its rubbing direction is 90° to the first, or for an anti-parallel cell the glass is placed such that the rubbing directions are anti-parallel.The glasses must also be placed so as to leave areas of ITO free in order to make electrical contacts. Figure 4.5 and figure 4.6 show the cell construction where the rubbing directions shown indicate an anti-parallel rubbed cell.

Two opposite sides are glued with a thin strip of epoxy resin applied with a syringe. If an optically flat cell was being made then ITO coated optical grade glass was used so that the inner surfaces of the cell were flat. However when assembling it is necessary to ensure each glass is parallel to the other to avoid making a wedge shaped LC layer. It is possible to see thin film interference fringes caused by the air gap with the cell viewed with just the clean rooms fluorescent strip lighting. Before the bonding glue dries the glasses are carefully manipulated, by hand, so as to extinguish these fringes, indicating a flat film. When the glue has dried the cell can be filled with liquid crystal.

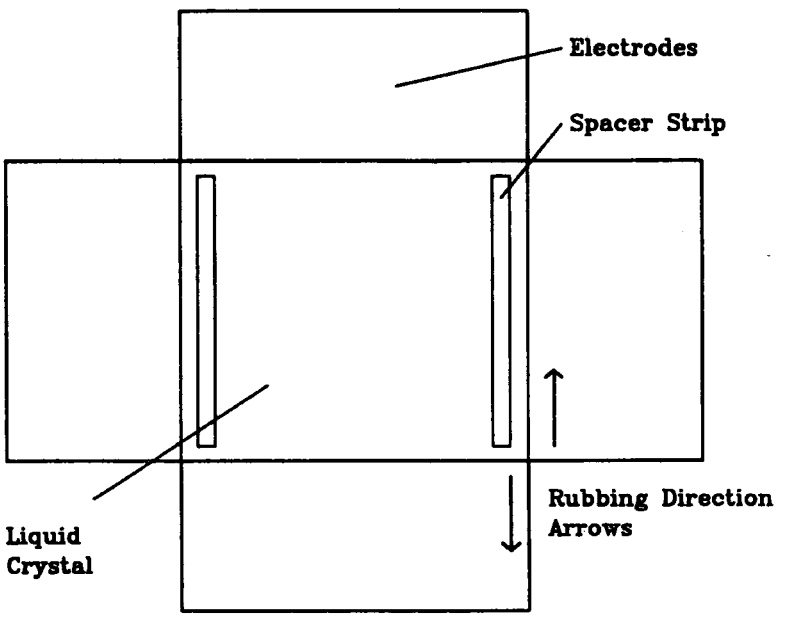

Figure 4.5: Construction of an anti-parallel nematic liquid crystal cell

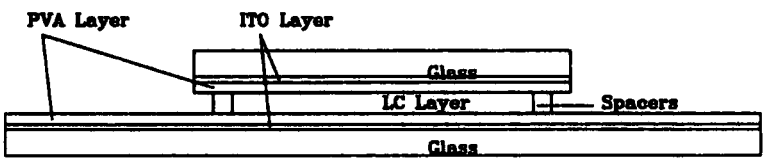

Figure 4.6: LC Cell Cross Section (not to scale)

The E44 is introduced via a capillary tube so that capillary action ensures that all the cell is filled. The rest of the gap can then be sealed in the same way as before with epoxy resin. Electrical contacts to the ITO are made by applying conductive paint to the free areas of glass and then soldering wires onto this paint. Some sources recommend that the cell should be heated to above the isotropic point (100°C) in order to promote correct molecular alignment, but it was found that this was not necessary. Indeed heating sometimes distorted the flatness of the cell.

Once the cells were finished, the first test was to check for correct molecular alignment. Simple eye inspection of the cell shows whether the LC layer appears milky (due to disclinations, see chapter 2) or if it is clear (good alignment). This test can be made more rigorous by placing the cell between crossed polaroids in laser light and rotating the cell. If the cell is well aligned then the light is extinguished completely when one of the crystal axes is parallel to one of the polaroid axes. Areas of disorder show up by patches of light transmitted by the second polaroid.

If the alignment is good and the connections have been made properly the cell is now ready for use. The next chapter describes how the cells were tested in greater detail.

Chapter 5

Preliminary Testing of Liquid Crystals

5.1 Introduction

Before the prismatic properties of a liquid crystal cell could be investigated, the fundamental parameters of the cells needed to be assessed. These are cell thickness and homogeneity, wavelength dispersion, voltage characteristics and optical quality.

5.2 Determination of Cell Thickness, Homogeneity,Dispersion and Voltage Characteristics from Edser-Butler fringes

The measurement of thickness, optical flatness, and refractive indices is well documented in the literature. Thin film thicknesses can be measured using a variety of interferometric techniques, for example Pohl interferometry (KINZER [37]). Refractive indices are measured by the the manufacturers (Merck Chemicals) using Abbé refractometry and optical flatness can be assessed very easily by observing the straightness of wedge fringes obtained by viewing the cell in laser light. However for this particular purpose each alternative method has some disadvantage, so a new technique was developed using Edser-Butler fringes which allows 3 measurements to be made. These are fringes of equal chromatic order, first used to calibrate spectrometers (EDSER AND BUTLER [23]). They provide a convenient way of measuring

LC cell thickness and wavelength dispersion, and give an extremely accurate result for the cell homogeneity. The fringes can also be used to determine the voltage characteristics of a LC cell across the visible spectrum. The following sub-sections give an account of how the fringes are formed, and how results are obtained.

5.2.1 Experimental

Fig. 5.1 shows the experimental apparatus. A pinhole is illuminated by a white

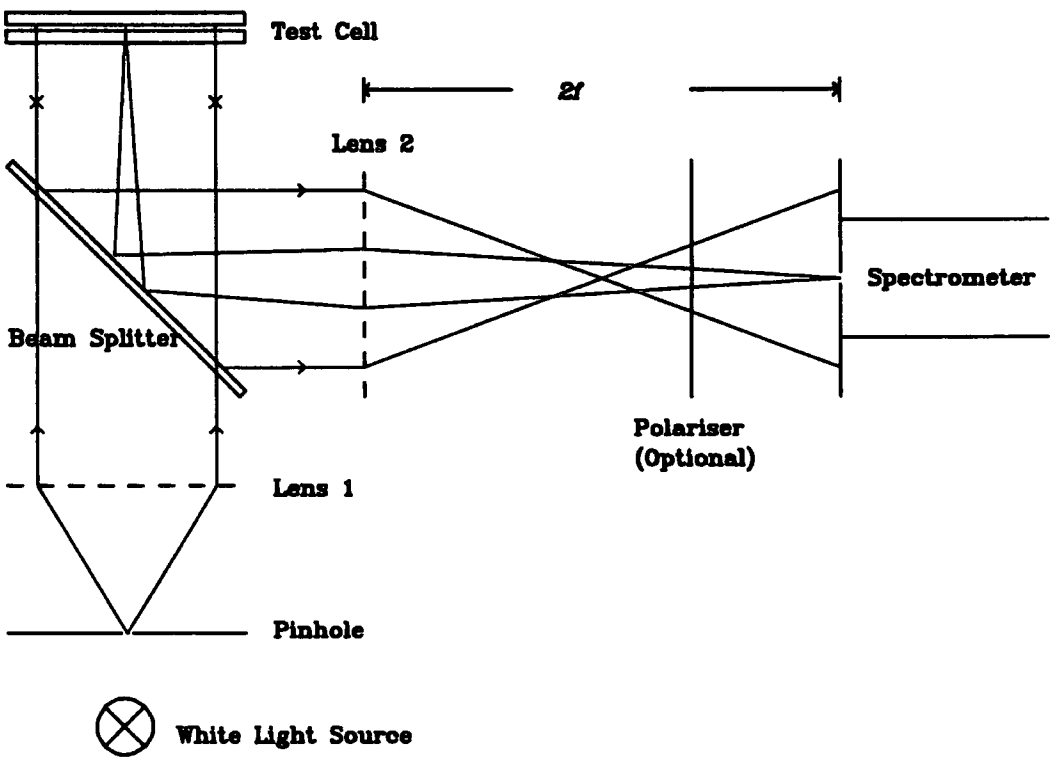

FIG 1. Experimental Apparatus

Figure 5.1: Experimental Apparatus for observing Edser-Butler fringes

light source and the light from this pinhole is then collimated by lens 1 in order to illuminate the test cell with a parallel beam. Lens 2 is arranged so that there is unit magnification between the test cell and the spectrometer slit, hence an area on the test cell the size of the slit is being imaged on the spectrometer. This means that the detailed structure of a test cell may be investigated, by traversing the cell across the imaged slit.

Reflection of white light occurs from the inner front and back surfaces of the

liquid crystal giving two, and more, interfering beams governed by the interference equation $2\mu t \cos\theta = n\lambda$ (for a refractive index μ, thickness t, wavelength λ, and angle of incidence θ). In the case of fig. 5.1, θ $(= 0)$ and t are constant. Consequently whenever a wavelength in the white light spectrum satisfies the equation then extinction by destructive interference occurs. The observed effect in the spectroscope is a familiar white light spectrum crossed by a series of dark vertical bands, the spacing of which is inversely proportional to the cell thickness. It can be shown that the intensity of these fringes is given by :

$$I \sim \sin^2\left(\frac{2\pi\mu t}{\lambda}\right) \tag{5.1}$$

Fig. 5.2 shows an example using a grating spectrometer where the refractive medium is the ordinary index of mica. Since the fringes are equally spaced in terms of wavenumber, $1/\lambda$, then in a grating spectrometer, they are more widely spaced towards the red end of the spectrum. There will also exist fringe patterns corresponding to the reflection from the outer surfaces of the test cell, however these patterns are too closely spaced to be seen.

5.2.2 A Birefringent Cell

If the cell is constructed with a birefringent filling, e.g. liquid crystal, then two fringe patterns are formed corresponding to each optical thickness, $\mu_o t$ and $\mu_e t$. When polarised light is used, such that its direction is parallel to either the ordinary or the extraordinary axis then one set of fringes is observed. If the polariser is rotated through 90° then the orthogonal fringe pattern can be seen with a different spacing.

An interesting effect is observed when the polaroid axis is not parallel to either crystal axis (or if the polariser is removed). Both fringe patterns occur simultaneously and 'beats' are seen, that is a modulation of the fringes having a relatively long periodicity. Fig. 5.3 shows an example of fringes produced by liquid crystal E44 taken with a prism spectrograph. In fig. 5.3a. the polaroid axis is parallel to the extraordinary axis. In fig. 5.3b. the polariser has been rotated through 90° hence fringes produced by the ordinary crystal axis are being observed. The fringe spacing is now broader since $\mu_o < \mu_e$ which corresponds to a lesser optical thickness. In fig. 5.3c. the polaroid axis is at 45° to both crystal axes. This is phenomenolog-

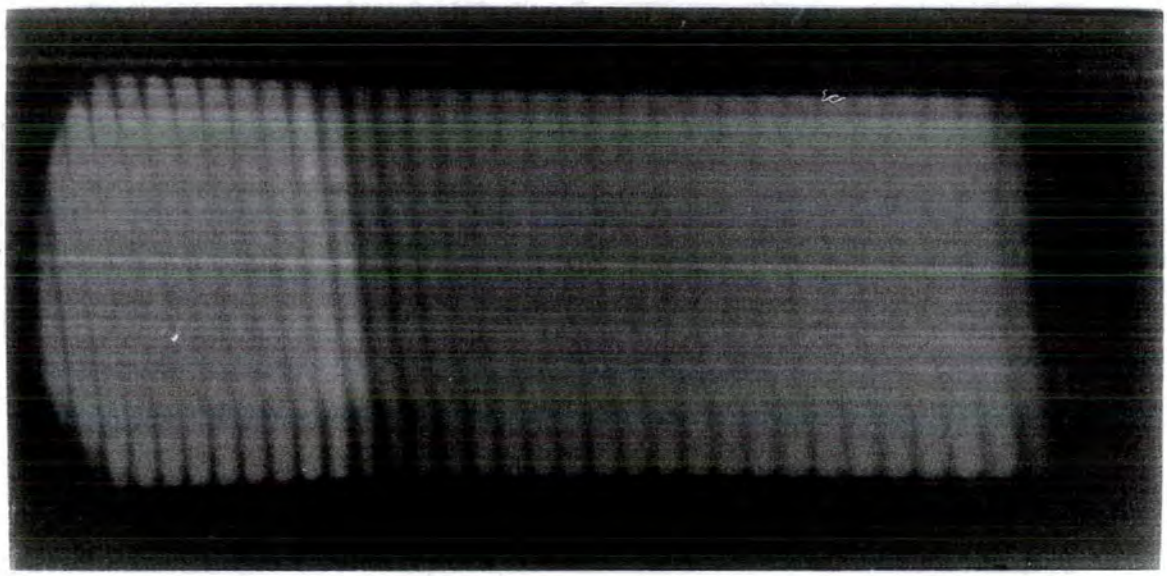

Figure 5.2: Edser-Butler fringes observed using a mica film

ically the same as removing the polariser and hence both sets of fringes are seen but in modulation. The fringes are curved because the liquid crystal film thickness is not constant. (See section 5.2.3. for more details). It should be noted that the photograph was taken with a UV spectrograph so the spectra extend into the ultra-violet.

It can be shown that the intensity of the modulated fringes is given by:

$$I \propto 1 - \cos\left[\frac{4\pi t}{\lambda} \cdot \left(\frac{\mu_e + \mu_o}{2}\right)\right] \cos\left[\frac{4\pi t}{\lambda} \cdot \left(\frac{\mu_e - \mu_o}{2}\right)\right] \qquad (5.2)$$

The first cosine term,determined by the average of the refractive indices, describes the general structure of the fringes; the second term, determined by the birefringence, $\mu_e - \mu_o$, describes the modulation of the fringes. In an isotropic sample where μ_e and μ_o are identical, the second factor reduces to unity and no modulation is seen. When an A.C. voltage is applied across the liquid crystal cell so that the birefringence decreases, then the periodic length of the modulation is seen to increase.

5.2.3 Examination of Optical Flatness

As described in section 5.2.1, the test cell is imaged onto the spectrometer slit so that the magnification is unity (by arranging both the object and image distances to be twice the focal length, f). The variations in the observed fringes, along their individual lengths, then represent changes in optical thickness along the area of the cell being imaged. For example, in fig. 5.3c. the ends of the fringes are curved in the direction of the red end of the spectrum. This implies that the cell was also bowed in a similar, but not so exaggerated, way as the fringes. The total variation in the fringe positions is about 3 fringe widths (where the fringe spacing is about 10nm), therefore the change in optical thickness due to the bowing is about 30nm. By turning the test cell through 90°, or by traversing the cell across the imaged slit, the optical flatness in the other direction can be investigated.

The fine detail of the fringes yields information about the small scale structure of the cell. Again referring to fig. 5.3c., one can see variations in the fringes of the order of a tenth of a fringe width. This implies changes in optical thickness of 1nm. When the cell glasses are coated to a high reflectance (as in the next section) to

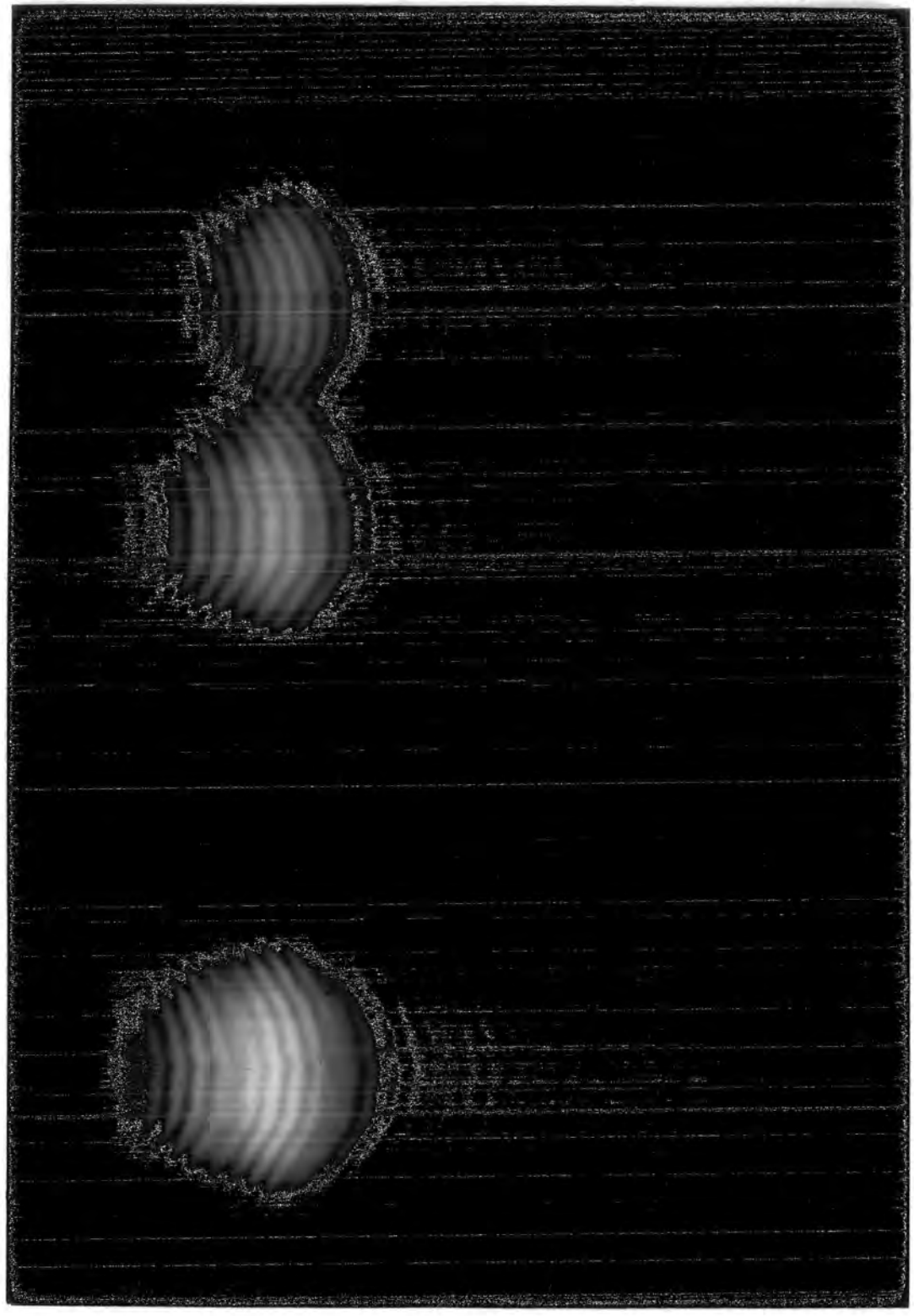

Figure 5.3: Edser-Butler fringes observed using a birefringent film

make the fringes sharper, then changes in fringe positions as small as 0.1nm can be detected. The technique is therefore very sensitive to variations of optical thickness.

5.2.4 Determination of the Optical Thickness of a Non-Dispersive Film

The determination of the average optical thickness of a non-dispersive thin film only requires counting the number of fringes, m, within an angular spread. It can readily be shown that the optical thickness of the cell is given by:

$$\mu t = \frac{m\lambda_1\lambda_2}{2(\lambda_1 - \lambda_2)} \tag{5.3}$$

where, λ_1 and λ_2 specify the wavelength range (determined by the spectrometer) corresponding to the angular spread. For a typical cell thickness of 10 μm, the fringes are about 10 nm apart and m is ~ 20 across the visible spectrum. For example, the thickness of an air filled cell of 15 μm nominal thickness was measured, where 23 fringes could be seen over an wavelength range of 447.8 nm to 663.0 nm. Using equation 5.3, the optical thickness was determined to be $(15.87 \pm 0.01)\,\mu$m.

5.2.5 Experimental Determination of the Dispersion and Liquid Crystal Thickness of a film such as BDH–E44

When the cell is filled with a dispersive medium, the method above has to be modified to take dispersion into account. Consider two fringes which are m fringes apart. Then

$$2\mu_1 t = n\lambda_1 \tag{5.4}$$

and

$$2\mu_2 t = (n+m)\lambda_2 \tag{5.5}$$

where n is the fringe order and μ_1 and μ_2 are the refractive indices at wavelengths λ_1 and λ_2 respectively. Combining these equations to eliminate n gives

$$2t(\mu_2\lambda_1 - \mu_1\lambda_2) = m\lambda_1\lambda_2 \tag{5.6}$$

Now the spacing of adjacent fringes (m=1) is determined by the dispersion; from precise measurements of these spacings, the dispersion in approximately 10 nm

intervals should be available. However the accuracy is limited since the fringes are broad and close together. A large improvement can be made by coating the glasses from which the test cell is constructed in aluminium to a reflection coefficient of $\sim$ 90% to produce a multi-reflection device similar to a Fabry-Perot etalon. The fringes become much sharper and correspondingly easier to locate. In this case the contrast of the fringes is much greater if the apparatus is set up in transmission mode, where the test cell is placed between lens 1 and lens 2. Measurements are also made easier by using a fine grating (2400 lines mm^{-}1).

Interferometric techniques always display optical thickness, therefore to separate the thickness from the refractive index the results need to be 'normalised' to a known value of refractive index at a standard wavelength. Even then, because of the complexity of equation 5.6, the separation of index and thickness has to be made in a model dependent way, as described in the next section.

A test cell with aluminium coated surfaces was filled with liquid crystal BDH-E44; the molecules were aligned with a layer of rubbed PVA. When viewed in the spectrometer, Edser-Butler fringes corresponding to both polarisations were seen and each set was selected independently using the polariser. Careful measurements of the fringe positions were made, from which the fringe wavelengths were determined.

As described in section 5.2.3, the fringe positions are very sensitive to changes in optical thickness; atmospheric pressure and temperature variations alter the physical thickness of the cell, by the order of a few nanometres. These very small thickness changes do not appreciably affect the fringe spacing, from which the results are obtained; however they do affect the absolute fringe positions. Measurements between adjacent fringes were therefore made using an eyepiece micrometer so that the fringe spacings were obtained simultaneously, before any movements could affect the results.

For both the extraordinary and ordinary fringes, the pair of fringes straddling the position of the sodium D lines were identified. At the D line (589.6 nm) the manufacturer's values of μ_e and μ_o are known precisely (μ_e=1.7904 and μ_o=1.5277). These indices are used to normalise the data.

Knowing these wavelengths and the corresponding indices it is possible to find both the dispersion and the thickness of the E44 cell as described in the next sections.

Initial Approximate Method of Data Reduction

The assumption is made that μ_1 and μ_2 can be replaced by an average μ over the m fringes in the interval $\Delta\lambda$. Hence equation (5.6) reduces to

$$2\mu t = \frac{m\lambda_1\lambda_2}{\lambda_1 - \lambda_2} = \frac{m\lambda_1\lambda_2}{\Delta\lambda} \tag{5.7}$$

where $\Delta\lambda = \lambda_1 - \lambda_2$. At a standard wavelength, λ_s, where the index, μ_s, is known precisely from manufacturer's measurements, the fringes on either side of λ_s will give (m=1)

$$2\mu_s t = \frac{\lambda_s^2}{\Delta\lambda_s}. \tag{5.8}$$

Here the assumption $\lambda_1\lambda_2 = \lambda^2$ (where $\lambda = \frac{1}{2}(\lambda_1 + \lambda_2)$) has been made. This is acceptable for adjacent fringes $\sim$ 10 nm apart. Combining the two equations to eliminate t gives

$$\mu = \mu_s \frac{\Delta\lambda_s}{\Delta\lambda} \frac{m\lambda_1\lambda_2}{\lambda_s^2}. \tag{5.9}$$

This value is defined as the apparent index, μ_{app}. This is the quantity initially calculated from the data. However the approximation that μ is constant over a 10 nm interval, whilst seemingly valid, can affect the values of μ and t. Consequently these values of thickness and refractive index need to be corrected using a more precise procedure as explained in the next section.

Model Dependent Corrections to the Approximate Method

In equation (5.6) above, μ_1 and μ_2 are replaced by $\mu_1 = \mu - \delta$ and $\mu_2 = \mu + \delta$ where $\mu = \frac{1}{2}(\mu_1 + \mu_2)$ is the index at a wavelength, Λ, between λ_1 and λ_2 and $2\delta = \mu_2 - \mu_1$ To find Λ assume μ is given by a simple Cauchy formula

$$\mu = A + B/\Lambda^2, \tag{5.10}$$

therefore

$$\frac{1}{2}(A + B/\lambda_1^2 + A + B/\lambda_2^2) = A + B/\Lambda^2. \tag{5.11}$$

Then

$$\Lambda = \sqrt{\frac{2\lambda_1^2\lambda_2^2}{\lambda_1^2+\lambda_2^2}} \tag{5.12}$$

is the wavelength corresponding to the refractive index, μ.

When μ_1 and μ_2 are replaced in equation (5.6)

$$2t[\mu(\lambda_1-\lambda_2)+\delta(\lambda_1+\lambda_2)] = m\lambda_1\lambda_2 \tag{5.13}$$

or

$$2t(\mu\Delta\lambda+2\lambda\delta) = m\lambda_1\lambda_2 \tag{5.14}$$

and similarly, at the normalisation wavelength

$$2t(\mu_s\Delta\lambda_s+2\lambda_s\delta_s) = \lambda_s^2, \tag{5.15}$$

Eliminating t between equation (5.14) and (5.15) gives

$$(\mu\Delta\lambda+2\delta\lambda)\lambda_s^2 = (\mu_s\Delta\lambda_s+2\delta_s\lambda_s)m\lambda_1\lambda_2 \tag{5.16}$$

from which

$$\mu = \mu_s\frac{\Delta\lambda_s}{\Delta\lambda}\frac{m\lambda_1\lambda_2}{\lambda_s^2}+\frac{2\delta_s m\lambda_1\lambda_2}{\lambda_s\Delta\lambda}-\frac{2\delta\lambda}{\Delta\lambda} \tag{5.17}$$

$$= \mu_{app}+\frac{2\delta_s m\lambda_1\lambda_2}{\lambda_s\Delta\lambda}+\lambda\left(\frac{\partial\mu}{\partial\lambda}\right)_\Gamma \tag{5.18}$$

where

$$\frac{2\delta}{\Delta\lambda} = -\left(\frac{\partial\mu}{\partial\lambda}\right)_\Gamma \tag{5.19}$$

at some wavelength, Γ, in between λ_1 and λ_2. From the simple Cauchy expression above

$$-\left(\frac{\partial\mu}{\partial\lambda}\right)_\Gamma = \frac{\mu_2-\mu_1}{\lambda_1-\lambda_2} = \frac{2B}{\Gamma^3} \tag{5.20}$$

and

$$\Gamma = \sqrt[3]{\frac{2\lambda_1^2\lambda_2^2}{\lambda_1+\lambda_2}} \tag{5.21}$$

hence

$$\mu = \mu_{app}+\lambda\left(\frac{\partial\mu}{\partial\lambda}\right)_\Gamma-\frac{\Delta\lambda_s}{\Delta\lambda}\left(\frac{\partial\mu}{\partial\lambda}\right)_{\lambda_s}\frac{m\lambda_1\lambda_2}{\lambda_s}. \tag{5.22}$$

It is not possible to obtain a suitable analytic expression for $\frac{\Delta\lambda_s}{\Delta\lambda}$. However the numerical value of this quantity, ξ, is known directly from the measurements of the fringe spacing at λ and λ_s. Therefore

$$\mu = \mu_{app}+\lambda\left(\frac{\partial\mu}{\partial\lambda}\right)_\Gamma-\xi\left(\frac{\partial\mu}{\partial\lambda}\right)_{\lambda_s}\frac{m\lambda_1\lambda_2}{\lambda_s}. \tag{5.23}$$

Defining $h_\lambda = \mu_{app} - \mu_s$ and using the Cauchy expression in equation (5.23)

$$h_\lambda = A + \frac{B}{\Lambda^2} - A - \frac{B}{\lambda_s^2} + \frac{2\lambda B}{\Gamma^3} + \xi\left(\frac{-2B}{\lambda_s^3}\right)\frac{m\lambda_1\lambda_2}{\lambda_s} \tag{5.24}$$

and hence

$$B = h_\lambda\left(\frac{1}{\Lambda^2} - \frac{1}{\lambda_s^2} + \frac{2\lambda}{\Gamma^3} - \frac{2\xi m\lambda_1\lambda_2}{\lambda_s^4}\right)^{-1} \tag{5.25}$$

where all the quantities in (5.25) are measured directly or easily calculated from the measurements. Then with

$$\mu = A + \frac{B}{\Lambda^2} \text{ and } \mu_s = A + \frac{B}{\lambda_s^2} \tag{5.26}$$

the corrected value of the measured index is

$$\mu = \mu_s + B\left(\frac{1}{\Lambda^2} - \frac{1}{\lambda_s^2}\right). \tag{5.27}$$

Data Reduction Method for Adjacent Fringes

When adjacent fringes are measured, (m=1), then λ,Λ, and Γ can be replaced by λ and and $\lambda_1\lambda_2$ by λ^2 (where $\lambda = \frac{1}{2}(\lambda_1 + \lambda_2)$). Then equation (5.25) reduces to

$$B = h_\lambda\left(\frac{3}{\lambda^2} - \frac{1}{\lambda_s^2} - \frac{2\xi\lambda^2}{\lambda_s^4}\right)^{-1} \tag{5.28}$$

and equation (5.27) becomes

$$\mu = \mu_s + B\left(\frac{1}{\lambda^2} - \frac{1}{\lambda_s^2}\right). \tag{5.29}$$

Determination of thickness

Once the dispersion curve is known for a material then the thickness of other cells may easily be measured. As in section 5.2.4, the angular spread of a number of fringes is measured. The indices, μ_1 and μ_2 are determined from the dispersion curve at wavelengths λ_1 and λ_2, respectively. Using equation 5.6 gives

$$t = \frac{m\lambda_1\lambda_2}{2(\mu_2\lambda_1 - \mu_1\lambda_2)} \tag{5.30}$$

For example, the extraordinary fringes of a 10 μm nominal thickness liquid crystal cell were measured. 22 fringes could be seen over a wavelength range of 643.5nm to

478.1nm. Using the results from the previous section, these wavelengths correspond to indices of 1.771 and 1.861 respectively. Using equation (5.30) gives $t = (9.65 \pm 0.02)\,\mu$m.

5.2.6 Results for BDH–E44

The wavelengths of the Edser-Butler fringes for a liquid crystal filled with BDH–E44 were measured for both extraordinary and ordinary indices. The two Edser-Butler fringes straddling the sodium D lines were identified and their wavelengths measured. From the manufacturer's value of either μ_e or μ_o at this wavelength,the apparent indices between other adjacent fringes were found from equation (5.9). These apparent indices were then corrected in the model dependent way described above; calculating $\lambda, \Gamma, \Lambda, B$ and h_λ en route and

$$\mu = \mu_s + B\left(\frac{1}{\Lambda^2} - \frac{1}{\lambda_s^2}\right) \tag{5.31}$$

was found for each fringe pair.

Fig. 5.4 shows three dispersion curves of liquid crystal BDH–E44 after the data has been corrected as described above These corrections are small, the maximum being 7%. Curve (a) shows the extraordinary index, curve (b) shows the ordinary index, and curve (c) represents the extraordinary index when a voltage of 1.5 V is applied across the cell. It is important to note here that this voltage is a square wave. The liquid crystal responds slightly more to a similar RMS sine wave. This voltage partially rotates the molecules of the liquid crystal and reduces the extraordinary index. The solid lines represent the fit of the points to a Cauchy curve and the error bars show one standard deviation. The crosses show the points where the data were normalised.

Although the values of index are shown plotted at discrete wavelengths, they are actually an average index of the wavelength range in between the points. This means that there are no hidden anomalies, such as a very sharp resonance peak due to molecular absorption.

The curve for μ_e (V=1.5V) required an index for normalisation; this was measured for sodium light by placing the cell in one arm of a Jamin interferometer as described in section. 6.2.1.

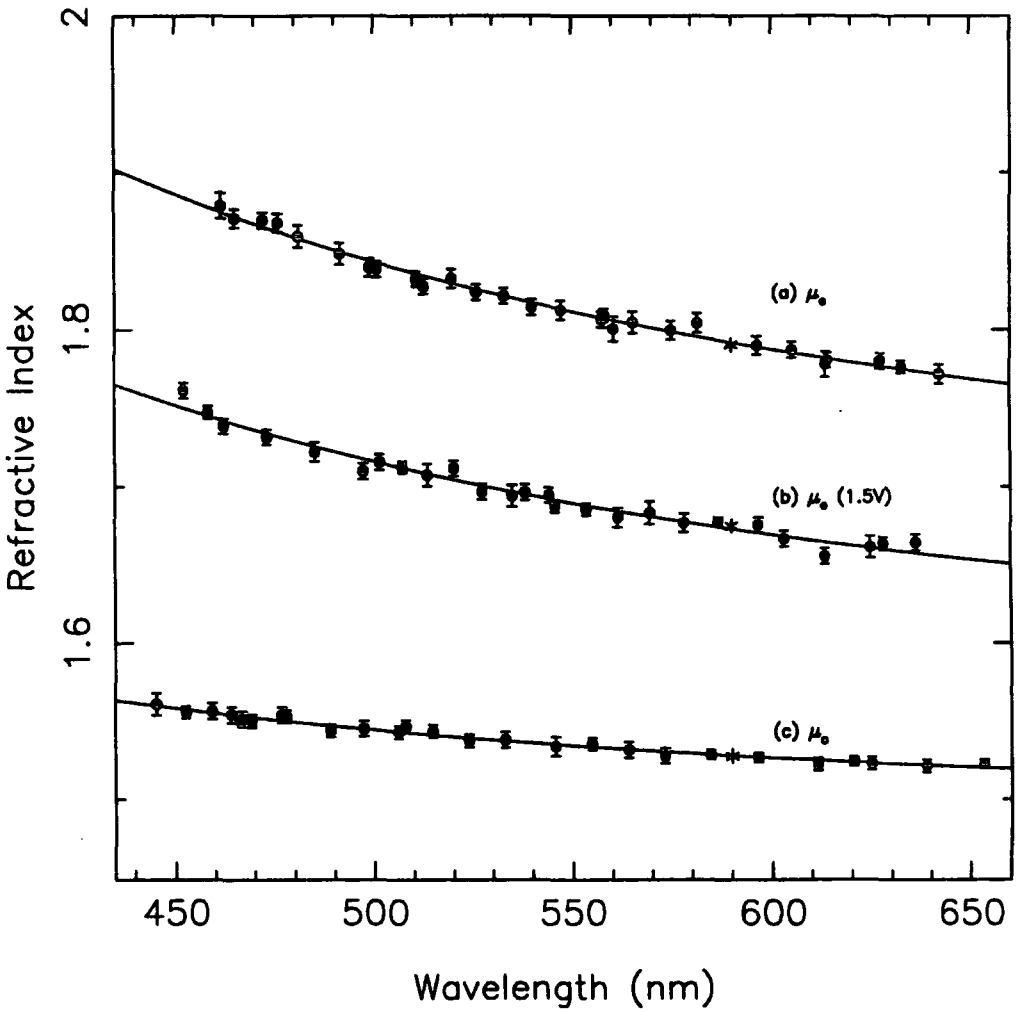

Figure 5.4: Indices of LC E44 as determined from the Edser-Butler technique

For a particular sample, once it has been demonstrated that a simple Cauchy curve is sufficient to characterise the dispersion, then other curves may be obtained in a simple fashion. Figure 5.4 shows three dispersion curves for the liquid crystal. The intermediate curves for μ_e for other applied voltages may be found by using an aluminium coated cell and by measuring only the fringe positions at each end of the spectrum and the two normalisation fringes, and by knowing a normalisation index. Using the data reduction method described in section 5.2.5 gives a value for B using equation (5.25) which is all that is needed to determine the whole dispersion curve. For example 24 ordinary index fringes were measured over a range of 477.4nm to 637.8nm. The fringes straddling the sodium D line were also measured, and together these gave $\mu_{app} = 1.549$. This gave a value for B of $1.5 \times 10^3 \text{nm}^2$, which is also the result obtained by averaging the individual values of B used in the data reduction to obtain each individual point as explained in section 5.2.5.

A birefringence dispersion curve may be plotted by subtracting the μ_e (V=0) and μ_o curves. This is shown in Fig 5.5 The cross shows the normalisation value and the vertical line shows a typical error bar. This curve is in good agreement with results taken by alternative methods (WILLIAMS et al. [63]).

Critique

The main analysis above is model dependent and based on the assumption that the dispersion of index is given by a simple Cauchy curve. Simulations have been carried out which justify this approach. Obviously if the dispersion curve were of a more complicated shape then higher power terms would be needed. As a final check on the validity of the method, some simulated values of μ_{app} were obtained from the final dispersion curve. These values compared well with the measured data for μ_{app}.

5.2.7 Determination of Voltage Characteristics.

When an electric field is applied across a LC cell the Edser-Butler fringes formed from the extraordinary thickness move towards the blue end of the spectrum as the refractive index decreases. By measuring the fringe shift then the change in

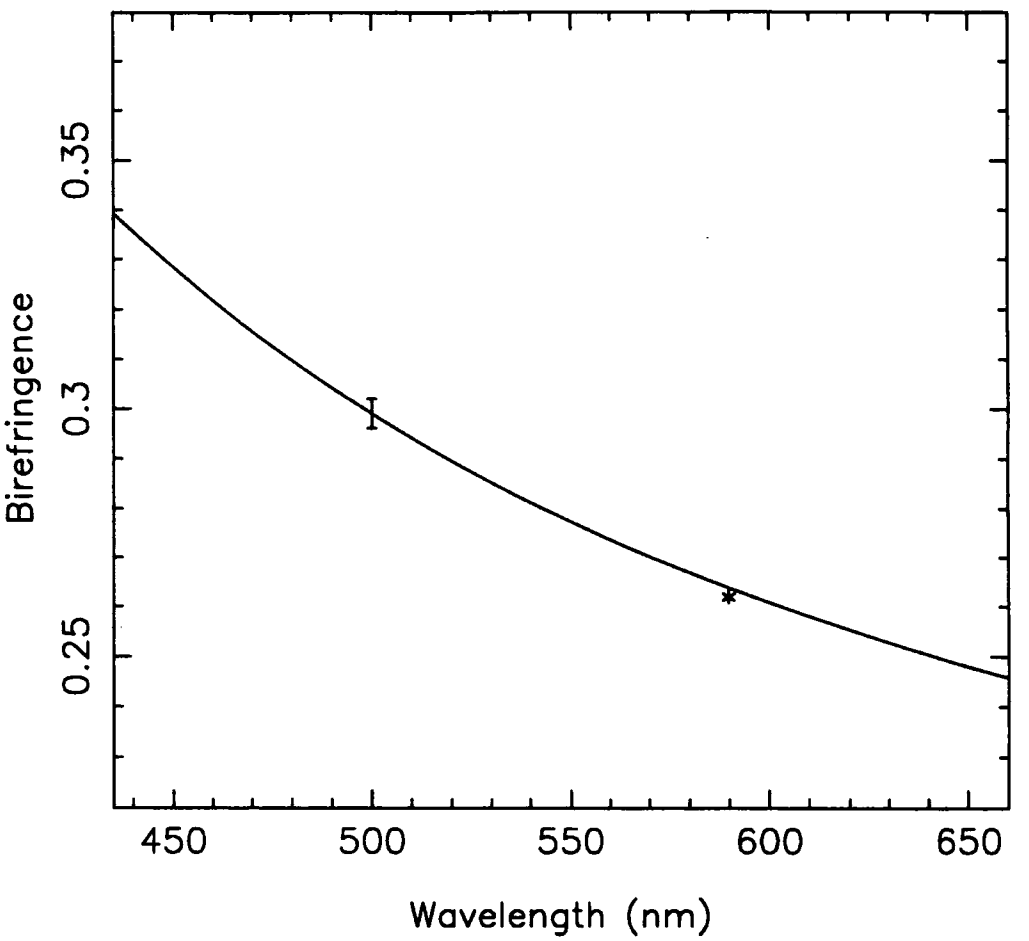

Figure 5.5: Birefringence of LC E44 as determined from the Edser-Butler technique

refractive index may be calculated from the equation

$$2\Delta\mu_e t = m\lambda. \tag{5.32}$$

where m is the fringe shift and $\Delta\mu_e$ is the change in refractive index[1]. The spectrometer's telescope crosswire is positioned on a fringe (from which the wavelength can be determined) and then the voltage across the cell is increased until the adjacent fringe moves to the same position. The voltage is recorded and then increased again to position a third fringe on the crosswire. For a nominal LC thickness of 10μm, then about ten fringe shifts occur. The whole procedure can then be repeated for another fringe, and hence another wavelength. The method is extremely quick, since the actual fringe positions are not required for the results. The results are shown in figure 5.6. The field used was an AC sine wave. The points are joined by a quadratic least squares fit formula. Figure 5.7 shows the same results plotted on a single graph. It can be seen that the curves are nearly identical for low voltages, and that wavelength dispersion is very small below about 2V. The errors on the curves are very good for low voltages, but the errors increase rapidly above about 3V due to the birefringence becoming less sensitive to the applied field. Hence individual results are only really useful below 3V although the general trend of dispersion increasing at higher voltages can be seen. The accuracy of the points corresponding to higher voltages could be increased by using a cell made with silvered glasses, as in section 5.2.5, to sharpen the fringes.

By taking the results from each individual curve, then a fit may be made of $\Delta\mu$ versus λ for various values of voltage. The results are shown in figure 5.8. Each curve shows the wavelength dispersion for equally spaced values ($\sim$ 0.05V) of the applied voltage. By combining the results of $\Delta\mu$ versus both V and λ a $\Delta\mu(V,\lambda)$ plane may be drawn, as shown in figure 5.9.

The physical principle used behind the results in this section, i.e. that of counting interference fringe shifts, is very common. It is effectively the same technique described in section 6.2.1 using the Jamin interferometer. However using Edser-Butler fringes has two advantages over other techniques. Firstly the fringes are produced

[1]It is important here to distinguish between 'birefringence' and '$\Delta\mu_e$'. Birefringence is at a maximum when no there is no applied field and it decreases until the cell becomes isotropic at saturation voltage. $\Delta\mu_e$ is zero at zero applied field and increases as the voltage is increased up to a maximum. The two quantities are therefore just different ways of describing the same physical property

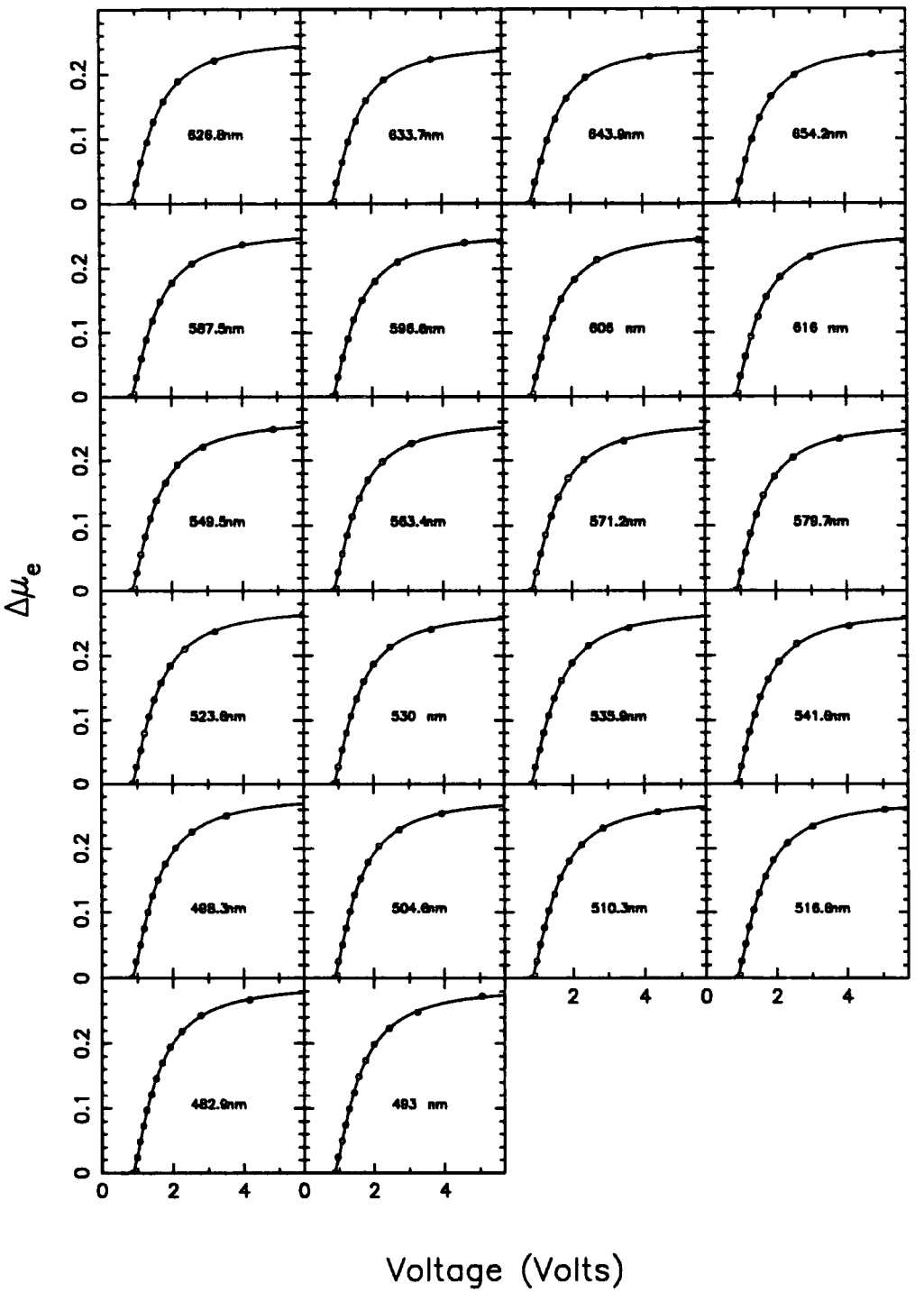

Figure 5.6: Voltage (AC sine wave) characteristics of E44 for different wavelengths

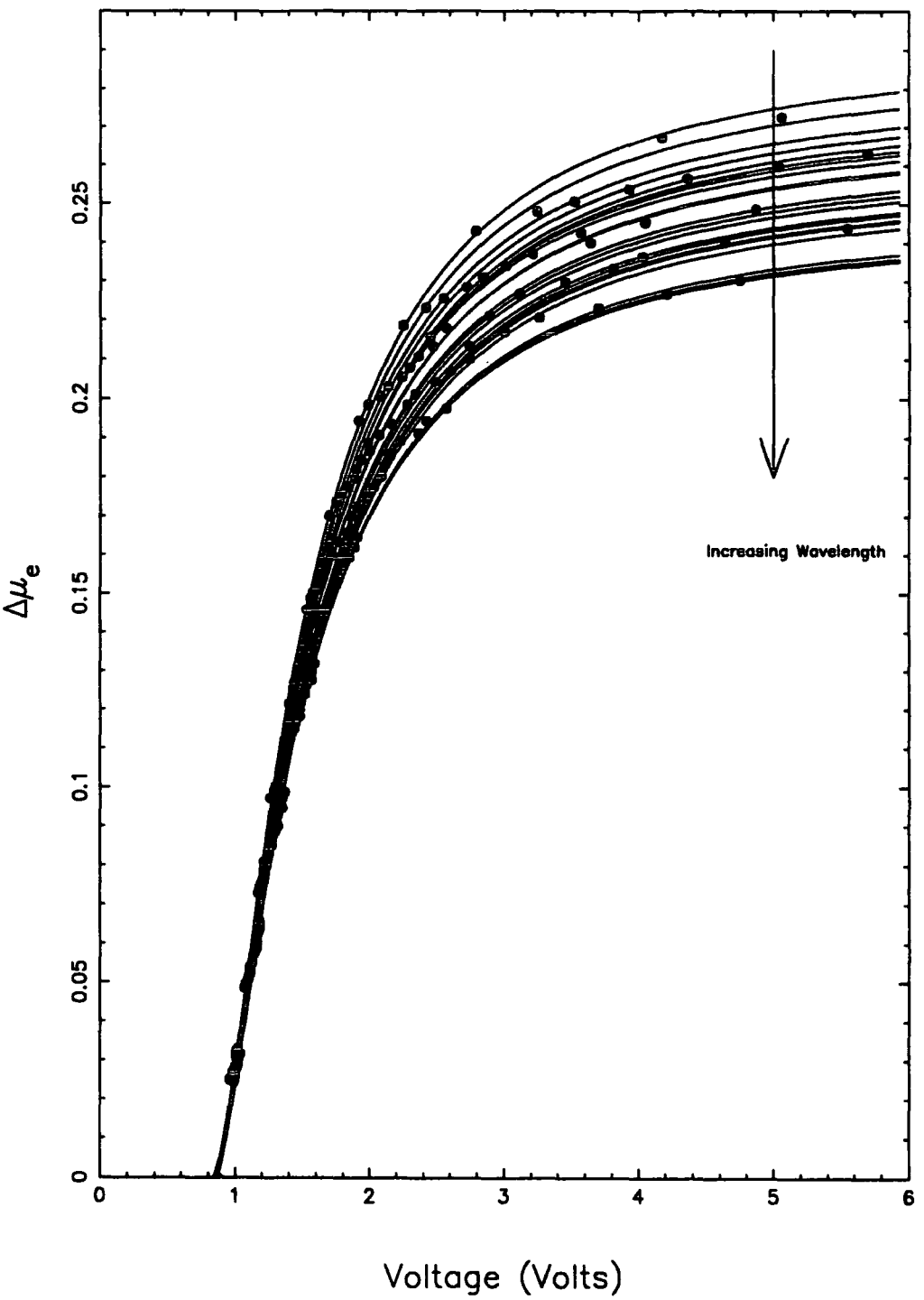

Figure 5.7: Voltage characteristics of E44 for different wavelengths

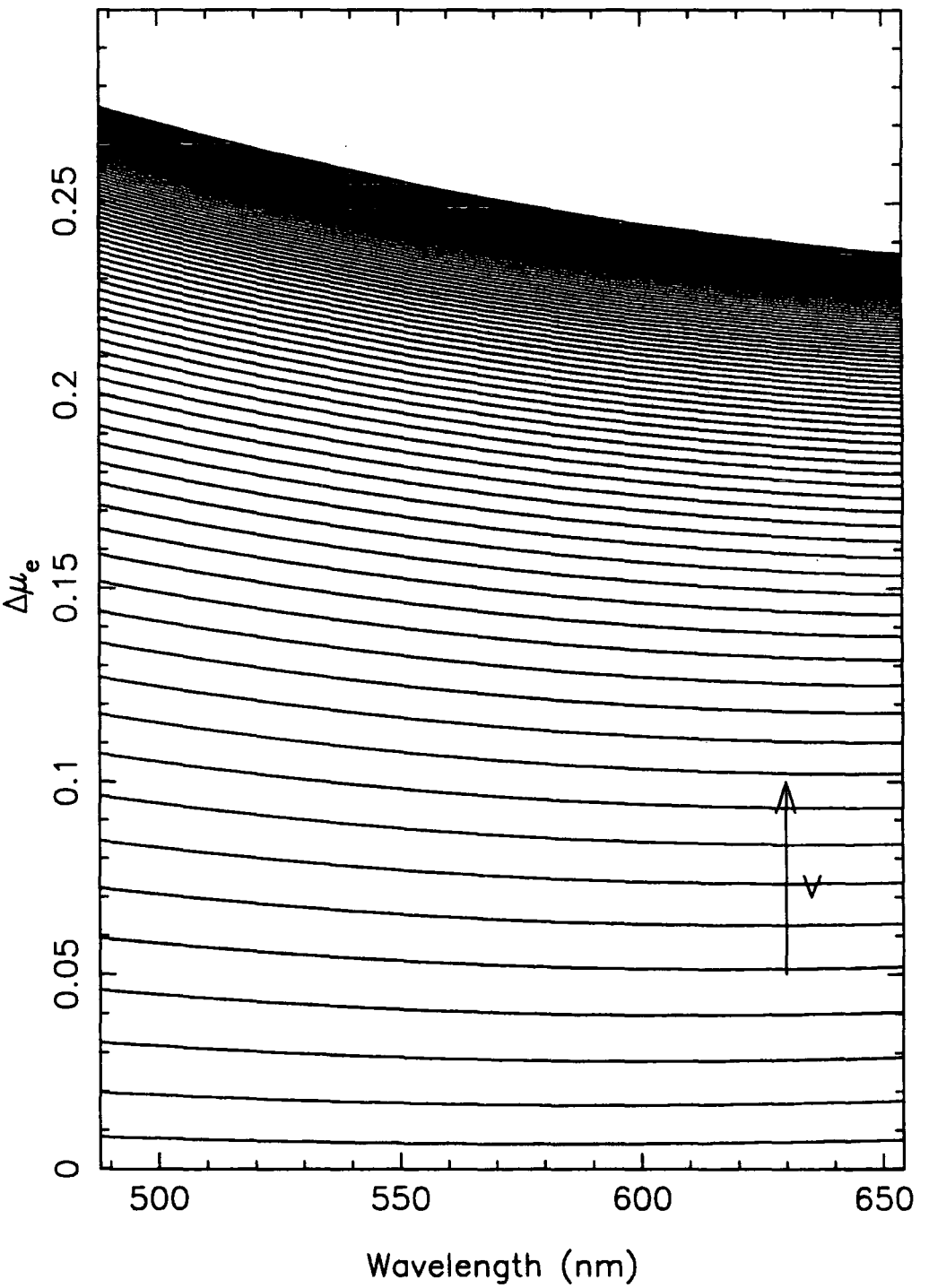

Figure 5.8: Birefringence dispersion of E44 for different voltages

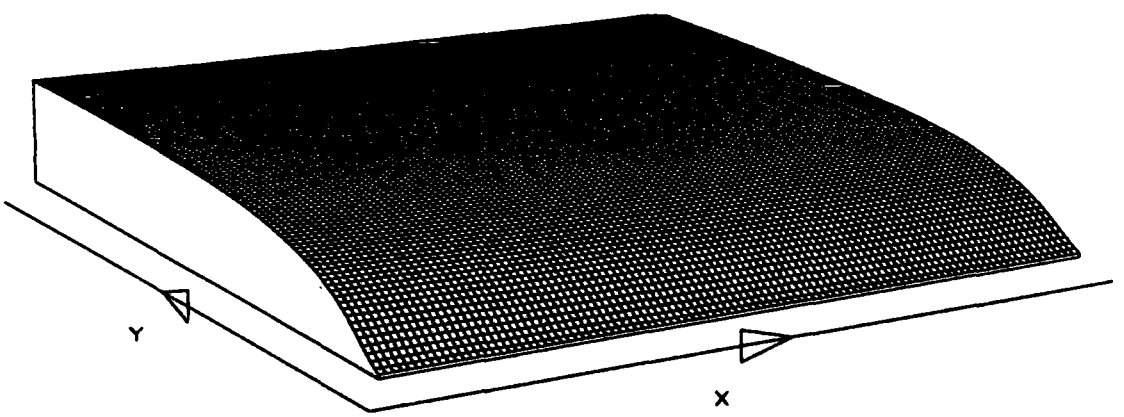

Figure 5.9: Birefringence as a function of both wavelength and voltage for E44. X-axis shows wavelength and Y-axis shows voltage

by a double passage of the light through the cell meaning that twice as many fringe shifts are observed for a given phase shift, and more importantly, there is a fringe for many different wavelengths throughout the spectrum (at approximately 10nm intervals) so a whole series of results can be taken by using a simple white light source and normal laboratory equipment. Over a period of time the fringe positions shift due to very small thickness changes in the cell so if the results are repeated a virtually continuous series of results can be built up.

The previous sections have described how Edser-Butler fringes can be used to measure cell thickness, flatness, and dispersion of both index and electric field response. The next chapter describes how the sensitivity of the technique may be fully exploited in measuring the prismatic properties of LC cells.

5.2.8 The Effect of Dispersion on Image Quality

How does the dispersion introduced by the liquid crystal affect the quality of a telescope image? There are two dispersion effects to consider. The first is the dispersion of refractive index and the second is the dispersion of *change of* refractive index (or birefringence). Figure 5.4 shows the dispersion of refractive index. It can be seen that the μ_e curve has a stronger wavelength dependence than the μ_o curve. However in this application, where a very thin film is being used, this variation in refraction will have a negligible effect on the light and it is the dispersion of the change of refractive index that is of importance. The angle of deflection of a LC prism is given by equation 4.15 as

$$\theta = \frac{\Delta\mu t}{W}$$

where W is the cell length. Any variation in birefringence over the spectrum is the directly related to the angle of deflection. It can be seen that the full birefringence varies from 0.34 at 450nm to 0.25 at 650nm[2]. Therefore, a 10μm by 1cm cell designed to deviate light by 58 arcseconds (i.e. the maximum possible) at 550nm, will deflect it through 70 arcseconds at 450nm and 52 arcseconds at 650nm. After taking into account the magnification of the telescope this would give a blurring in the image of

[2]These figures are taken from figure 5.8 because this shows the *usable* index variation. From figure 5.5 both the birefringence and the dispersion appears to be greater. This is because figure 5.5 is a direct measure of $\mu_e - \mu_o$ whereas figure 5.8 is a measure of $\mu_e(V = 0) - \mu_e(V \sim 5)$ so the liquid crystal was not full saturated.

about 0.23 arcseconds, which is a considerable fraction of the uncorrected image size ($\sim$ 1 arcsecond). However this value is very much an upper-bound on the amount of dispersion and in practice will be much less for a number of reasons. Consider figure 5.7. If the applied voltage is below 2V (see section 6) then the dispersion over the spectrum (483-654nm) is about 0.02 which corresponds to a blurring of only 0.06 arcseconds in the final image. From section 4.2.1 it can be seen that the average angle of required deviation is around 10 arcseconds which requires a birefringence of 0.05 where the dispersion is very small. Secondly the vast majority of astronomy involves the use of filters (e.g. UBV etc.) which limits the wavelength range and therefore reduces the dispersion (or cuts it out totally in the case of, for example, an OIII filter). So, although dispersion is a potential problem that cannot be totally ignored, its effect will be small. The third reason is that the sharpened results from a device a recorded on a CCD (see chapter 3) which is red sensitive, i.e. the part of the spectrum where the LC dispersion curve is flatter (figure 5.8).

5.3 Optical Quality

Light intensity is of paramount importance when observing faint stellar objects so if liquid crystals are to be used in astronomical devices then the amount of light absorbed and scattered in a LC cell must not be too high. This is especially important considering that any actual device would probably be made with two liquid crystal layers in order to correct for each polarisation state. There are two parameters to be measured; what fraction of incident light on a cell is transmitted and what fraction of that transmitted light is scattered? Another way of asking this second question is how much information in an object is transmitted to the image? A useful way of quantifying this is to measure the modulation transfer function (MTF).

In order to measure both the transmission and the MTF a CCD (charge coupled device) was used.

Index	Transmission
μ_e (V=0)	71.0 ± 0.8%
μ_e (V=6)	72.3 ± 0.8%
μ_0	72.4 ± 0.8%

Table 5.1: Transmission of LC-E44 cell at 550nm (FWHM 14nm)

5.3.1 Transmission

In order to measure the total amount of light transmitted through a liquid crystal then a number of CCD frames were taken, with and without a liquid crystal cell in place, and the two light intensities were then divided to determine the transmission. The CCD was cooled (by liquid nitrogen) in order that the signal was not noise dominated. The exposure times and shutter mechanism are controlled by a PC onto which each frame is displayed. The result is a 2 dimensional array of numbers corresponding to each pixel element intensity. A white light source was used with a broadband monochromator and a diffuser to give a uniform light distribution. Light was allowed to fall, unfocussed, onto the aperture of the CCD. The total light intensity was found by integrating all the individual pixel values. The CCD has a dark current (noise) and there is a very low level of spurious light in the laboratory which was accounted for by taking a *bias frame* and subtracting it from the signal before integration.

The transmission was measured for the extraordinary index with no applied voltage (μ_e (V=0)), the extraordinary index with 6.0V applied (μ_e (V=6)), and for the ordinary index (μ_o). Each index was selected with the polariser. The results are shown in table. 5.1. As can be seen, the transmission is about 70%. A LC cell is a multi-layer device so the majority of the loss in transmitted light will occur because of reflections between layers of different refractive index. There appears to be a small difference in the transmission between the extraordinary axis with no applied voltage and the other two measurements, and whilst it is difficult to be conclusive because of the large errors compared to the small effect, this could be because of changes in reflective coefficients.

Any LC device built for an actual instrument would be commercially made, and therefore of higher quality than laboratory made cells. The device could also be improved by applying anti-reflection coatings to the glasses, which is indeed already implemented in commercial devices. For example A.G. Electro-Optics[3] produce a 'Liquid Crystal Variable Retarder' (a simple liquid crystal cell) which is anti-reflection coated and has a transmission of $> 92\%$ (400nm to 700nm).

To conclude, a well constructed device will have a good transmission properties, however they are not as perfect as a mirror based device with near 100% reflection. This is discussed in greater detail in chapter 8.

5.3.2 Modulation Transfer Function

The spatial amplitude distribution of an image is known as the point spread function (PSF). The fourier transform of the PSF for on-axis imaging systems is the modulation transfer function. It is a measure of the modulation or contrast of features which exist in the image at various spatial frequencies. The MTF has become a widely used method of specifying the optical performance of a variety of systems, for example telescopes, the atmosphere, the eye, photographic film, and CCDs.

To illustrate the physical meaning of MTF consider that the input to an imaging system has a sinusoidal intensity distribution in the object plane with a spatial frequency of ω cycles/mm. Then the object modulation is defined as (see fig. 5.10)

$$M_o(\omega) = \frac{I_a - I_b}{I_a + I_b}. \tag{5.33}$$

After passing through the imaging system, the image modulation becomes

$$M_i(\omega) = \frac{I'_a - I'_b}{I'_a + I'_b}. \tag{5.34}$$

The ratio between the image modulation and object modulation is then the MTF at spatial frequency ω,

$$\mathrm{MTF}(\omega) = \frac{M_i(\omega)}{M_o(\omega)}. \tag{5.35}$$

The structure of a general object is expressed as a spectrum of spatial frequencies for each of which an MTF(ω) exists. These comprise the complete MTF for the

[3]Meadowlark Optics, c/o A.G. Electro-Optics, Tarporley, Cheshire, CW6 0HX

system. There is a maximum spatial frequency, ω_c, that can be transmitted by any optical element, often referred to as the diffraction limit. In an unabberated system this is related to the aperture of the system. It is given by

$$\omega_c = \frac{D}{2.063 \times 10^5 \lambda} \text{ cycles/arcsec} \tag{5.36}$$

where D is the diameter of the aperture and 2.063×10^5 is the conversion factor between radians and arcseconds. In terms of linear spatial frequencies, τ, it is given by

$$\tau_c = \frac{D}{f\lambda} \text{ cycles/mm.} \tag{5.37}$$

where f is the focal length of the system in mms. These equations can be obtained directly from Abbé theory (see e.g. STEWARD [54]).

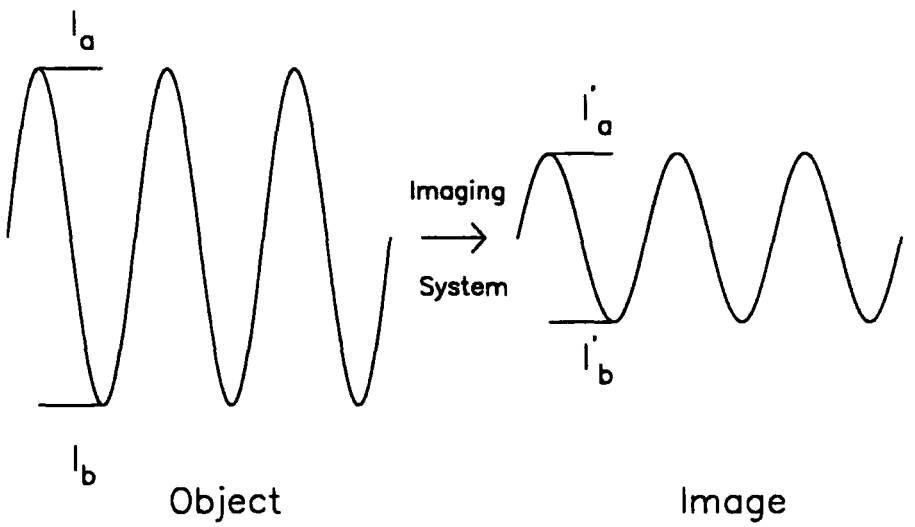

Figure 5.10: Harmonic object and resulting image

The MTF is therefore a useful method of quantifying the image quality, or how much information in the object is transmitted to the image. Each element in an optical system will have an individual MTF, the MTF of the whole system is product of the individual MTF's. Thus, in a telescope system, the MTF is given by the product of the MTF's of the atmosphere, the telescope optics, the liquid crystal, and the recording device (CCD or photographic plate). Here it is the MTF of the liquid crystal that is being measured, so first the MTF of the optical system used

to make that measurement is tested, and then the same system with liquid crystal. The liquid crystal MTF is then given by the quotient of the two.

MTF of the Telescope System

The question arises as to what is the maximum spatial frequency that the liquid crystal must be able to transmit. The MTF was measured up to the maximum spatial frequency that can be transmitted by a typical sub-aperture in the MARTINI device since all higher spatial frequencies will be lost. A typical sub-aperture size is 60cm. This value indicates the equivalent aperture size at the layer of atmospheric turbulence ($\sim$ 3.6km above ground). The actual aperture is at the conjugate focus and is therefore demagnified by the WHT optics (demagnification factor 77) to 7.8mm as shown in figure 5.11. The angular cut-off spatial frequency, given by equation 5.36 will be different depending on whether one considers the real aperture at the conjugate focus, or the equivalent aperture size at the turbulent layer. This apparent problem is solved by considering the Abbé theory of image formation whereby the image is made up of a series of fourier frequencies, the smallest periodicity of which is the linear cut-off spatial frequency. The focal distance of each aperture from the focal point also scales in the same way as the aperture diameters, therefore, although the larger aperture has a greater resolving power than the smaller aperture, it is further from the focal point and so needs to resolve smaller angles. Thus it is the linear spatial frequency that is of interest here. Using equation 5.37 the maximum spatial frequency transmitted by a 60cm WHT aperture at 550nm (effective focal length is 46.2m) is 24 cycles/mm. Any detail in an object of higher spatial frequency will not be transmitted by the telescope, therefore a liquid crystal device must be capable of good transmission of spatial frequencies up to this limit.

Experimental Determination of MTF

There are two main methods to experimentally determine the MTF. The first is by interferometric techniques, generally by using a shear interferometer whereby the light passing through an imaging system is amplitude-split and then recombined with a shift between the two beams. The MTF can be calculated by analysing

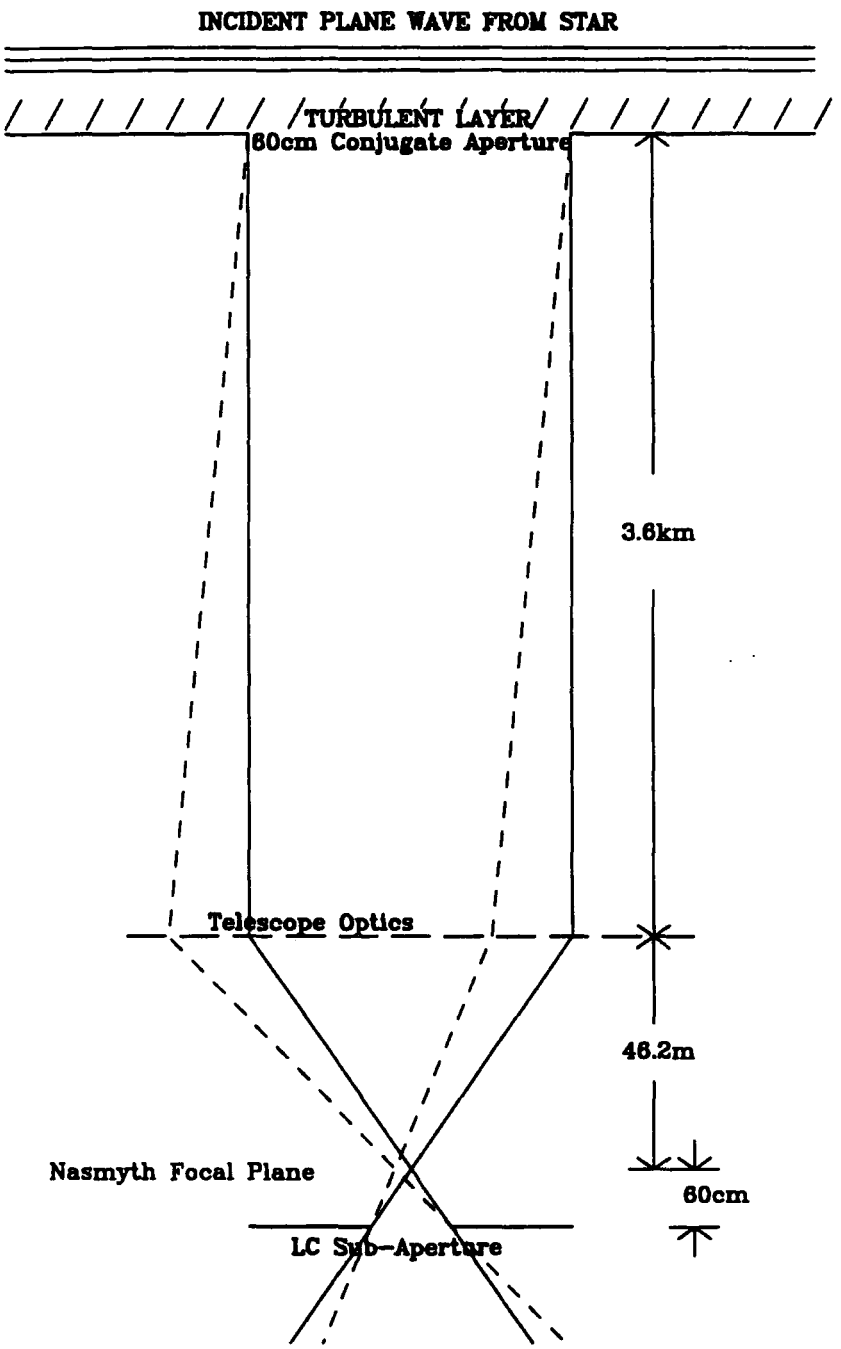

Figure 5.11: Telescope Effective Optics. The telescope is shown as a single focussing element. The ray paths show how two incident plane waves, one at normal incidence and the other tilted (greatly exaggerated), are focussed pass through the LC correcting element (no correction shown in this case).

the phase differences between the two beams, shown up in the quality of interference fringes obtained (e.g. DUNLOP [20]). The second technique is to measure the modulation in the image obtained from a grating-like test target having decreasing line separations (increasing spatial frequencies). The latter was chosen because of its ease and because it provides a clear physical demonstration of the modulation transfer function. Figure 5.12 shows the experimental apparatus used.

A diffuse quasi-monochromatic light source is incident onto the test card. This is focussed onto the CCD via a collimator of two lenses, then the addition or removal of the LC cell does not change the focussing of the test card on the CCD.

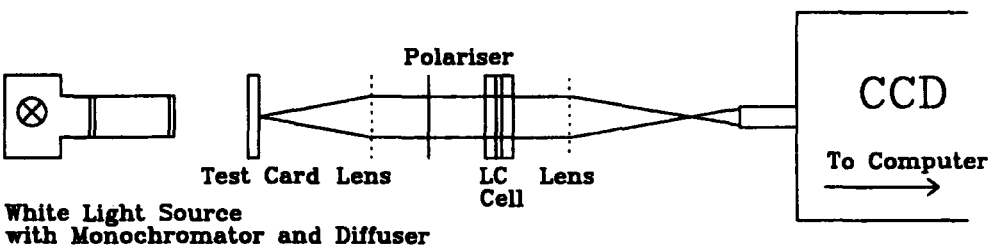

Figure 5.12: Experimental apparatus used to determine the LC MTF

CCD frames were taken both with and without the LC cell in place using light of wavelength 550nm. The polariser selected different polarisation states so that any differences between light polarised along the two crystal axes could be studied.

The CCD frames were manipulated on the Durham Node of the Starlink Vax Computer using *Figaro* software. First of all the bias frame was subtracted from all the images. Then they were *flat-fielded* by dividing the subsequent frames by an image taken without the test card in place. This corrects the intensity data for the inhomogeneities in the light distribution from the lamp and also from any variation in sensitivity across the CCD chip. The images could then be transferred to a simple 2-dimensional matrix of intensities that could then be analysed by a fortran programme.

Figure 5.13 shows a contour plot of the test card pattern taken with the LC cell in place. Notice how the large resolution elements are distinct, whereas the

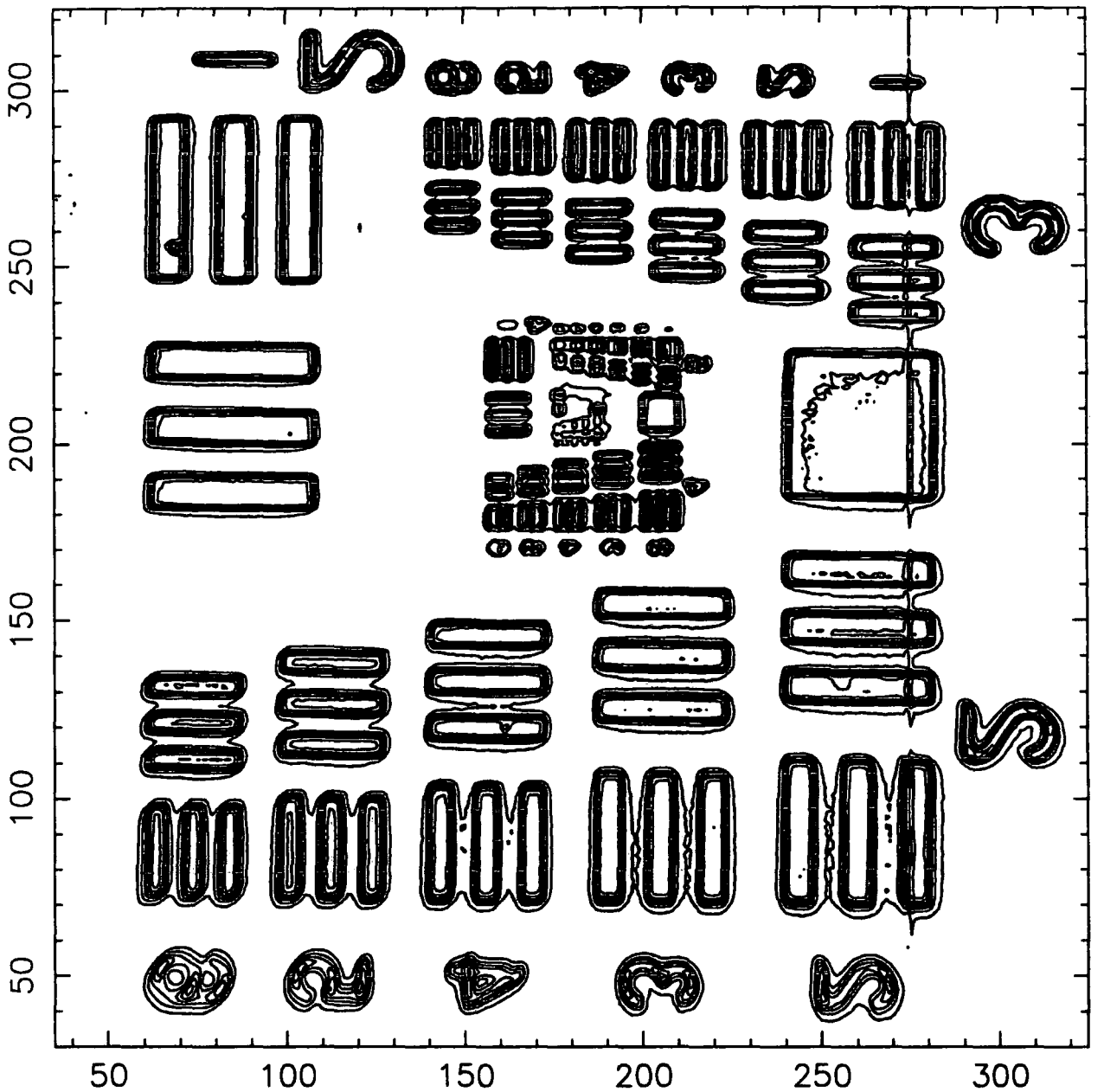

Figure 5.13: Contour Plot of Test Card Pattern. The numbers on the axes correspond to pixels

finer elements become less distinct until eventually the smallest are unresolvable. By looking at the numbers each element can be identified and the spatial frequency (lines per mm) determined.

Figure 5.14 shows an intensity cross section through the frame showing how the modulation of the approximately sinusoidal intensity distribution starts to decrease as the spatial frequency increases. The modulation can be calculated using equation 5.34 for each spatial frequency. The maximum and minimum intensities are found by scanning through the data. Occasionally spurious points are included but each frame contains a large amount of data so these are averaged out.

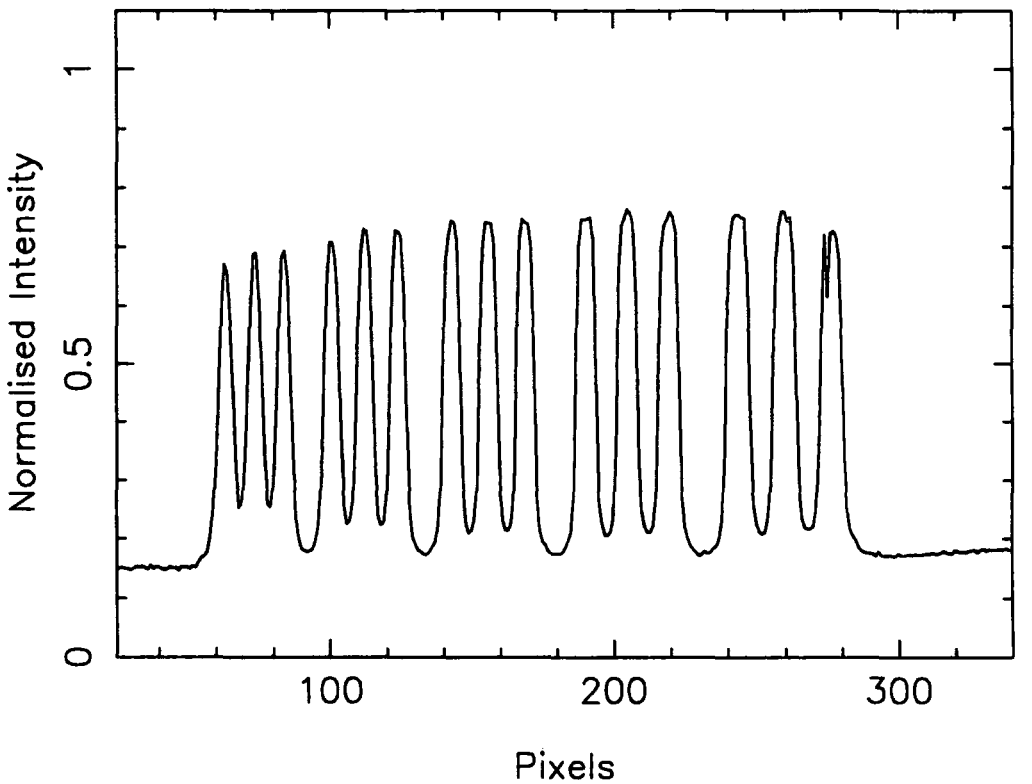

Figure 5.14: Slice through CCD frame Y=86

Figure 5.15 shows two diagrams of the modulation obtained in this way, with and without the LC cell in place. The general trend can be seen that as the spatial frequency is increased the modulation decreases. However there are some anomalies whereby the modulation sometimes increases. Consider figure (b) whereby the modulation increases for the first few points, and there seems to be a discontinuity at around 9 lines/mm. However here it is the modulation of the lenses and CCD that is being tested. The test card has a size comparable to the lens so that the full

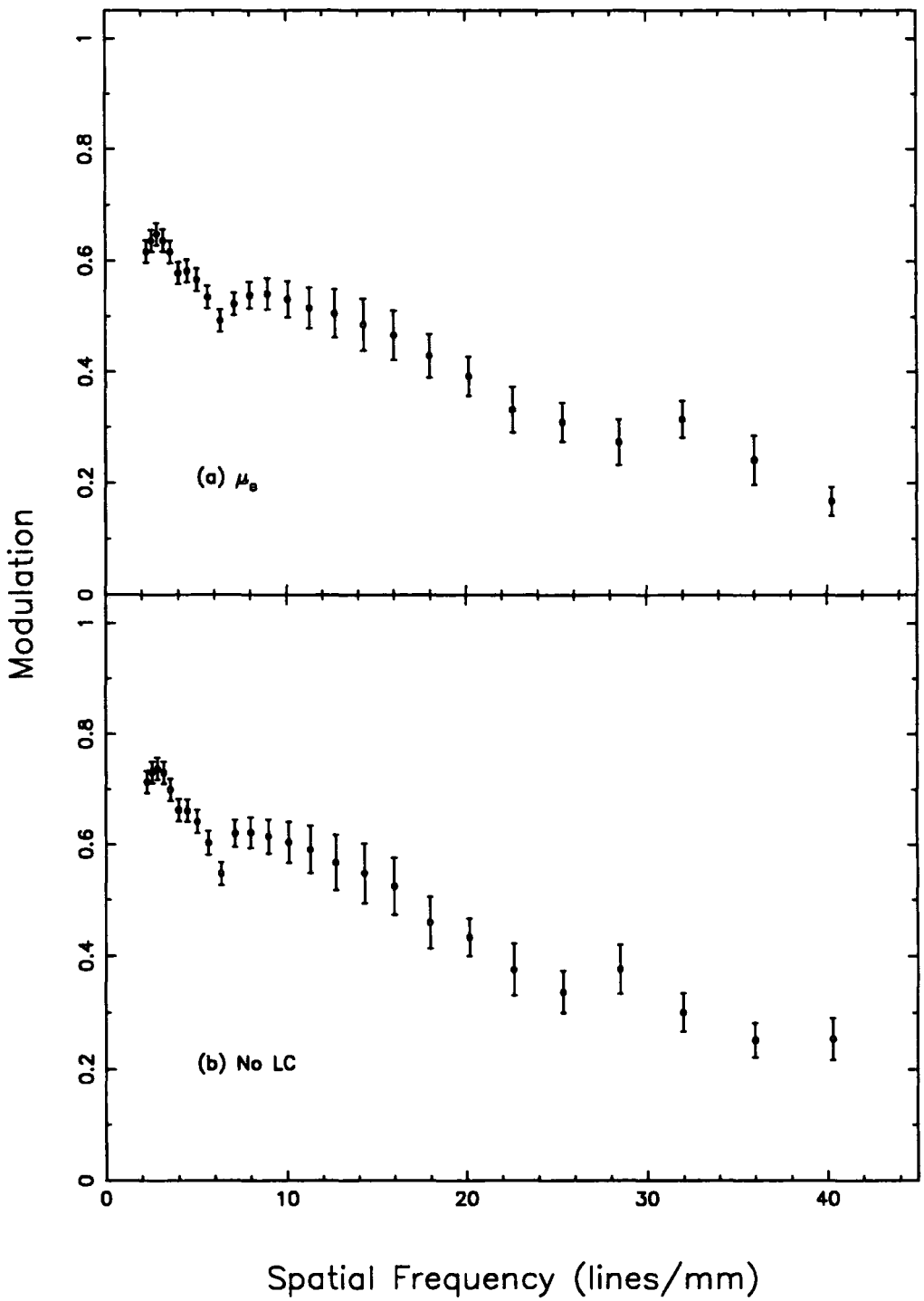

Figure 5.15: Modulation (a) with the LC cell in place (μ_e axis) and (b) without the LC cell.

aperture of the lens is being used, and different resolution elements will image in different ways through the lens giving a difference in modulation. The spatial frequencies where a sudden jump occurs correspond to a large shift in where adjacent resolution elements are situated on the test card. As can be seen in figure (a) the shape remains the same when the LC cell is inserted into the apparatus indicating the anomalies are not an artifact of the LC cell.

In order to calculate the modulation transfer function of the LC cell the modulation calculated with the cell in place is divided by that calculated with only the lenses, i.e *diagram (a)* $\div$ *diagram (b)*. The MTF should be normalised to the value at zero spatial frequency, but since this was not available the MTF at the lowest spatial frequency was used. The highest spatial frequency that this experiment can test for is not governed by the LC cell, or the lenses, but by the size of the CCD pixels. These are 17μm in size so obviously any detail smaller than this cannot be resolved. This can be improved by changing the two lenses so that the image of the test card pattern on the CCD is magnified. Thus the final data is presented from two sets of results, one measuring the lower spatial frequencies, and the second measuring the higher spatial frequencies. The spatial frequencies also need to be re-scaled because the first lens in figure 5.12 has a different f/number[4] to the WHT.

Figure 5.16 shows the results for four different cell configurations obtained by rotating the polaroid and by applying different voltages. Figures 5.16a and 5.16b show the MTF calculated with the light polarised parallel to the μ_e axis and μ_o axis respectively. Figures 5.16c and 5.16d again show the MTF calculated with the light polarised along the μ_e axis, but with an applied voltage of 6V and a applied voltage ramp (prism switched on) respectively. The vertical dotted line shows the cut-off frequency of the WHT with a 60cm sub-aperture. It can be seen that all four graphs are consistent with an MTF of unity up to the cut-off frequency. This indicates that the cell is of good optical quality and light is not been distorted or scattered. The MTF measured in this way is made up of two components, firstly the MTF of the glass used to make the cell, and secondly the sandwiched material, i.e. the PVA, the ITO, and the actual liquid crystal. It is to be expected that the glass exhibits good characteristics because it is optical quality grade, but this experiment shows that the other cell components do not degrade the light quality.

[4] f/6.5 as compared with f/11

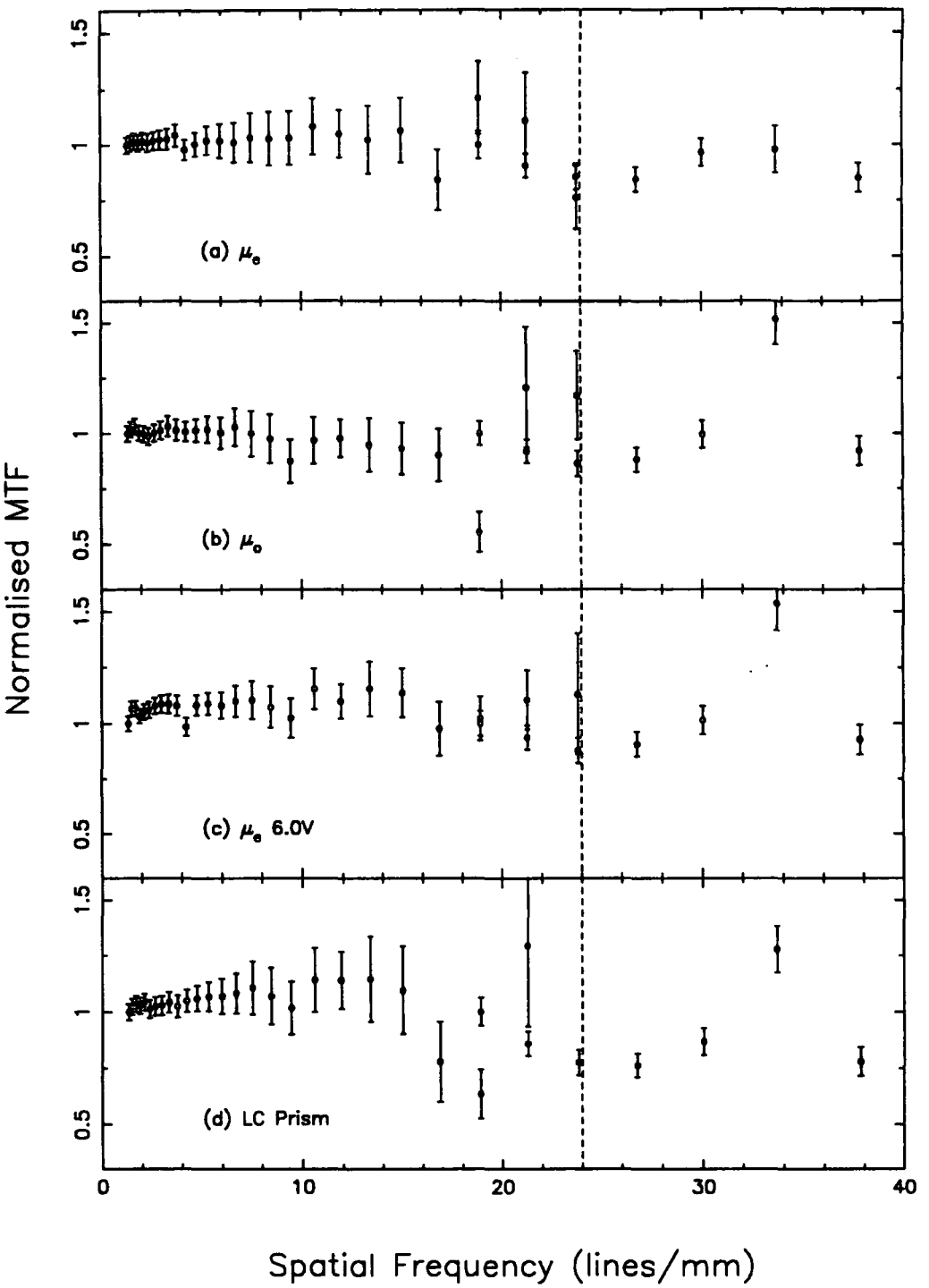

Figure 5.16: Modulation Transfer Functions for different configurations of the LC cell. (a) μ_e axis (no applied field). (b) μ_o axis. (c) μ_e axis (6V applied) and (d) μ_e axis with voltage ramp applied so cell acts as a prism.The vertical dotted line shows the WHT cut-off frequency for a 60cm sub-aperture.

There are a number of other remarks to be made, firstly the points are somewhat unevenly spaced, with the first point not being at zero spatial frequency. The resolution elements are governed by the test card and cannot be therefore changed, and there is an assumption that if the MTF is constant for spatial frequencies above 1.18 lines/mm, it will also be so for lower frequencies. Secondly the errors increase with increasing spatial frequency; this is because of two reasons. Consider figure 5.15, it can be seen that the MTF for high spatial frequencies are obtained by dividing two small numbers, therefore the relative error increases. Secondly the errors for the modulation calculated for the higher spatial frequencies are higher because there are less data points; it can be seen from figure 5.13 that the resolution elements get smaller with increasing spatial frequency.

To summarise this section. The liquid crystal cell has a transmission of around 70% and good optical quality up to spatial frequencies necessary for astronomy. These results are really a 'lower bound' on quality, as any device actually used would be commercially made and therefore have higher quality than laboratory made cells.

In this chapter the fundamental parameters of a liquid crystal cell have been measured. The next chapter goes on to discuss how liquid crystals may be used in a prismatic way.

Chapter 6

An Active Prism

6.1 Introduction

This chapter considers the design, operation, and testing of an active liquid crystal prism. Four different experimental techniques were used to measure LC prism angles. These experiments are described first, and then the results from the experiments are presented in section 6.3.

As explained in Chapter 1 a liquid crystal cell operates as a phase wedge by the application of a ramped voltage along one of the sides of the cell. This modulates the refractive index from a maximum value at one end of the wedge to a minimum at the other in order to simulate a phase wedge.

6.2 Testing of a Static Prism

Four different ways of observing the prismatic properties of a LC cell were used. Each has its advantages, and combined together they provide a comprehensive description of the LC cell.

6.2.1 Measurement of Phase Changes using a Jamin Interferometer

The *Jamin* interferometer (see e.g DUNLOP AND MAJOR [21]) is a variation on the basic two-beam interferometer, of which one of the most common examples is the Michelson interferometer. Figure 6.1 shows the experimental apparatus used. Light from an expanded, collimated laser is focussed to give a converging beam. The light is amplitude split by the first glass block. The reflected beam is directed to the second block, whilst the transmitted beam is reflected from the silvered back surface of the block to be then transmitted again towards the second block. The

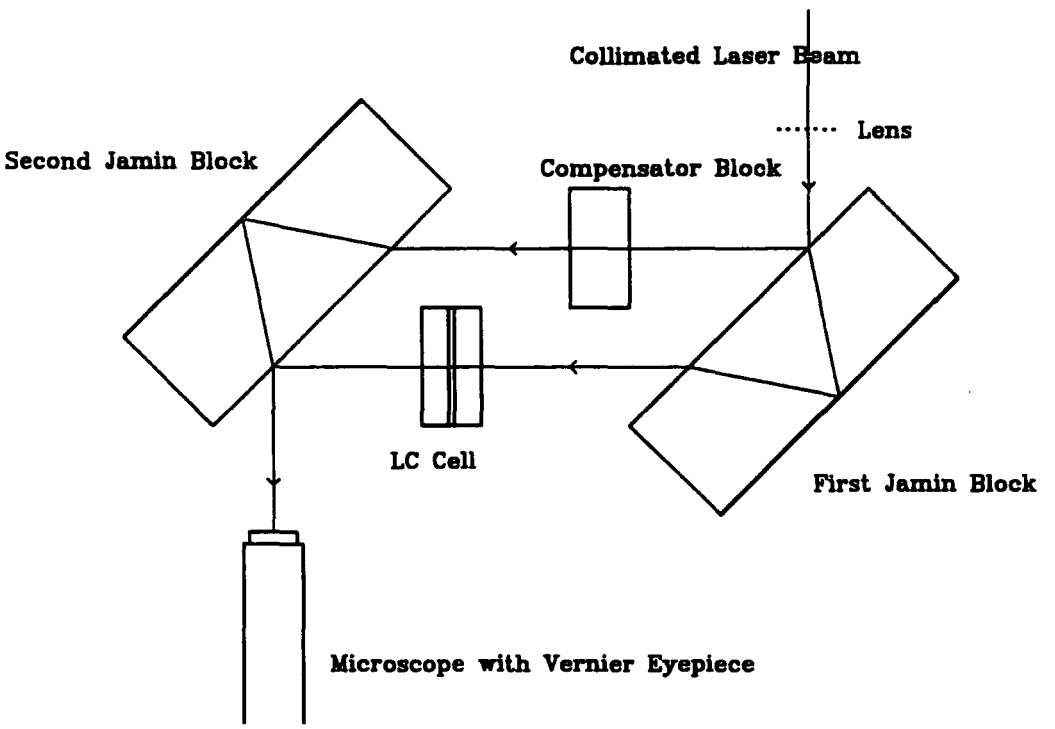

Figure 6.1: Experimental Apparatus to measure $\Delta\mu_e t$ with a Jamin Interferometer.

reverse procedure occurs to recombine the beams at the second glass block. If nothing is inserted between the jamin blocks (i.e. the glass blocks) and they are exactly parallel, then the optical path length is identical for both paths traversed and no fringes are produced. The blocks are mounted in an adjustable frame and by slightly tilting one of them straight wedge fringes appear. Alternatively, by inserting a parallel sided glass into one of the beams circular fringes are seen.

In the configuration shown, the compensator block is not imperative since fringes are very easy to form with the high coherence of laser light, however it reduces the large curvature of the fringes caused by the thick walls of the LC cell, and makes the fringe positions slightly easier to measure. The blocks are tilted until a convenient number ($\sim$ 10) of wedge fringes can be seen in the field of view. When an electric field is applied across the LC cell, the refractive index changes and the corresponding change in optical path length cause the fringes to move. The basic fringe movement is governed by the interference equation,

$$\Delta\mu_e t = m\lambda, \tag{6.1}$$

where $\Delta\mu_e t$ is the change in extraordinary optical thickness (in this case produced by a change in refractive index), λ is the wavelength, and m is the fringe shift. Thus by making an accurate measurement of how much the fringes move by using the travelling eyepiece microscope, the change in optical thickness may be determined. If the thickness of the LC cell is known (see section 5.2.5) then the change in refractive index may be calculated. The absolute refractive index is known at zero applied field, and therefore the index at any applied field can be measured. The lens is arranged so that the light is brought to focus in the plane of the liquid crystal so that then only a very small area on the liquid crystal is being examined. By recording the change in optical thickness at various places along the cell as the voltage ramp is applied then the refractive index variation along the cell may be calculated. The method is accurate; however it is quite lengthy and is insensitive to very small phase variations. This technique was also used to determine the normalisation index as used in section 5.2.6.

6.2.2 Measurement using Rotary Power

A LC cell is placed between crossed polaroids such that the LC axis is 45° to the polaroid axes as shown in figure 6.2. Light is transmitted through the crossed second polariser due to the LC acting as a wave plate (as mentioned in chapter 2). Equation 2.5 gives the phase difference between the emergent ordinary and extraordinary rays. For maximum transmission of light through the crossed polaroids the LC must act as a half-wave plate therefore this phase difference must be equal to

an odd integral multiple of π. For extinction of light then

$$\frac{2\pi\Delta\mu t}{\lambda} = n_{\text{even}}\pi, \tag{6.2}$$

where n is an integer, or

$$\Delta\mu t = n\lambda. \tag{6.3}$$

Therefore when an increasing voltage is applied to a cell the transmission varies between a number of minima and maxima. Whenever light is extinguished then the LC cell is said to be in a π-state. The number of π-states as the electric field is increased is then a measure of the birefringence of the cell. The technique is a

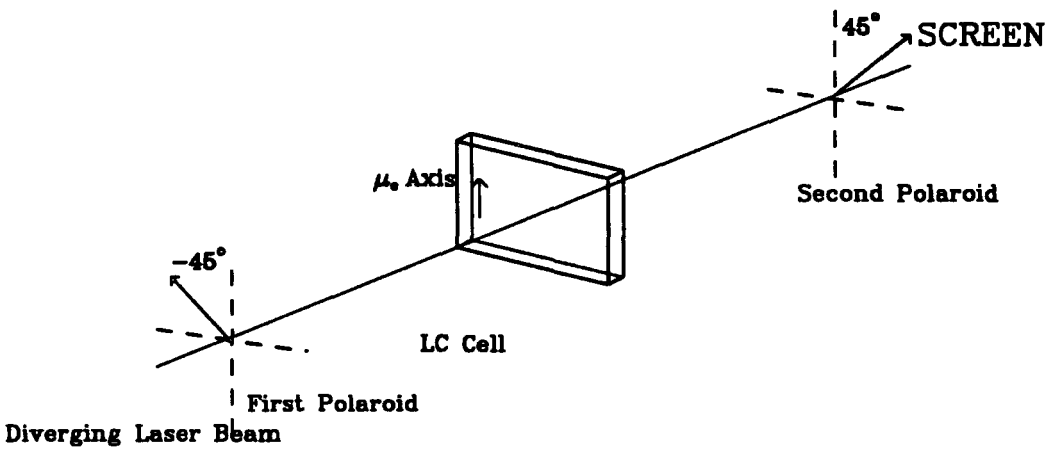

Figure 6.2: Apparatus to observe π-States.

common way of examining liquid crystals (e.g. Wu et al. [66]). A slight variation can be used to measure the phase variations along a cell. The apparatus is set up in the same way as before and a voltage ramp is applied to the cell. A number of dark lines appear across the image on the screen whenever the optical thickness satisfies equation 6.3. The number π-states seen is then a measure of the change in optical thickness across the cell, and using equation 4.15 the effective prism angle can be calculated. The spacing of the fringes across the cell is a measure of how linear the phase wedge is.

This technique is the easiest method by which to observe the prismatic properties of the whole of the cell. The equipment is very simple to set up and the results can be seen virtually instantaneously. However it is not particularly accurate since only a few π-states can be seen across the cell.

6.2.3 Direct Observation of Deflection

The angles of deflection obtained by a large cell are very small (< 30arcsecs) however these small deflections may be observed by combining a lens of long focal length with a microscope. The experimental apparatus is shown in figure 6.3. A collimated white

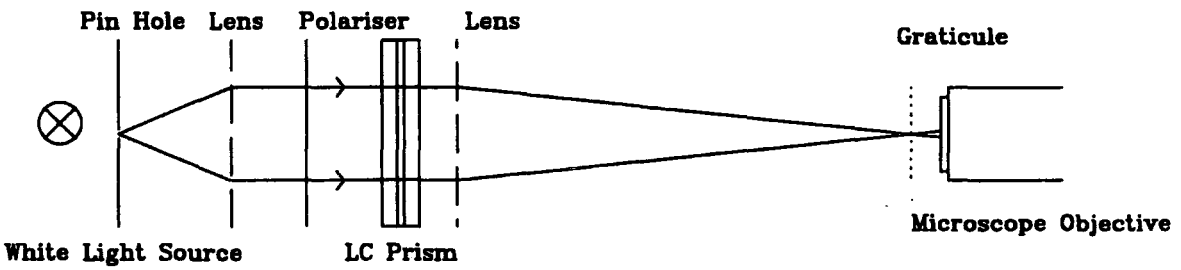

Figure 6.3: Apparatus to observe deflection of light by a LC prism.

light beam is produced by a 5μm pin hole and the first lens. The light polarised along the μ_e axis of the polaroid is deflected by the prism through a very small angle. This light is focussed by a 1m focal length lens onto a microscope graticule. The result is observed by a horizontally arranged microscope.

This is an attractive experiment because the operation of the prism can be seen directly. It also is a way of observing any abberations caused by the LC cell by looking at the quality of the light spot formed. The experiment is however difficult to set up and the results are not so precise because the movements are quite small in comparison to the spot size.

6.2.4 Measurement using Edser-Butler Fringes

As described [1] in chapter 5 Edser-Butler fringes provide a very sensitive method of examining the LC Cells. When Edser-Butler fringes are formed by a good quality cell they are straight and vertical. As a voltage ramp is applied to the cell to create a phase wedge the fringes tilt over towards the blue end of the spectrum (optical thickness decreasing). The amount of tilt is a measure of the prism angle. The straightness of the fringes indicates how linear the phase wedge is. Any change in phase across the whole of the cell is shown up by the whole fringe pattern moving. The position (in wavelength) of a fringe is given by

$$2\mu t = n\lambda. \tag{6.4}$$

Consider one fringe that is tilted due to a change in refractive index along the length of the cell. The thickness is constant therefore

$$\frac{\mu_1}{\mu_2} = \frac{\lambda_1}{\lambda_2}. \tag{6.5}$$

Thus if the refractive index is known for the wavelength of the end of the fringe that remains fixed, the refractive index at the other can be calculated. The thickness is known so therefore the prism angle may be calculated. The Edser-Butler technique is extremely sensitive and very small prism angles can be detected that the other techniques cannot.

6.3 Operation and Results of a Static LC Prism

6.3.1 Controlling the Prism

Figure 6.4 shows how the electric field is applied to a cell. By comparing with figures 4.5 and 4.6 it can be seen that one of the plates is kept at earth and a voltage ramp, varying from V_{max} at one end to V_{min} at the other, is applied to the second plate. V_{min} is generally close to earth. The voltages are AC (sine) wave in order to stop the LC from degrading.

[1] It is sometimes necessary to alter the focussing between the cell under test and the spectrometer in order to examine the whole of the cell, if it is longer than the height of the spectrometer slit. However this does not affect the method of data reduction

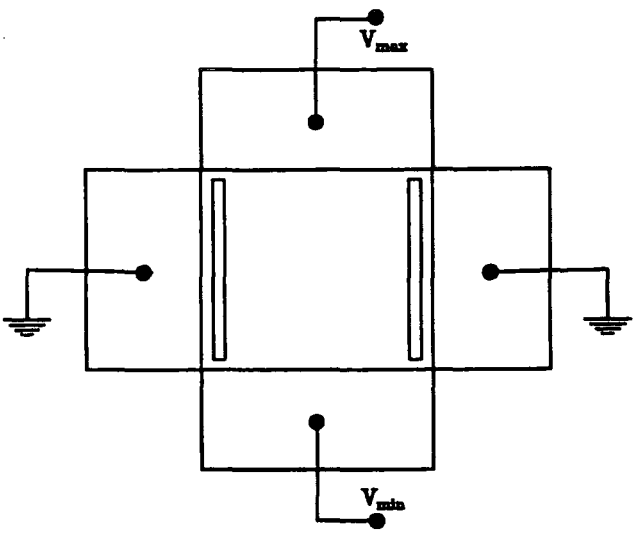

Figure 6.4: Electrical Connections to a Liquid Crystal Prism

One of the primary considerations is how does the voltage vary along the length of the cell? This cannot be easily determined in a completed cell so measurements were made by applying a voltage ramp along a piece of ITO coated glass and measuring the voltage at various places along the glass with a digital AVO meter. Figure 6.5 shows the results for two different sizes of glass. It can be seen that the results are linear for most of the length of the glass with some edge effects (the line is drawn as a guide to the eye). The longer glass showed much greater edge effects. This can be attributed to the fact that the connections were much better for the shorter glass. The longer glass was connected to the supply via bulldog clips whereas the connections to the shorter glass were made with conductive paint as described in chapter 4.

The results shown are for an ITO resistance $\sim 200\Omega$. If low resistance ($\sim 20\Omega$) ITO is used then firstly, the edge effects increase, and secondly the current flow through the ITO increases and it therefore tends to heat up changing the optical properties of the cell. These two undesirable effects mean that higher resistance ITO must be used. ITO is actually a mixture of indium oxide and tin oxide. By controlling the relative concentrations of the oxides the transparency and the resistance

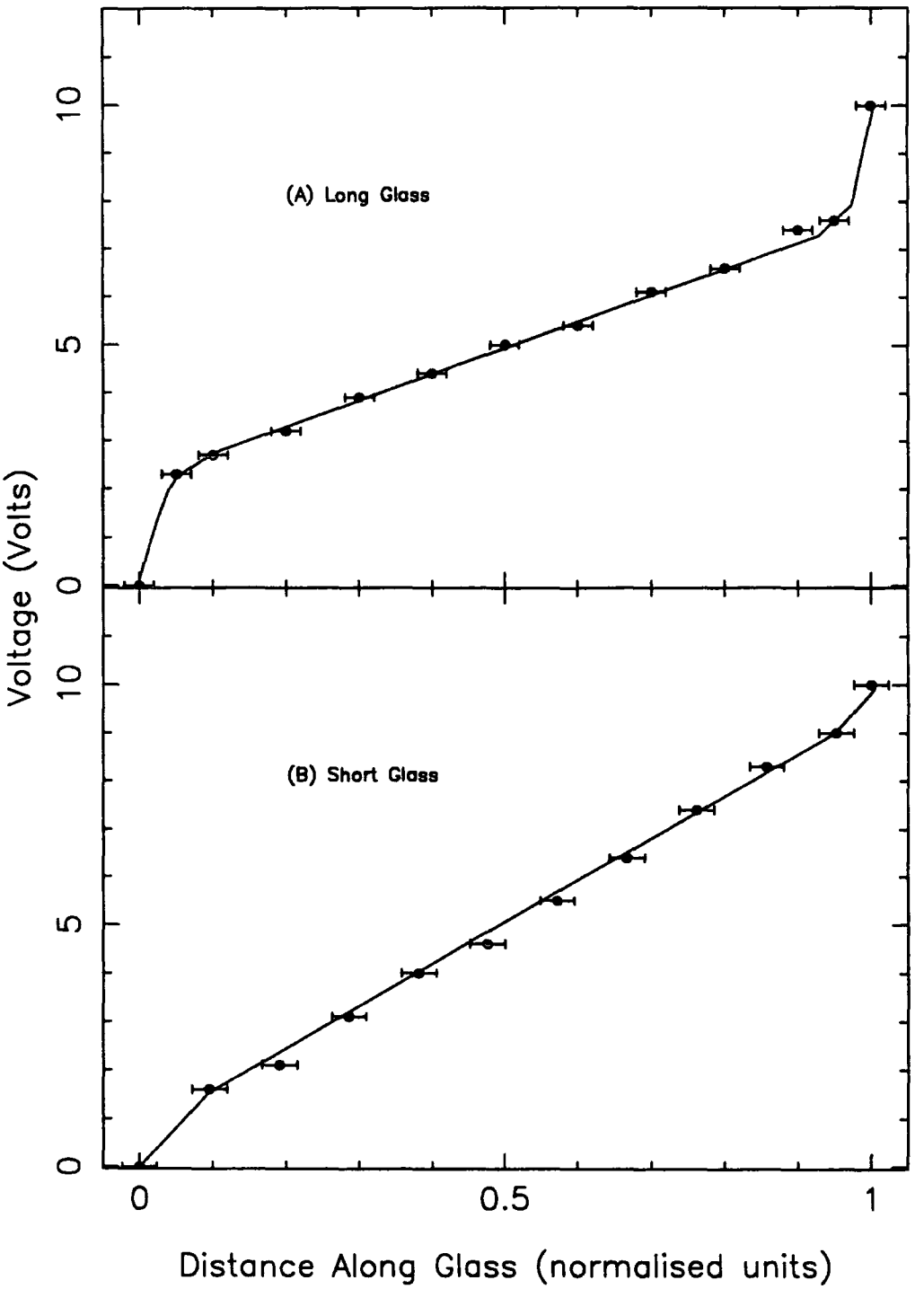

Figure 6.5: Variation of Voltage along an ITO Coated piece of Glass. Length (a) 50mm (b) 10.5mm. Resistance (a) 280Ω (b) 160Ω. Applied field 10.0V D.C.

may be controlled.

The voltage variation across a cell is therefore linear. There are some edge effects but these can be minimized by ensuring good electrical connections. The edge effects also only effect the parts of the cell away from the active liquid crystal area. The results only show the one-dimensional voltage distribution, however the electric field did not vary appreciably along the other glass axes as is desired. These results were taken using a DC field. The assumption has been made that the use of an AC field in a LC cell (a capacitor) does not effect the voltage distribution along the cell. As can be seen from the following results this seems to be valid.

For the phase to vary in the same manner as the voltage requires that the refractive index be linear with voltage. However, as shown in figure 5.6, $\Delta\mu_e$ varies according to a quadratic function, and accordingly, also the phase. Figure 6.6 shows an example of this. The results were taken using the Jamin interferometer. The thickness was previously determined by the Edser-Butler method. The curve shows the refractive index gradient that is expected from the results of section 5.2.7. The maximum voltage in the voltage ramp is unknown so the comparison has to be made by fitting the end point. The points and the curve are in good agreement therefore the phase wedge is acting in the expected manner.

In order for the phase wedge to be approximately linear then the usable birefringence is restricted to ~ 0.15. Therefore more measurements of change in optical thickness were taken with the jamin interferometer using lower voltages. Figure 6.7 shows the results for 5 values of applied voltage. It can be seen that the points lie in an approximate straight line (shown by the linear least squares fit). The graph for 2.99V is beginning to curve slightly so voltages much above this cannot be used. The graphs show another problem that occurs when lower voltages are used. At the minimum end of the voltage ramp the electric field across the LC layer is less than the threshold voltage required to produce a change in birefringence.

There are therefore three considerations when applying voltages to a prism. Firstly, for linear variation of index, the maximum voltage must be kept below $\sim 3V$. Secondly, if a small voltage ramp is applied then a positive[2] bias voltage

[2]Here the word positive is used to mean positive compared to V_{max}, however it is still an AC voltage.

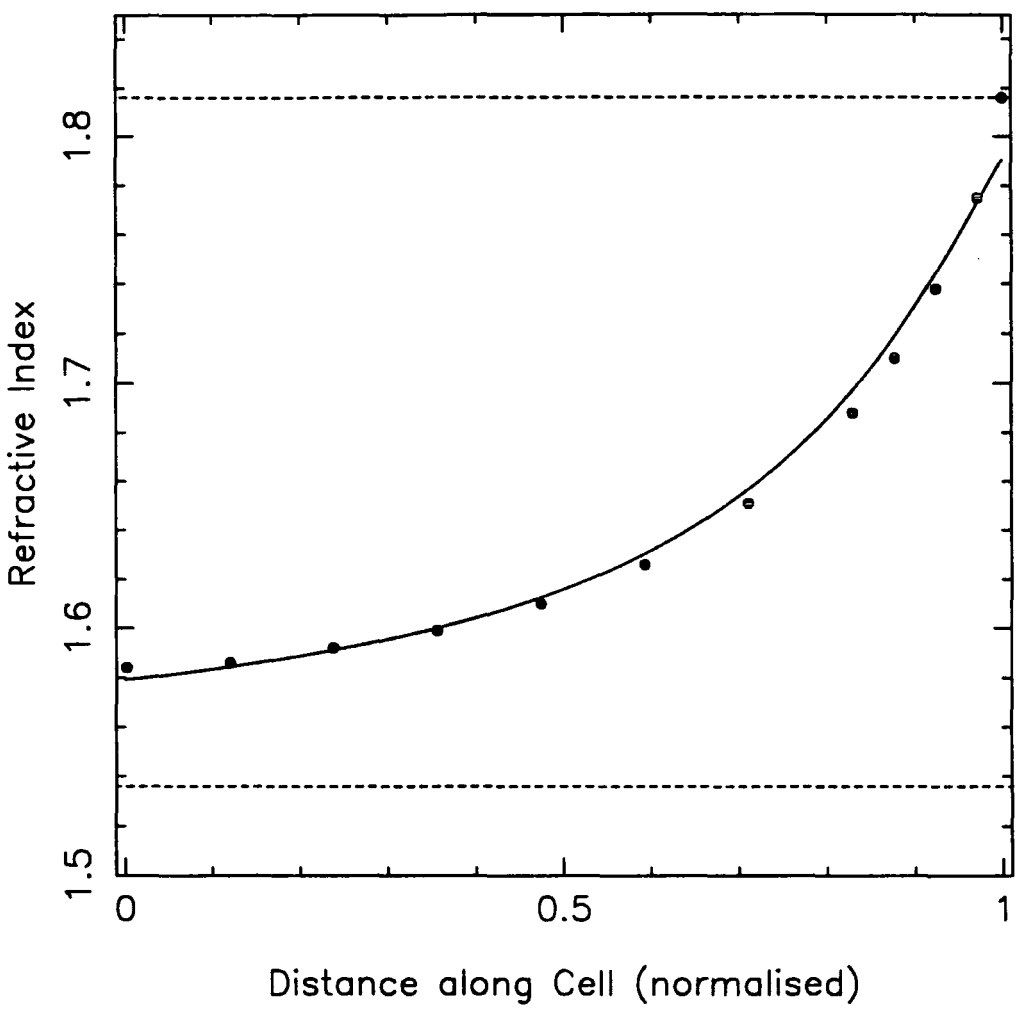

Figure 6.6: Variation of Refractive Index across a LC cell. Cell thickness 9.80μm. Cell length 21.9mm. 5.7V RMS 50Hz sine wave. $\lambda = 543$nm. The horizontal dotted lines show the values of μ_o and μ_e with no applied field. The line shows the variation expected from measurements of voltage characteristics.

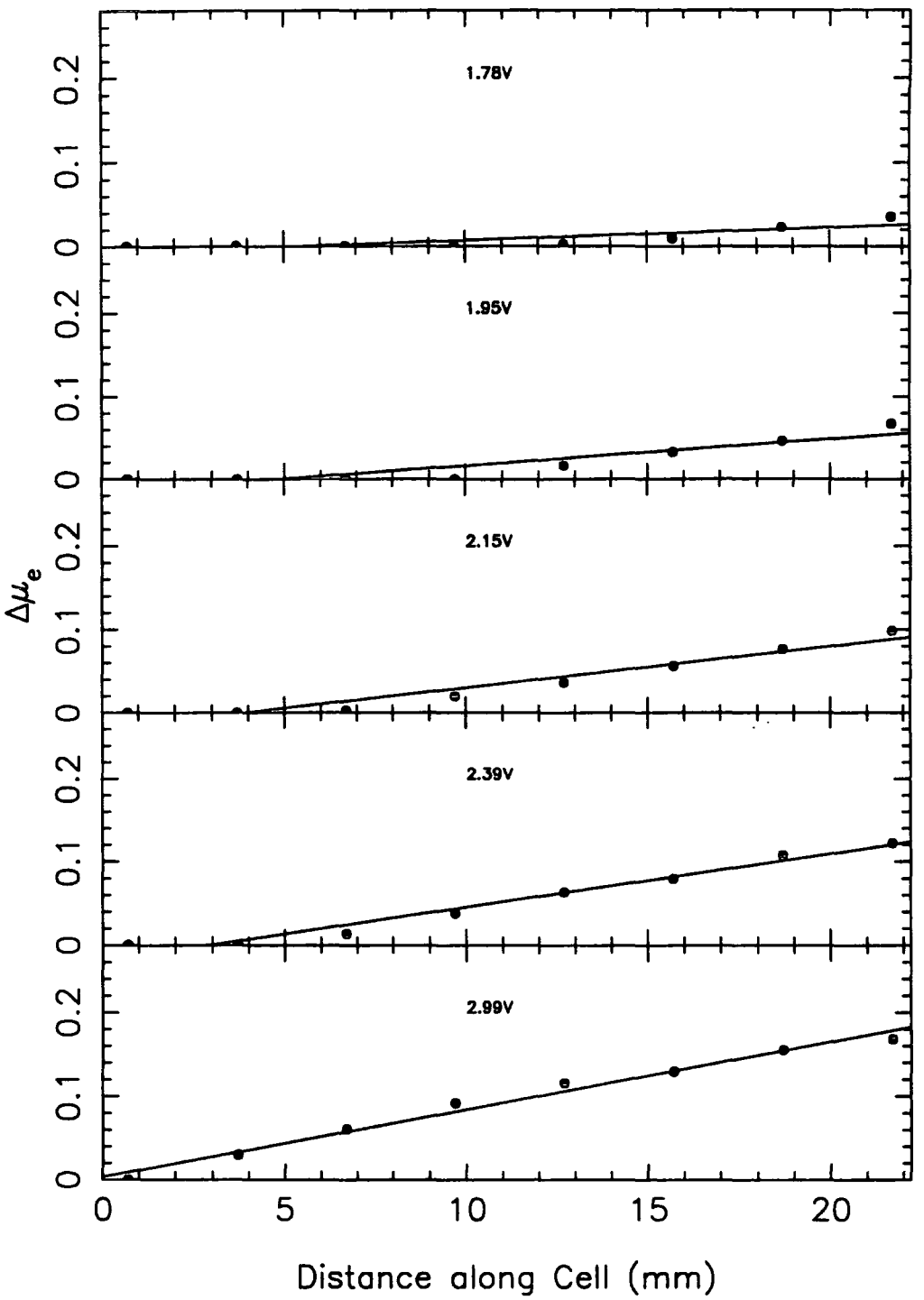

Figure 6.7: Variation of Refractive Index across a LC cell for different values of the applied voltage ramp. Cell thickness 9.80μm. Cell length 21.9mm. Applied field as indicated (RMS), 50Hz sine wave. Cell thickness 9.85μm. λ = 543nm. The solid lines are linear least squares fits.

must be added to V_{min} so that the voltage at the lesser end of the wedge is the threshold voltage. Conversely when the voltage is high the voltage at the lesser end of the wedge is greater than the threshold voltage so that a negative bias voltage must be applied. The details of the circuit used to provide these voltages is shown in Appendix B.

6.3.2 Results

The easiest and most accurate way to determine the necessary voltages to apply to produce a given linear phase wedge is by using Edser-Butler fringes. The voltages are varied so that the fringes are tilted, yet they remain straight. The bias voltage is adjusted so that the end of the fringes corresponding to the 'thick' end[3] of the wedge remains fixed. Measurement of the shift of the other end of the fringes gives the change in refractive index. Figure 6.8 is a photograph showing Edser-Butler fringes produced with and without the applied voltage ramp. Once the necessary voltages were determined, then the measurements could be made using the observations of direct deflection of a light beam. Figure 6.9 shows photographs of the direct deflection of light. They are double exposures showing the prism switched on and off. The graticule can be seen from which the angle of deflection can be calculated. Notice the first diffraction maxima can be seen. The light spots remain circular with the prism switched on, and there is no evidence of elongation due to dispersion effects. The results from both methods are shown in table 6.1. The results show good agreement, within the experimental accuracy, between the two methods. They also show that the dispersion is small over the wavelength range 524-650nm. The dispersion effect is only beginning to manifest itself in the largest deflection. The results show one limitation of using the Edser-Butler technique for measuring prism angles across the spectrum, that is that 'blue' corresponds to only 524nm (a green-blue colour). If a fringe further into the truly blue end of the spectrum is used, then as the voltage ramp is switched on the fringe moves towards the ultra-violet and cannot be seen. The voltages shown are somewhat irrelevant because they show only the actual voltages applied to the cell and not the voltages over the actual active area of liquid crystal. The same prism was tested using the optical rotation method by observing the π-states across the prism. An example is shown in figure 6.10.

[3] i.e. the end of the fringe where the μ_e is at its maximum value (V=threshold voltage)

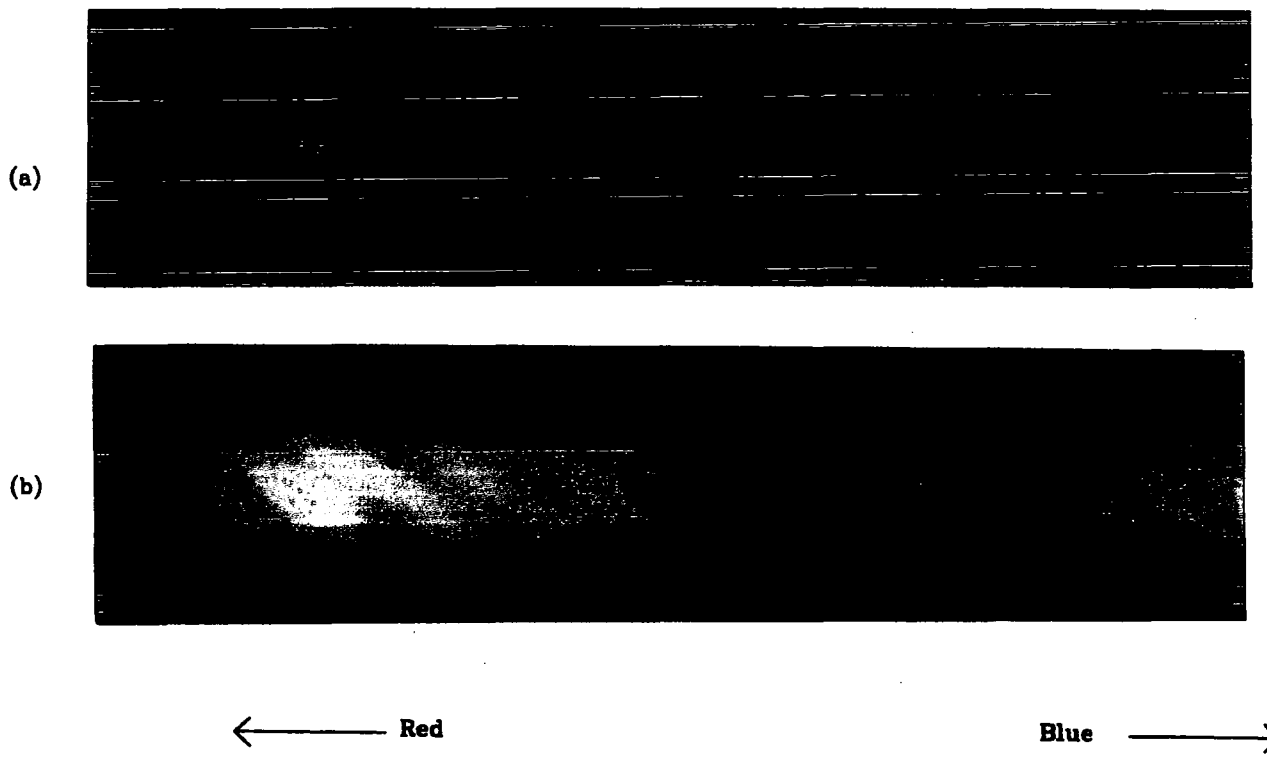

Figure 6.8: Edser-Butler fringes produced by a 10μm cell. Voltage ramp switched (a) off. (b) On, corresponding to $\sim 10''$ prism angle.

(a)

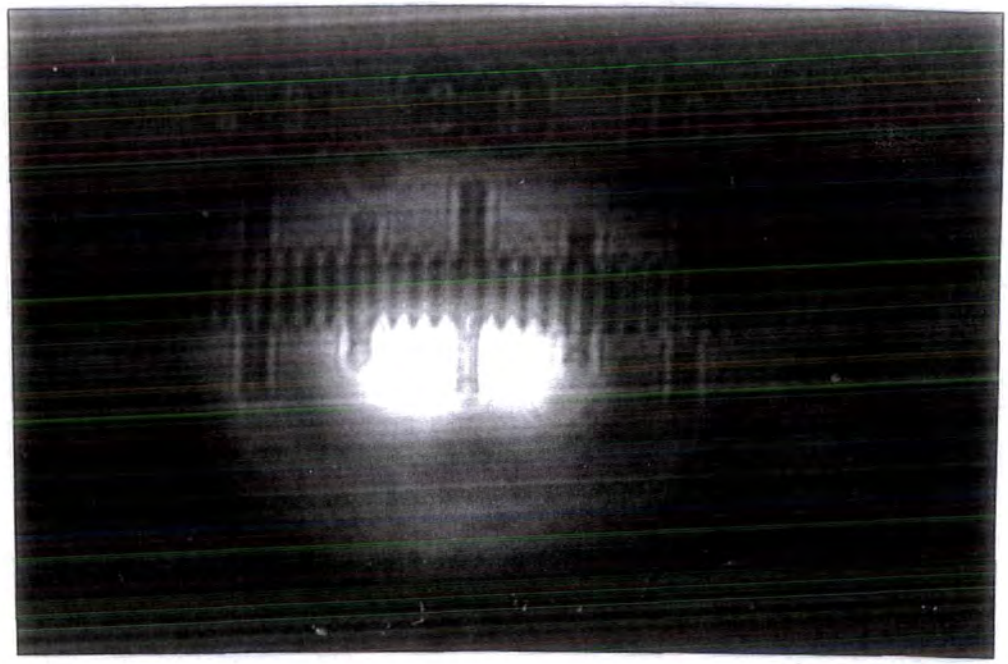

(b)

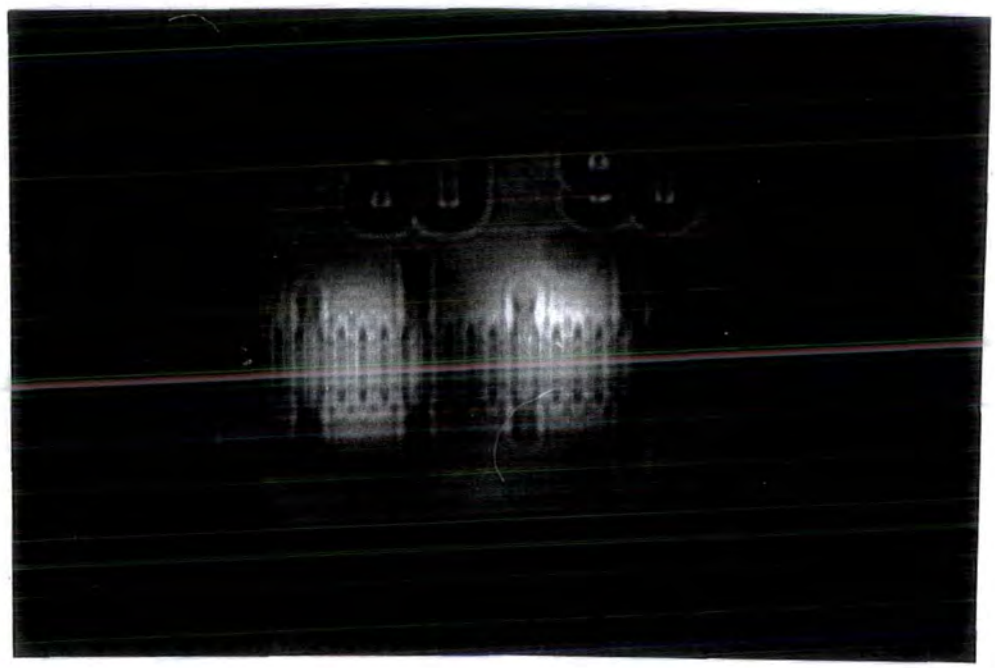

Figure 6.9: Direct observation of white light deflection by (a) an 8″ prism. ($V_{max} = 1.70V, V_{min} = +0.43V$) and (b) an 18″ prism ($V_{max} = 3.05V, V_{min} = -0.24V$)

Applied Voltage (V_{max}, V_{min})	Wavelength	$\Delta\mu$	θ	θ_{direct} (white light)
1.15, +0.80V	Red (~ 650nm)	0.025 ± 0.005	$2.8 \pm 0.5''$	
"	Green (~ 550nm)	0.026 ± 0.005	$2.9 \pm 0.5''$	$2 \pm 2''$
"	Blue (~ 524nm)	0.025 ± 0.005	$2.8 \pm 0.5''$	
1.52, +0.55V	Red	0.049 ± 0.005	$5.5 \pm 0.5''$	
"	Green	0.054 ± 0.005	$6.0 \pm 0.5''$	$6 \pm 2''$
"	Blue	0.051 ± 0.005	$5.7 \pm 0.5''$	
1.70, +0.43V	Red	0.059 ± 0.005	$6.6 \pm 0.5''$	
"	Green	0.069 ± 0.005	$6.0 \pm 0.5''$	$8 \pm 2''$
"	Blue	0.064 ± 0.005	$7.1 \pm 0.5''$	
2.19, +0.15V	Red	0.093 ± 0.005	$10.4 \pm 0.5''$	
"	Green	0.097 ± 0.005	$10.8 \pm 0.5''$	$10 \pm 2''$
"	Blue	0.099 ± 0.005	$11.0 \pm 0.5''$	
2.60 , 0.00V	Red	0.116 ± 0.005	$12.9 \pm 0.5''$	
"	Green	0.120 ± 0.005	$13.4 \pm 0.5''$	$12 \pm 2''$
"	Blue	0.121 ± 0.005	$13.5 \pm 0.5''$	
3.05, −0.24V	Red	0.132 ± 0.005	$14.7 \pm 0.5''$	
"	Green	0.137 ± 0.005	$15.2 \pm 0.5''$	$18 \pm 2''$
"	Blue	0.137 ± 0.005	$15.2 \pm 0.5''$	
3.78, −0.55V	Red	0.158 ± 0.005	$17.6 \pm 0.5''$	
"	Green	0.168 ± 0.005	$18.7 \pm 0.5''$	$21 \pm 2''$
"	Blue	0.170 ± 0.005	$18.9 \pm 0.5''$	

Table 6.1: Angles of deviation produced by a 9.98μm by 18.5mm cell for different wavelengths. θ indicates the results obtained from Edser-Butler fringes and θ_{direct} indicates the results from the direct observations of deflections.

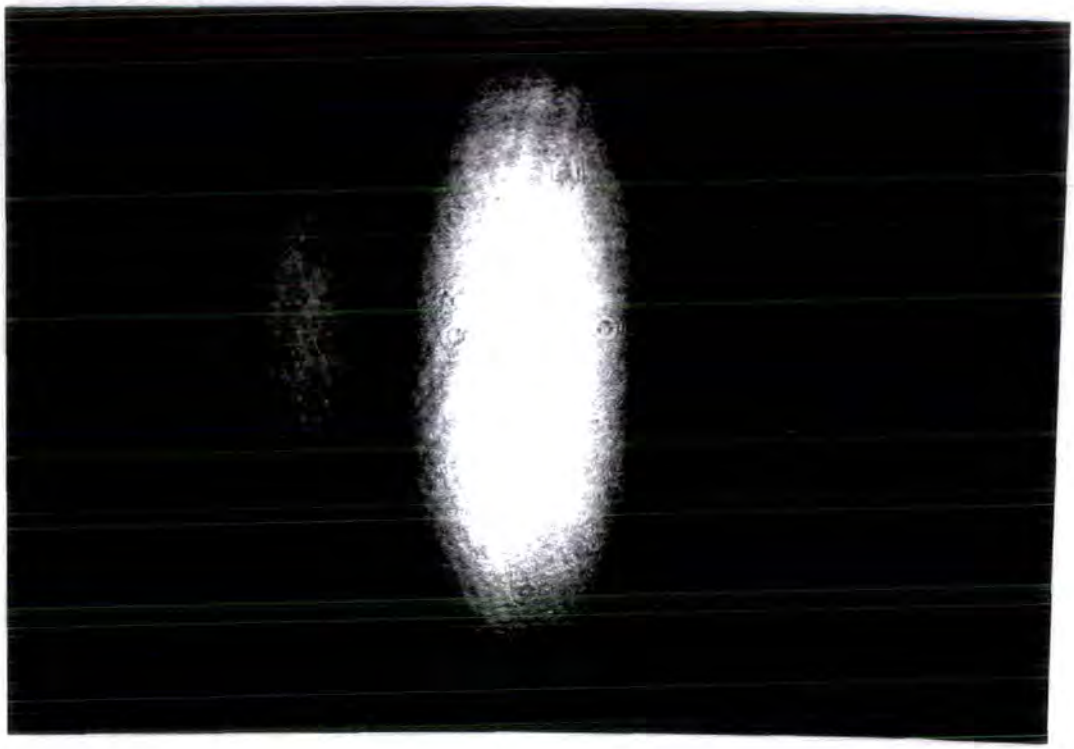

Figure 6.10: π-states observed in a liquid crystal prism. $V_{max} = 2.60V$ $V_{min} = 0.0V$.

The technique is not an accurate method of determining the prism angles but the results agree qualitatively with the above results. However they conveniently show the good optical quality over the whole of the cell, by the straightness of the fringes.

The prism angles produce for a given change in index along the cell will be different for cells of differing size. These results are for a relatively large prism (18.5mm) and so the prism angles produced are not as large as that required in astronomy (see section 4.2.1). Measurements were made with a smaller prism which gave larger deflection angles. A 7mm prism was tested (which corresponds to a 54cm aperture on the telescope). The results are as follows.

Cell Length	7mm
Cell Thickness	10.7μm
V_{max}, V_{min}	$4.26, -1.98$V
Prism angle from Edser-Butler fringes @ 547nm, $\Delta\mu = 0.13$	$41.0 \pm 0.5''$
Prism angle from direct observation of deflection @ 543nm	$45 \pm 5''$

Note on the Prism Size

This section has referred to prisms of different sizes giving different angles of deflection. It should be noted that the quantities 'size' and 'length' (W) refer to the active size of the liquid crystal area and not to the overall size. For example this section has referred to an 18.5mm prism and a 7mm prism. These were the same cell, with differing amounts of the cell being used. Therefore, in an actual device, the size of the liquid crystal cells being used does not have to be changed with different aperture sizes, only the voltage parameters.

6.4 Summary

In this chapter the use of liquid crystals as prismatic devices has been demonstrated. Prism angles of up to $45''$ have been experimentally measured. The important conclusion is that the liquid crystals are acting according to theory and that there appear to be no hidden problems in applying ramp voltages across a cell.

This chapter has just dealt with slowly varying the optical properties of a cell. The next chapter deals with the dynamics of liquid crystals so that they may be utilised in an adaptive way.

Chapter 7

An Adaptive Prism

7.1 Liquid Crystal Response Times

Chapter 2 described how the refractive index of a liquid crystal material depends on the orientation of long rod-like molecules that can be rotated by the application of an electric field. The molecules that are adjacent to the alignment layer of PVA (surface molecules) are anchored firmly and cannot be rotated. The molecules in the middle of the LC layer are free to move and can rotate in order to align with the electric field. When the electric field is removed the surface molecules cause bulk realignment of the molecules throughout the whole layer.

There are therefore three basic factors that govern the speed of molecular rotation. Firstly consider the electric field strength; the stronger the field the greater the torque on the molecules. The electric field is dependent on both the voltage applied and the thickness of the LC layer. The ability to rotate quickly is opposed by the viscosity of the material and the elastic constants governing the deformation of the structure.

When describing the elastic and viscous properties, the liquid crystal can be regarded as a bulk continuum without reference to the molecular structure (BLINOV [7]). Thus classical mechanics based upon Hooke's law can be used to derive formulae for response times. These are well documented (eg. JAKEMAN AND RAYNES [35] or LABRUNIE AND ROBERT [39]) and are given by,

$$\tau_r = \frac{4\pi\gamma}{\Delta\mu} \frac{d^2}{V^2 - V_{th}^2} \tag{7.1}$$

and

$$\tau_d = \frac{\gamma d^2}{\pi^2 K} \tag{7.2}$$

where τ_r (rise time) and τ_d (decay time) are the switch on and switch off times (from and to zero field) respectively. d is the LC thickness, γ is the rotational viscosity, and K is the elastic constant[1]. V is the applied voltage and V_{th} is the threshold voltage (below which no molecular rotation occurs).

τ_d is known as the *free relaxation time* and is independent of the applied field. When the field is removed the restoring torque is greater if the molecules have been rotated further from their equilibrium position, which leads to the relaxation time being independent of the initial electric field. Because it is the surface layer of molecules that provide the restoring forces, τ_d also has a strong dependance on LC thickness. τ_r is also dependent on the physical constants of the LC, but also on the strength of the applied field.

Thus, for a given LC cell, the dynamic range (i.e. available phase retardation) and the speed are conflicting parameters by their mutual dependence on LC thickness. The switch-on time can be improved by using a large voltage to give a large torque on the molecules. Switch-on times of the order of milliseconds can obtained by using $\sim$ 20V pk-pk. However the switch-off time is an intrinsic property of the liquid crystal cell, controlled by the aligning force of the surface molecules. Usually high birefringence is accompanied by high viscosity (see WU at al. [68]), again making response times and dynamic range complementary attributes. Free relaxation times, for a 10μm cell, are of the order of hundreds of milliseconds, obviously too slow for adaptive optics.

7.2 Experimental Measurements of Response Times

7.2.1 Experimental Technique

The ability of a liquid crystal cell to modulate the intensity of light propagating between crossed polaroids, as explained in section 6.2.2, is a convenient way to measure the dynamic behaviour of a cell. The rate of change of intensity of light

[1]There are three elastic constants depending on the type of molecular distortion. For a homogenous aligned cell it is K_{11}, the splay elastic constant (see BLINOV [7]) which is of relevance.

using a light detector which may be interfaced to an oscilloscope is a direct indication of the rate of change of liquid crystal refractive index. The apparatus used is shown in figure 7.1. A silicon photodetector was connected to one channel of a dual-beam storage oscilloscope to measure the light from the optical apparatus. Monochromatic red laser light was used (632.8nm). However the response time should be wavelength independent because it is a function of molecular rotation, not on any interaction with the light.

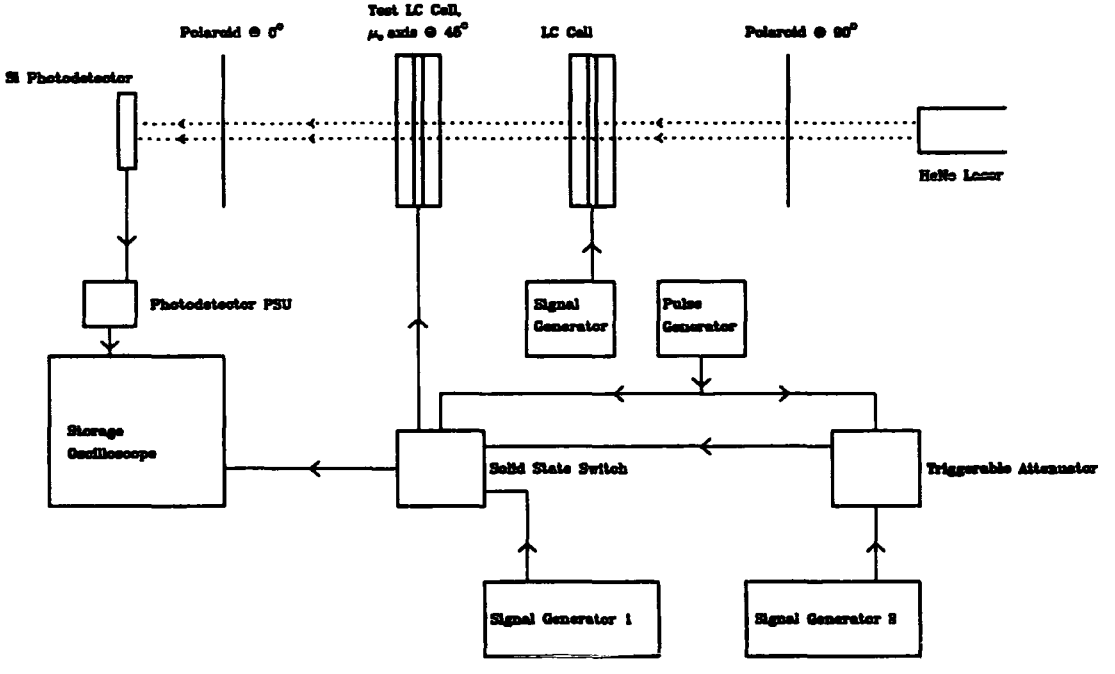

Figure 7.1: Experimental apparatus to measure liquid crystal response times.

There are two liquid crystal cells. One is the cell under test, and the second is to provide a tunable retarder, so that the light intensity falling on the photodetector may be tuned to be a minimum or a maximum when no voltage is applied to the test cell (i.e. in a pi or half pi-state). This enables the index change of the test cell to be calculated more easily by providing a suitable fiducial mark. The tunable retarder has its own power supply, separate from the other electrical equipment. This is an illustration of the ease by which liquid crystals may be used to control phase. If a piezo driven mirror had been used to produce a similar effect (as is used in some interferometers) then the apparatus would become much more cumbersome, and it

would be prone to vibrations.

The remainder of the electrical apparatus provides the ability to supply a variety of voltage forms to the liquid crystal cell. The pulse generator and signal generators (SGs) are conventional laboratory equipment. The triggerable attenuator is a device which is made inactive for a controllable time period ($\sim$ 5 to 50ms) when triggered by the pulse generator. It then switches on and attenuates the signal from SG2 by a controllable amount. The solid state switch is a device that switches its output to the liquid crystal from SG1 to SG2. The switching rate is controlled by the pulse generator. Because it is a solid state device it provides very fast bounce-free switching. The configuration of the equipment to give the required voltages is described below.

7.2.2 Preliminary Measurements

The switching times of a 10μm cell were measured as a function of voltage. Only one of the signal generators was needed. The pulse generator was adjusted so that the output to the liquid crystal consisted of a simple burst of a square wave voltage.

In this thesis switching times are measured as the full switching time. This introduces a certain level of subjectivity into the results, but this is small and in this context, as opposed to display devices, it is more important for the full switching time to be known. In the literature, response times are measured by different criterion. Sometimes the time to switch from 10% to 90% is quoted. When measuring the switch between light and dark states it is often the time for the intensity to fall by $1/e$. These different criterion tend to yield slightly shorter response times.

Two example oscillograms are shown in figures 7.2 and 7.3 Consider figure 7.2. The upper trace shows the output from the photodetector and the lower trace shows the voltage applied across the cell. It can be seen that as the voltage burst starts, the liquid crystal extraordinary index decreases as the cell switches on (after a short dead time), and therefore the cell goes through a number of pi-states. The reverse happens when the voltage burst stops, however the cell relaxes much more slowly. It can be seen that the phase change is approximately 4π, or 2.5μm. The cell is 10μm in thickness, and so this phase change corresponds to an index change of 0.25,

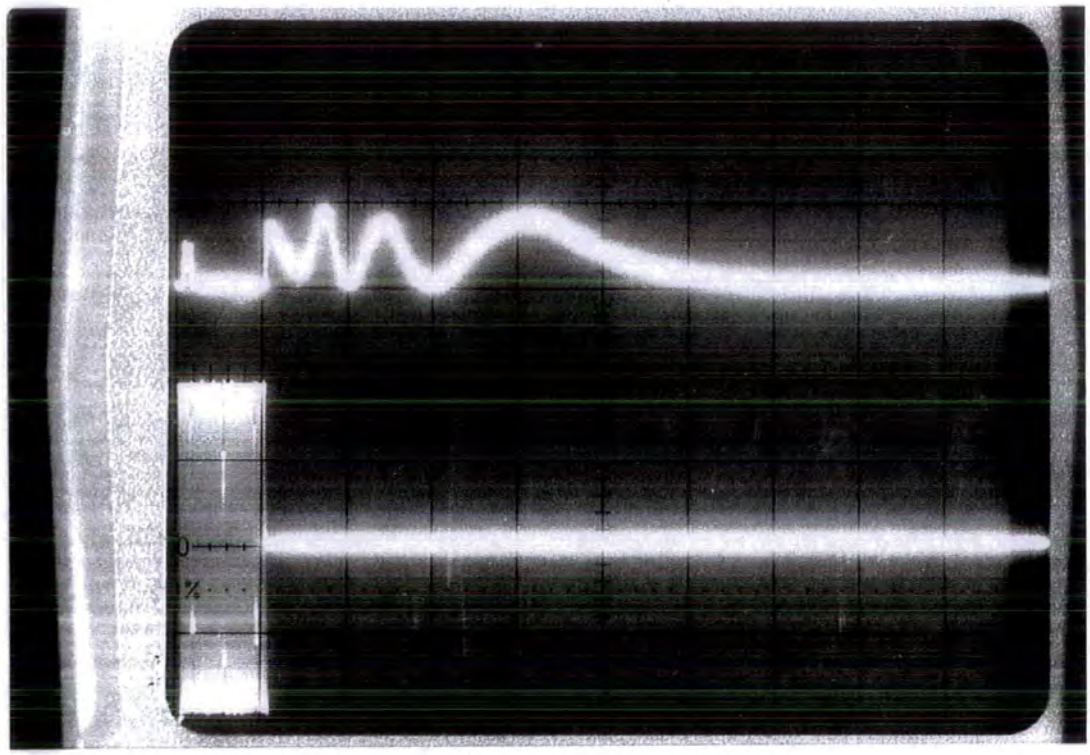

Figure 7.2: An example oscillogram. 10μm cell. 18V (pk-pk) 1KHz square wave burst for 0.1 seconds (time scale 0.1sec/div).

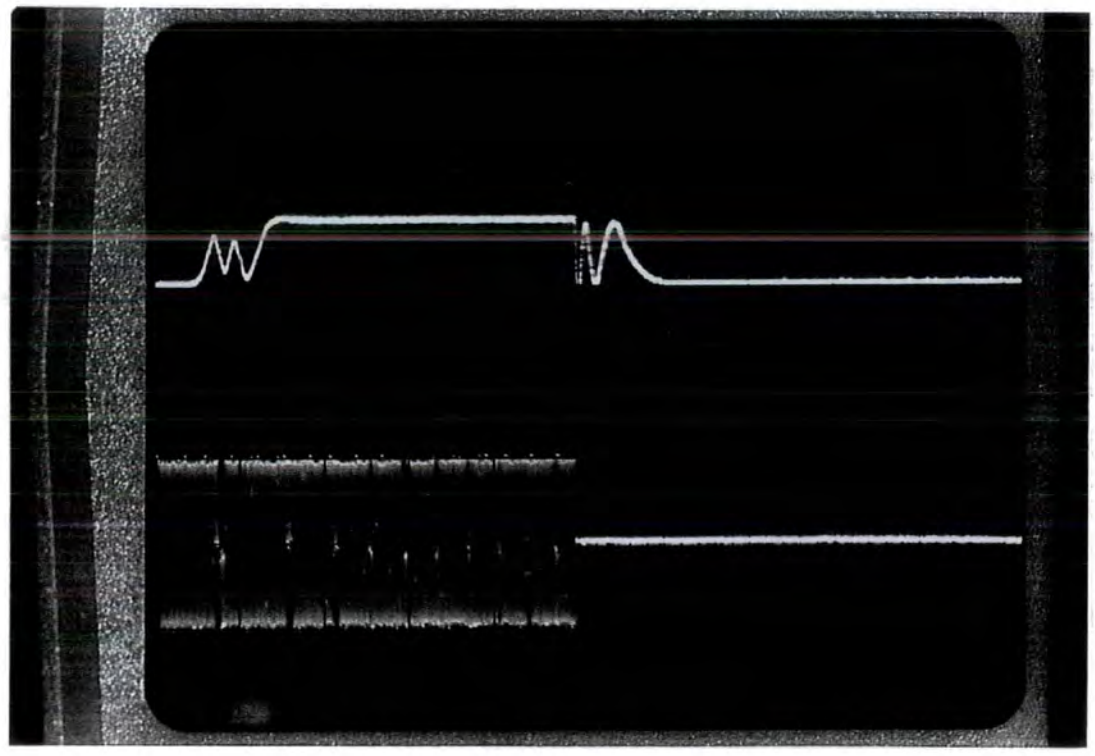

Figure 7.3: An example oscillogram. 10μm cell. 4V (pk-pk) 1KHz square wave burst for 2.5 seconds (time scale 0.5sec/div).

as expected. Notice how the photodetector output is initially at a minimum before there was a voltage across the cell. This is arranged to be so by adjusting the phase delay of the second liquid crystal cell.

Note how the switch on time is very short compared to the switch off time when the higher voltage is applied, whereas when only 4V is applied the switch on time is much longer and the switch off time remains similar to that for the lower voltage.

The full results are shown in figure 7.4 for a 10μm cell. According to equation 7.1 a graph of $1/\tau_{rise}$ against V^2 should be linear as shown. The least squares fit shown is calculated using only the points relevant to each diagram, so the two fits are slightly different because the theory that is behind equation 7.4 is an approximation.

The switch-off times should be field independent. Again the theory is not perfect so there was some variation, but the significant point is that they were all $\sim$ 400ms, i.e. too long for adaptive work.

7.3 Improving LC Response Times

There are various techniques for increasing the speed of liquid crystals. The surface or bias effect (FERGASON [24]) and the transient nematic effect (WU AND WU [69]) both utilise the fast decay time due to the small angled relaxation from highly deformed LC directors. The cell is placed between crossed polaroids, as explained in section 6.2.2, and modulated between the light and dark π-states nearest to the LC saturation voltage. The technique is primarily useful for LC displays, but it may also be applicable to phase control technology, as discussed in the next section. The dual-frequency effect and ferroelectric liquid crystals also may provide possibilities. They are discussed in section 7.4. The following section presents some experimental results of liquid crystal response times.

7.3.1 Improving the switch-on time

From figure 7.4 it can be seen that the LC rise time has a value of 15ms when a voltage of 9.1V (pk-pk) is applied across the cell. This corresponds to a phase

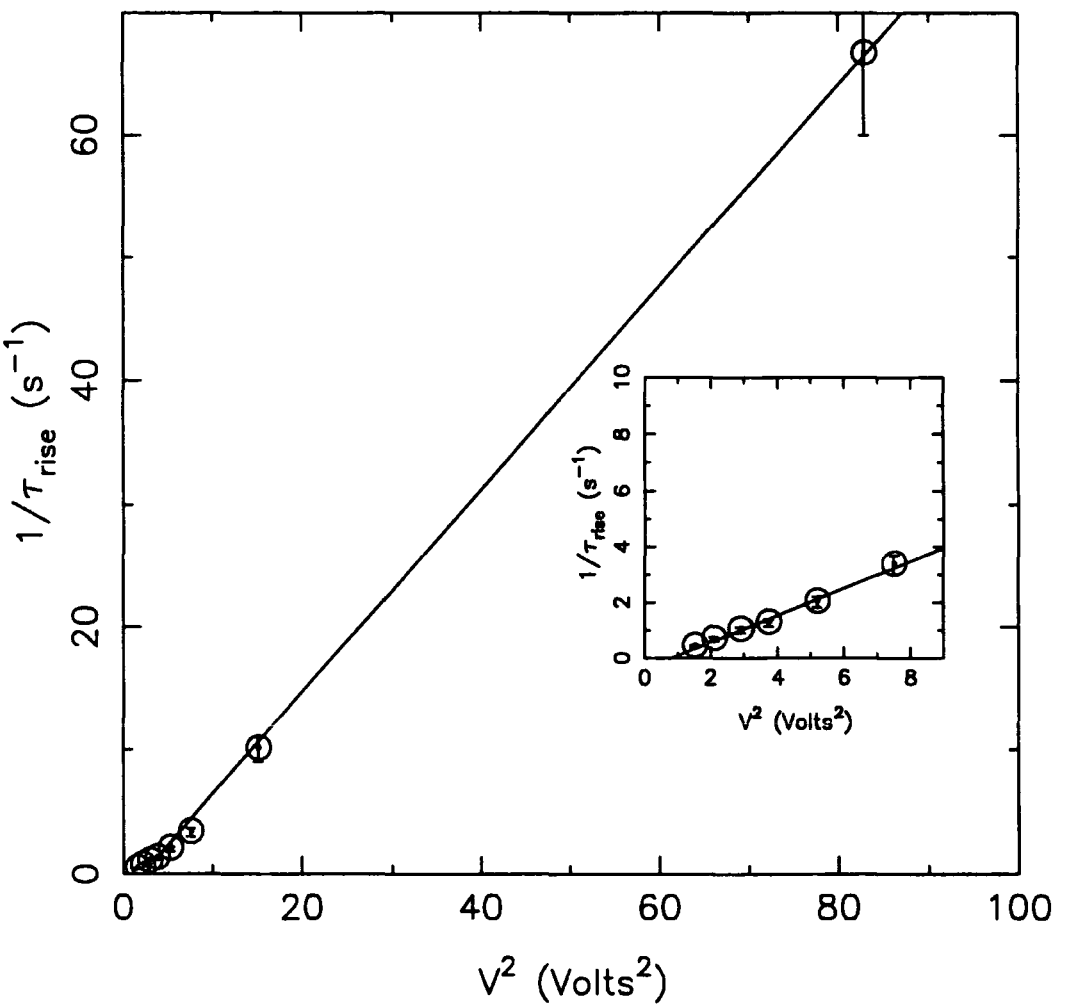

Figure 7.4: Switch-on times for a 10μm cell. The inset shows an expanded scale of the same graph. The straight line is a least squares fit to the points shown in each graph.

retardation of 4λ. On average the required phase retardation is much smaller, so a lower voltage is required which means a much longer rise time. For example a phase retardation of $\lambda/2$ (1.23V) corresponds to a rise time of 2.5 seconds. A possible solution to this problem is to apply a large voltage across the cell to rotate the molecules quickly, until the required phase retardation is reached, and then to apply the appropriate holding voltage. Measurements were made using SG2 and the triggerable attenuator, with the solid state switch being permanently switched to SG2. Figure 7.5 shows an example and the full results are shown in figure 7.6.

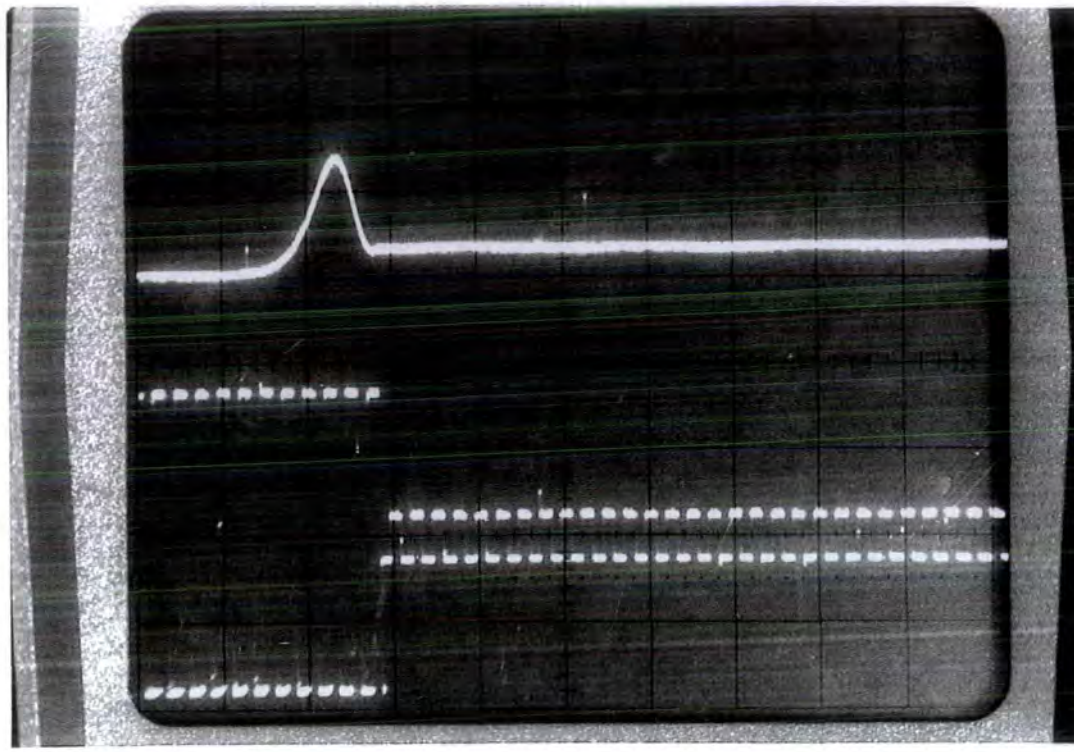

Figure 7.5: Improving the switch on time by applying a short high voltage burst. 10μm cell. 17V (pk-pk) for 14ms followed by a holding voltage of 2.6V (1KHz square wave) Timescale=5ms/div.

It can be seen that the switch-on times can be vastly improved for small values of phase retardation.

From the point of view of a LC prism it would be impossible to apply different pulse lengths to different parts of the cell so that each part of the cell switches on to the appropriate phase, however it would be possible to apply a voltage ramp across the cell for a fixed time interval, and then to switch to the holding ramp voltage.

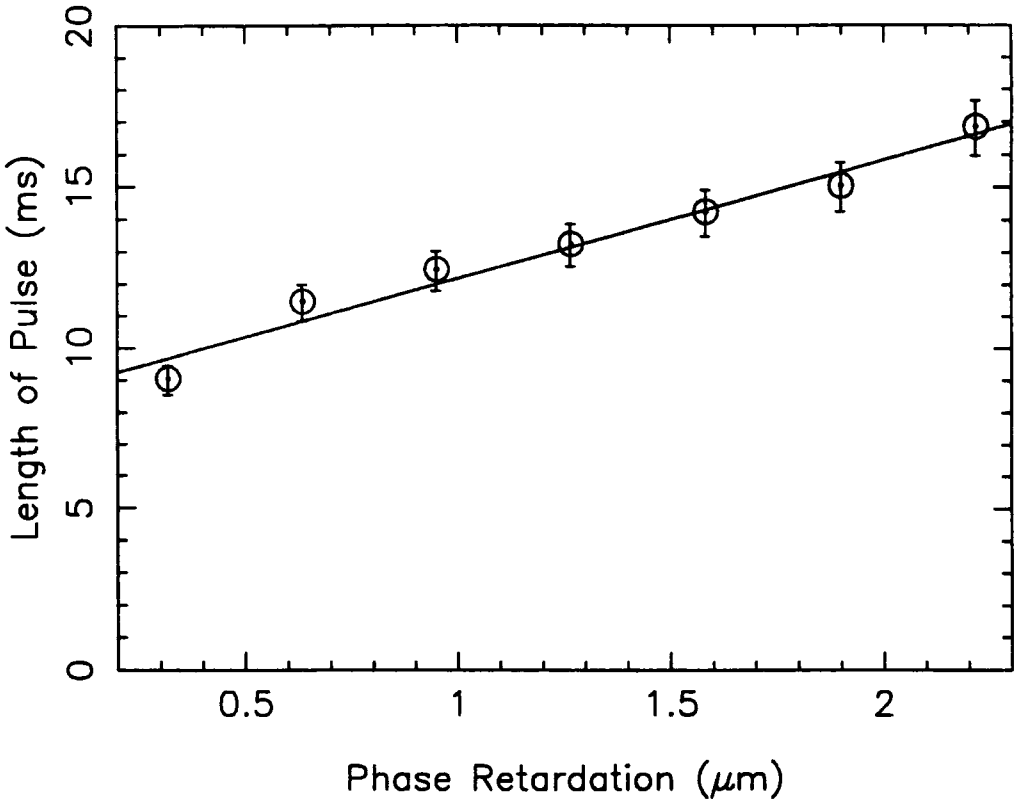

Figure 7.6: Length of voltage burst (19V pk-pk square wave, 1KHz) required to switch liquid crystal on. The solid line is a least squares fit. Cell thickness, 10μm.

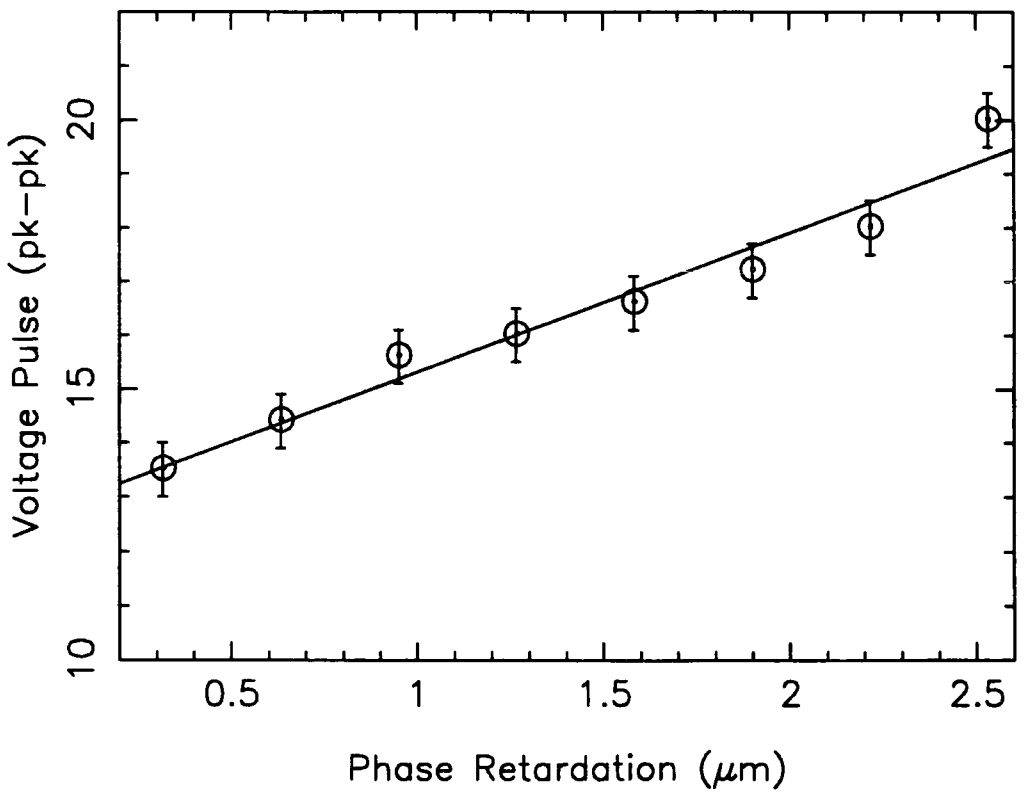

Figure 7.7: 18ms Voltage burst required to switch liquid crystal on. The solid line is a least squares fit. Cell thickness, 10μm.

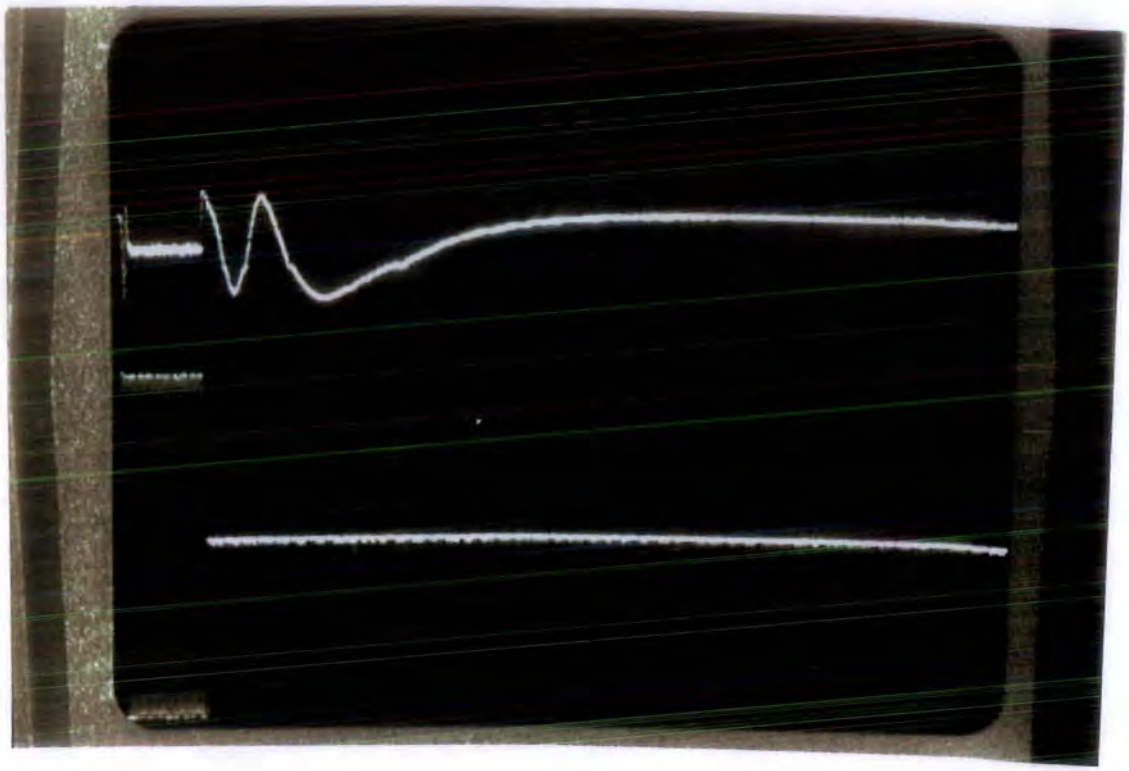

Figure 7.8: 5.6μm cell. 20V (pk-pk) 1KHz square wave burst for 50ms (time scale 50ms/div).

Some results are shown in figure 7.7. It can be seen that the voltage required is quasi-linear with phase retardation, as would be required.

These switch-on times ($\sim$ 18ms) are still not ideal. Measurements were made using larger voltages by amplifying the output of the signal generator with an audio power amplifier. The switch on time continued to decrease with increasing voltage, and a full switch on time of 0.2ms was achieved with a voltage of 120V (240V pk-pk).

7.3.2 Decay Time as a Function of Cell Thickness

As was mentioned at the beginning of this chapter, the cell thickness is an important parameter governing the response times. Cells were made of varying thickness by using different spacers[2] and their switch off times measured. Figure 7.8 shows an oscillogram taken with a 5.6μm cell. Notice that the switching times are faster, but that the dynamic range is less (shown by fewer pi-states). The full results are shown

[2]Thin cells are hard to make reliably because of the increased effect of contamination.

in figure 7.9. It can be seen that the switch off time for a 3μm cell is only 20ms, a huge improvement on the 10μm cell. However the dynamic range is much smaller being only about half a wavelength. Initially it would seem that a possible solution to improving the response times would be to use several thin cells sandwiched together so that the decay time was fast, and yet that the dynamic range is large enough. This is so; however simply plotting switch off times against thickness ignores much of the available information, as can be seen in the following sub-section.

7.3.3 The Transient Nematic and Bias Effects

Figure 7.10 shows change in optical thickness as a cell decays. Graphs (a) to (d) show the rates for differing cell thickness. The number of data points increases with cell thickness because more pi-states occur at which measurements can be made. If all the graphs are plotted on the same axes, as shown in 7.10(e), then it can be seen that the rate of change of optical thickness is approximately independent of cell thickness for small angled relaxation[3]. This fact is what is utilised in both the transient nematic effect and the bias (or surface) effect.

The transient nematic effect involves removing the field across a fully switched on cell so the molecules rotate quickly and then applying a field to hold the cell in the required state once the LC has relaxed by the required amount. In display devices, modulation times of a few milliseconds may be achieved. From figure 7.10(e) it can be seen that a switch off time, through 2π states (i.e. 1.27μm), of around 100ms can be achieved using the transient nematic effect. Figures 7.11 and 7.12 show two examples of cell modulation using the transient nematic effect. The voltages required were obtained by switching between the two signal generators, however the triggerable attenuator was adjusted so that after the time required for the 'high voltage' burst, SG2 was attenuated to a negligible level. In figure 7.11 the dynamic range is small and therefore the times are correspondingly short. The times shown correspond to a rate of about 40Hz (with a maximum possibility of about 60Hz). In figure 7.12 the dynamic range is larger and therefore the times are correspondingly slower. The times shown correspond to a rate of about 7Hz (with a maximum possibility of about 11Hz).

[3]Measurements of the decay rates of thick cells (30μm and 50μm) were made and the initial decay through 2π states was still $\sim$ 100ms.

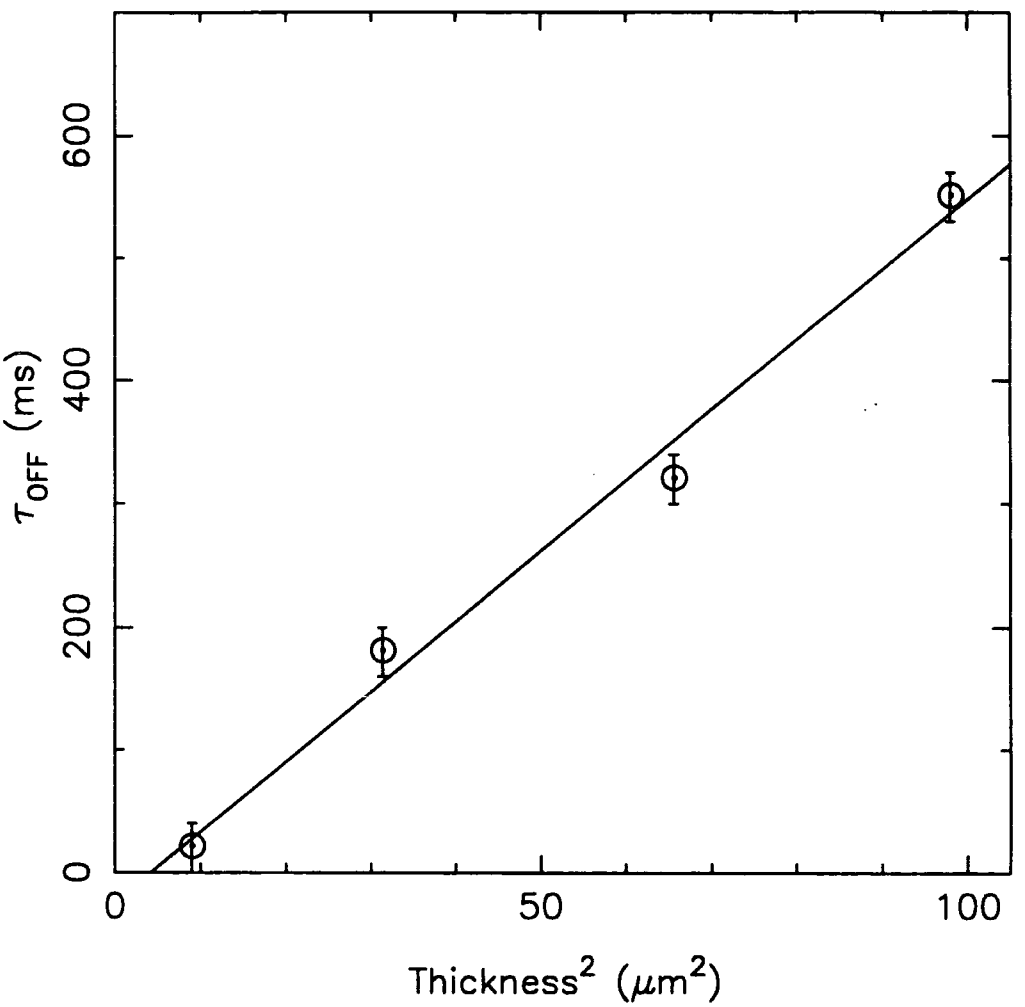

Figure 7.9: Effect of liquid crystal thickness on switch off time.

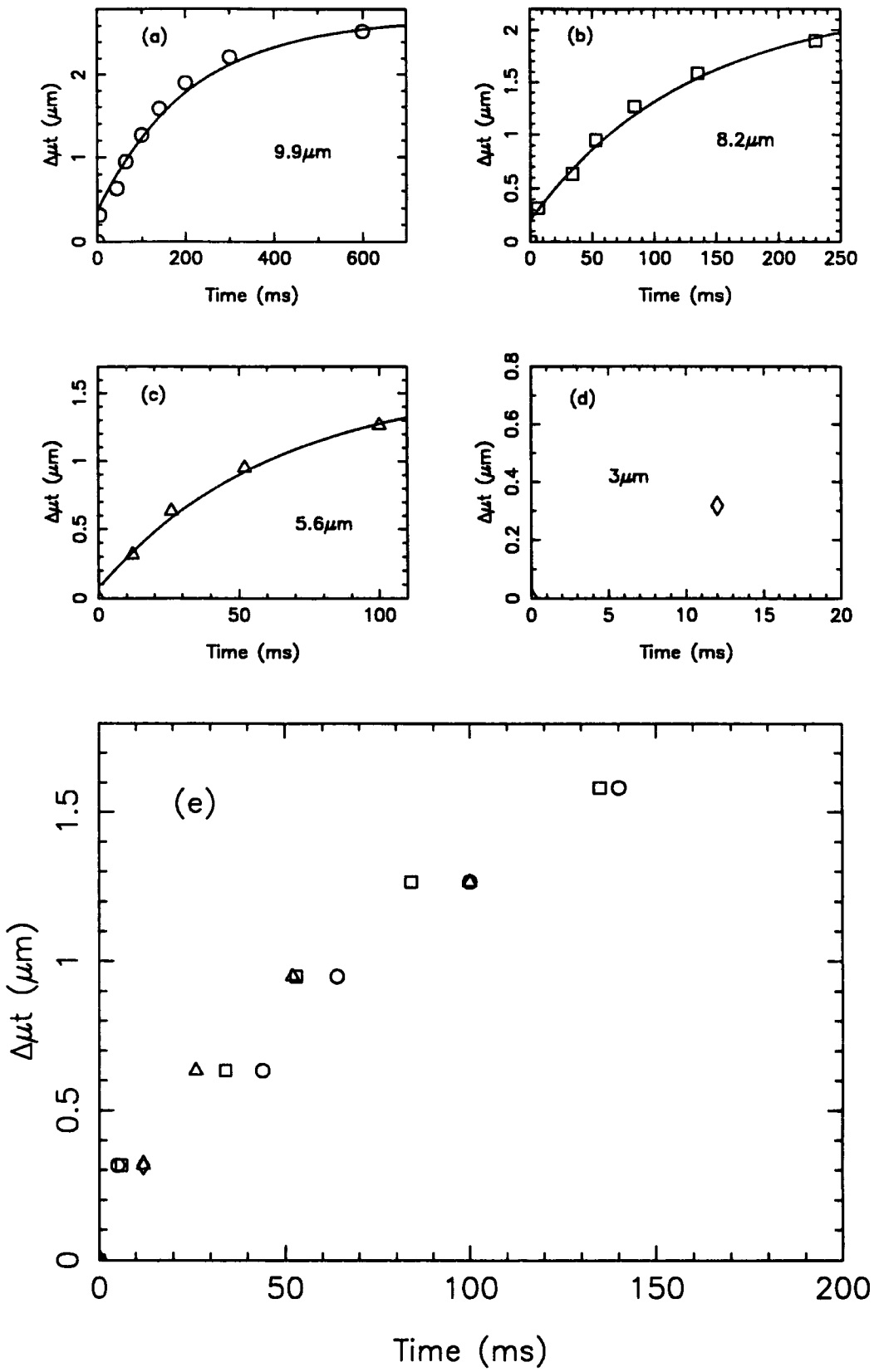

Figure 7.10: Switch off rate for differing cell thickness. The solid lines are for a guide only.

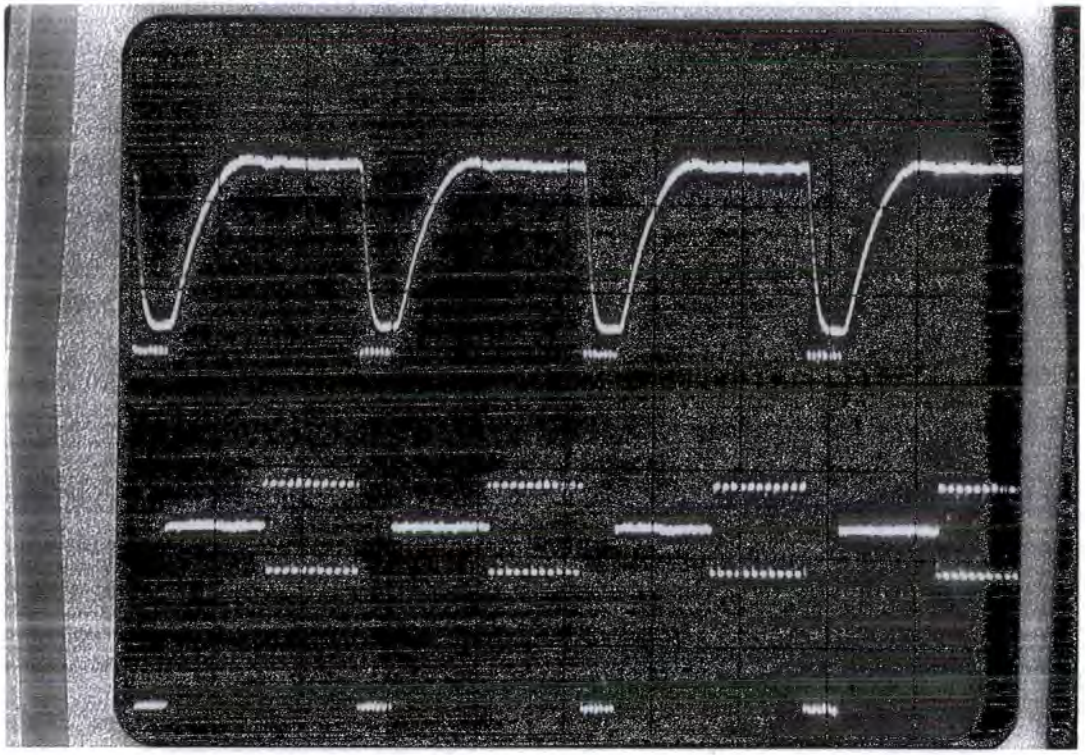

Figure 7.11: The transient nematic effect. 10μm cell. 20V for 4ms, 0V for 11.5ms, 5V for 10ms.Time scale 10ms/div. Dynamic range 0.32μm ($\lambda/2$).

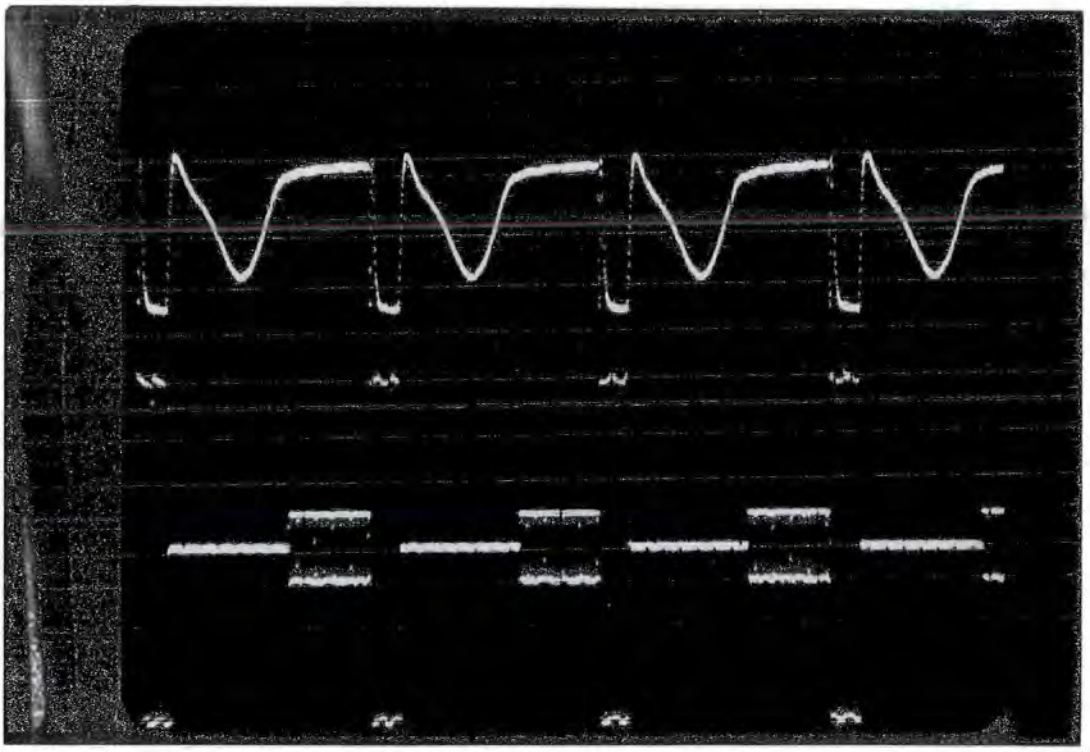

Figure 7.12: The transient nematic effect. 10μm cell. 20V for 17ms, 0V for 70ms, 4V for 50ms. Time scale 50ms/div. Dynamic range 0.95μm ($3\lambda/2$).

The bias or surface effect is very similar except that the holding voltage is applied immediately. This requires less driving electronics, however the decay is not as quick since some of the restoring force provided by the surface molecules is opposed by the holding field. Some results of LC decay times using the bias effect are shown in figures 7.13 and 7.14. The voltages were obtained by simply switching between the two signal generators without utilising the triggerable attenuator.

When only small relaxations occur then the bias effect gives similar decay times to the transient effect, however the decay time for a 2π relaxation is around 300ms, much longer than the transient nematic effect. However combining the transient nematic effect and the bias effect provides a possibility of switching a LC prism.

7.3.4 Controlling a LC Prism

A possible prism configuration for improved response times is to operate the cell so that the zero prism angle occurs when the cell is fully switched on across its whole length (i.e. the isotropic state) and then let the cell relax by varying amounts across the cell to produce a phase wedge. Consider the case where a phase ramp of height 2π is required. At one end of the cell the voltage is removed (for $\sim$ 100ms)so that the liquid crystal relaxes through 2π, and then the holding voltage is applied (transient nematic). At intermediate distances along the cell the voltage is reduced for the same time period, but the bias effect means that the cell will not relax so much. Figure 7.15 shows the voltage required to slow the relaxation to the required amount in 100ms. It is approximately linear which means that a voltage ramp may be used. At the other end no relaxation is required so that the full saturation voltage is maintained. Therefore in order to produce a phase wedge two voltage ramps are required. One to form the wedge, and the other to hold it. These are summarised for this particular example of a 2π phase wedge in table 7.1.

In this way a prism could be operated at a rate of $\sim$ 10Hz.

There are two apparent problems with this technique, namely phase wedge linearity and dispersion. In section 6.3.1 the linearity of the phase wedge was ensured by limiting the usable birefringence to a quasi-linear section, $\Delta\mu_e < 0.13$, and this also meant that the dispersion was low. Figure 7.16 shows figure 5.8 plotted so that

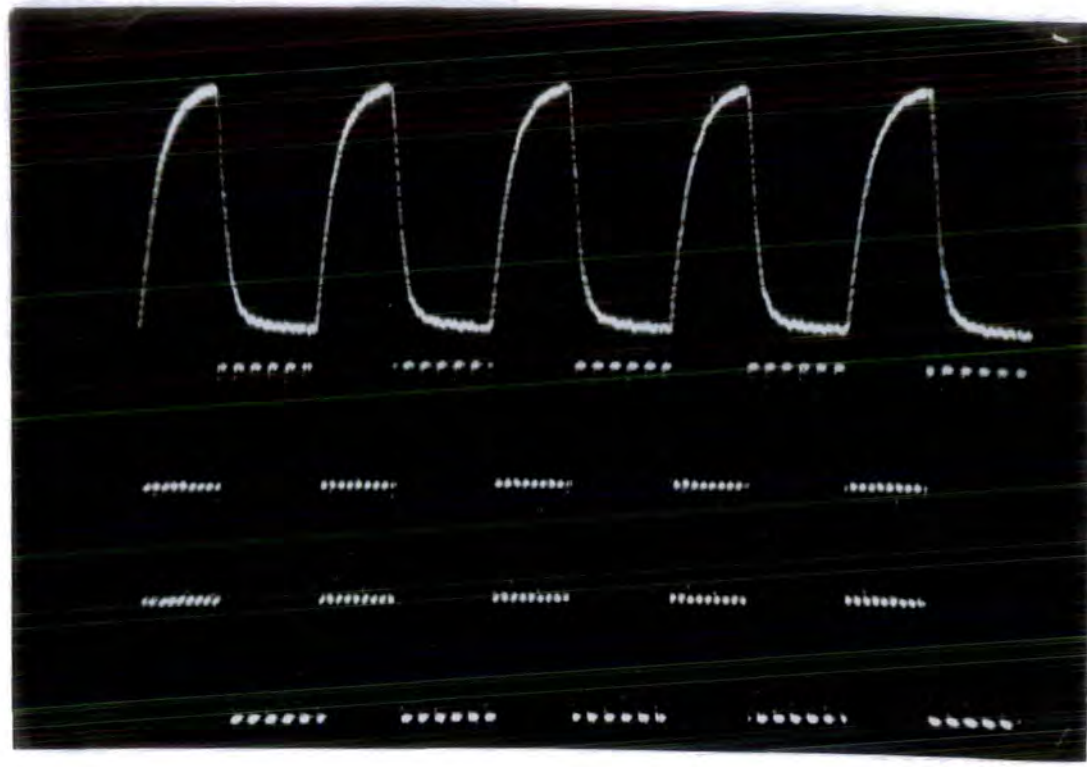

Figure 7.13: The bias effect. 10μm cell. 20V for 6ms, 0V for 4ms.Time scale 10ms/div. Dynamic range 0.32μm ($\lambda/2$).

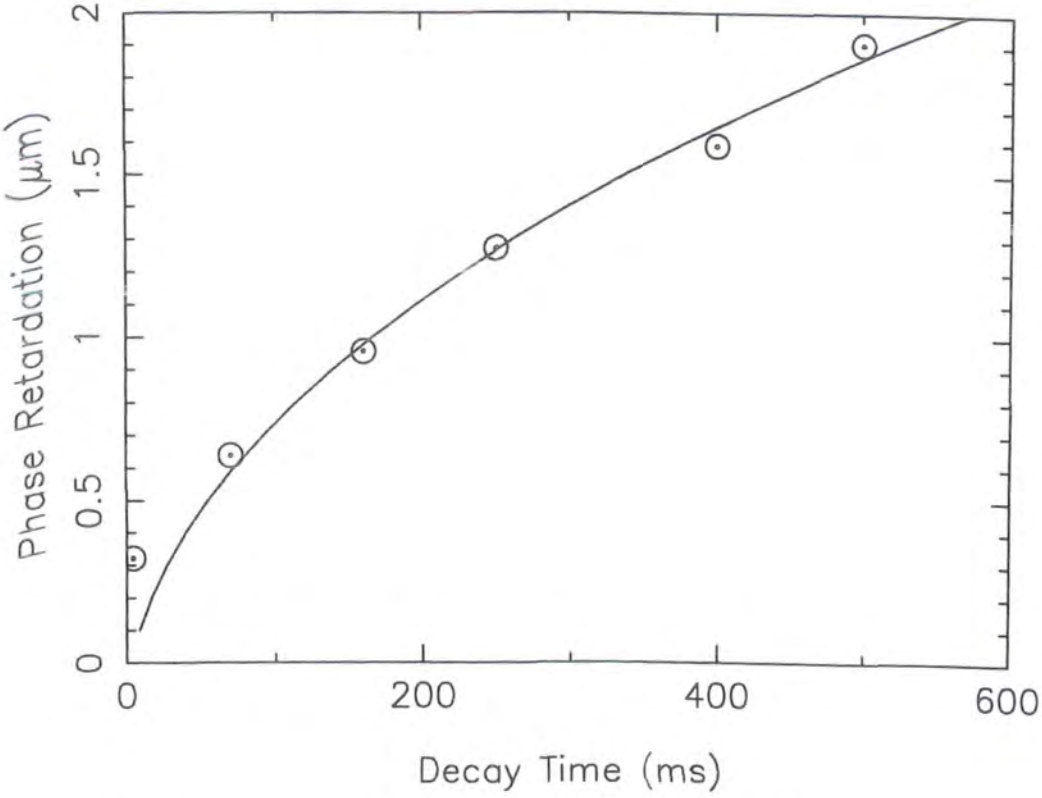

Figure 7.14: Decay times utilising the Bias Effect. The solid line is a guide only. Cell thickness, 10μm.

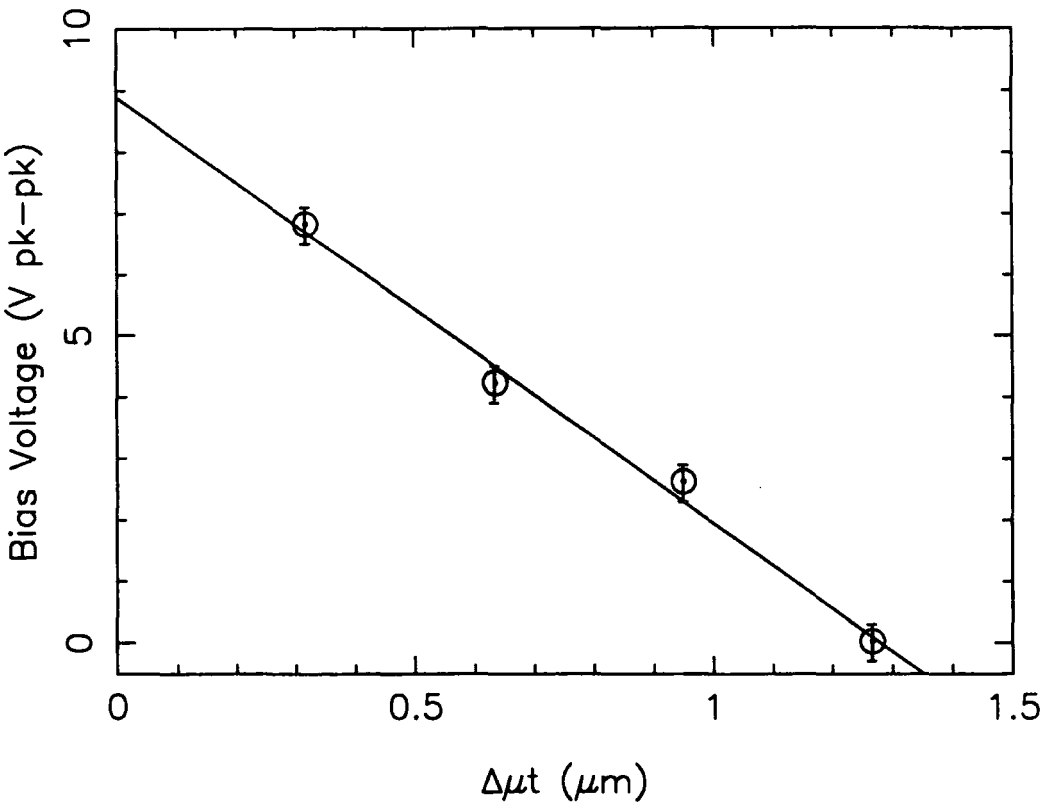

Figure 7.15: Voltage required using the bias effect to Cell thickness, 10μm.

Ramp Voltage	Duration	Prismatic State
LC Saturation Voltage 8.8V,0.0V 8.8V,1.5V $\sim 100V$ pulse	Required off-time 100ms Required on-time $\sim$ 1ms	Prism off. Prism switching on. Prism on Prism switching off

Table 7.1: Ramp voltages required to switch on a 2π phase wedge.

the zero line for $\Delta\mu_e$ is when the liquid crystal is fully saturated. It can be seen that the dispersion is 're-normalised' so that as long as only part of the birefringence is used then the the dispersion will be the same as that discussed in section 5.2.8. However there is still the linearity problem of $\Delta\mu_e$ against V. Figure 5.2.8 does exaggerate the problem because the lower (more negative $\Delta\mu_e$) parts of the graph would not be used, but it is nevertheless an effect.

7.3.5 Pi-Cells

In chapter 2 the pi-cell was mentioned along with the fact that the response time was faster than the anti-parallel rubbed cell. The reason for the improved relaxation times is the lack of *backflow* effects. In an anti-parallel aligned cell the molecular flow that occurs on relaxation is different on different sides of the cell and so re-alignment is mutually opposing. In a pi-cell the direction of flow when the cell is relaxing is the same for all parts of the cell, and therefore the relaxation is unimpeded. A 10μm pi-cell was made by rubbing the two glasses in the same direction. The free relaxation through 2π states was measured to be 17ms as shown in figure 7.17. This was however not perfectly repeatable. The pi-cell configuration is only quasi-stable and therefore the cell can revert to acting like an anti-parallel rubbed cell Recent results[4] indicate that problems of instabilities in pi cells have been solved so this would seem to be an attractive way forward.

7.4 Other Techniques for Improved Response Times

7.4.1 Dual Frequency Effect

This effect utilises the fact that in certain types of liquid crystal material, the sign of the dielectric constant (and hence the birefringence) is frequency dependent. Hence at one frequency of applied field, $\mu_e > \mu_o$ and at another frequency, $\mu_e < \mu_o$. This effect occurs because the liquid crystal molecules prefer to align with the director parallel to the electric field if the frequency is low, but prefer to align with the director perpendicular if the frequency is high[6]. The advantage of this is that

[4]Private discussions with RSRE Liquid Crystals Group[15].

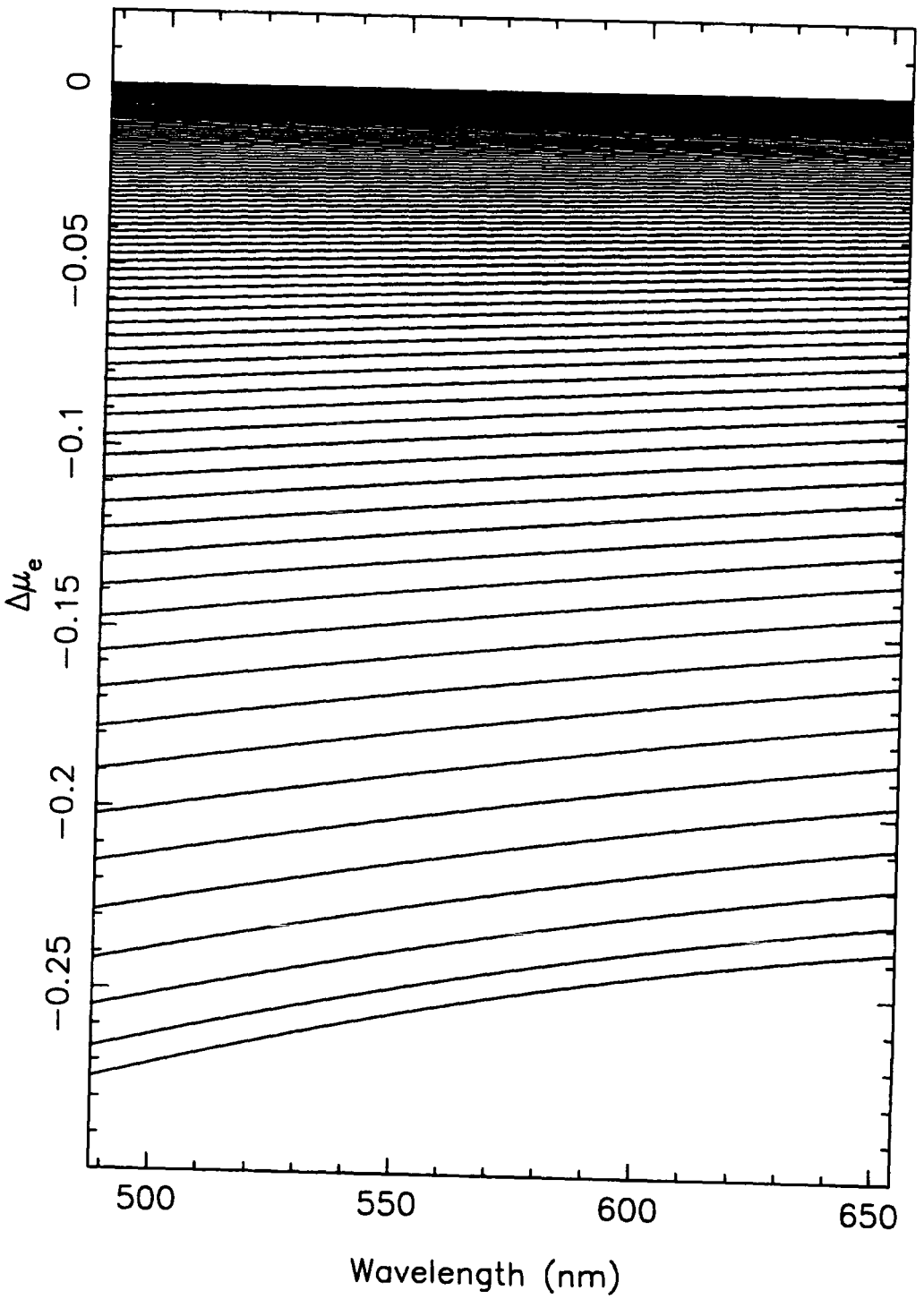

Figure 7.16: Birefringence dispersion of E44 for different voltages

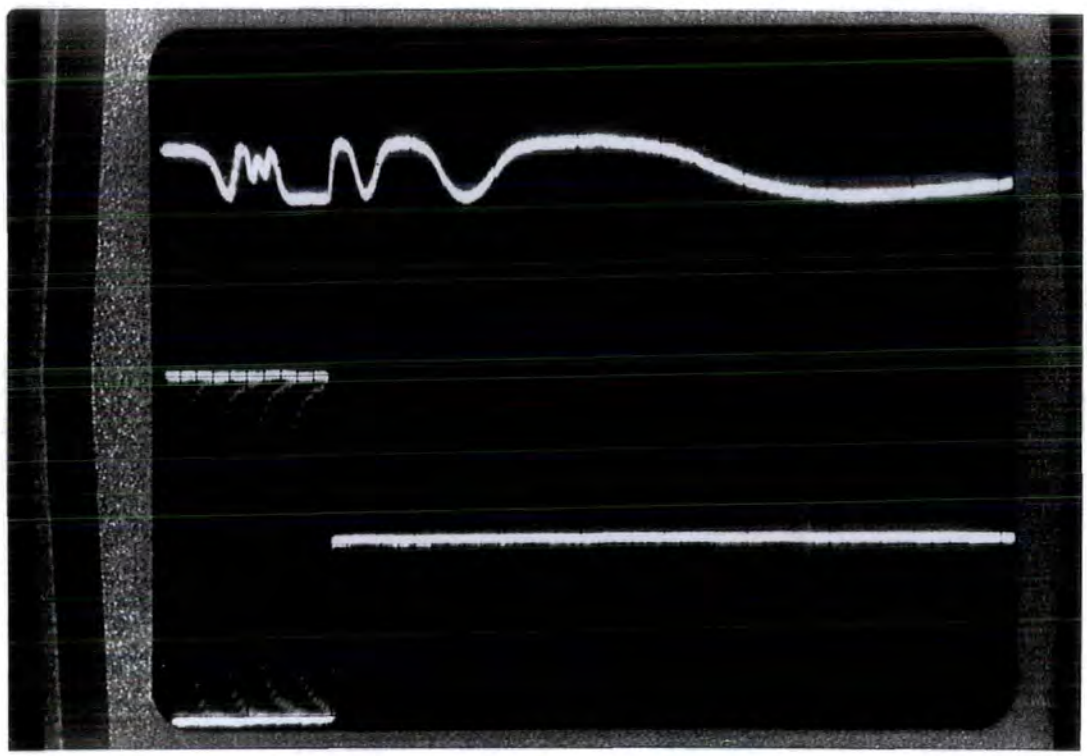

Figure 7.17: A 20ms 20V(pk-pk) 1KHz burst applied to a pi-cell. Time scale 10ms/div

the change of frequency of the applied field *drives* the molecular orientation in both directions. Hence the relatively weak alignment forces provided by the rubbing layer are not required. The effect is only manifest in certain liquid crystal materials (not BDH-E44). For example BONACCINI et al.[8] have demonstrated an (undefined) liquid crystal with a response time of $19.5\mu s^{-1}$ (this corresponds to a 2π phase shift in 65ms).

7.4.2 Ferroelectric Liquid Crystals

A different approach to improving response times involves the use of a different type of liquid crystal to a nematic. In 1974 MEYER et al.[43] realised that the smectic C liquid crystal phase ought to be ferroelectric, and in 1980 CLARK AND LAGERWALL[13] developed the Surface Stabilised Ferroelectric Liquid Crystal (SSFLC) which allows the smectic C liquid crystal to be utilised in a device. The (chiral) smectic C LC possesses a director which rotates in a cone in going from one smectic layer to the next. By using a thin cell (SSFLC) it is possible to produce a device with no rotation. The molecules have a net permanent dipole moment (ferroelectricity) and so by reversing the direction of the applied field the the LC can be made to switch between two states in less than a microsecond. However the device is binary and therefore only applicable to display technology and not the modulation of refractive index.

An effect which has potential for phase modulation is the *Electroclinic Effect* first reported by GAROFF AND MEYER[28]. Although not strictly a ferroelectric, the topic is generally discussed in the context of ferroelectricity because the Smectic A phase is formed in some chemicals by heating the smectic C phase, It utilises the smectic A phase to produce a cell where there is a direct coupling of the molecular tilt to the electric field. When an electric field is applied to a cell then the optical axis of the cell rotates[1], and therefore the refractive index that governs a particular polarisation state will also vary. There are however some problems. The chemicals used are in the smectic A phase at high temperature ($\sim 75°$ [3]), so the necessity of heating apparatus in the telescope dome is not an attractive one. The cells must be thin and the controllable birefringence is small so that the dynamic range is small. The transmission of the cells is also poor[15]. Therefore the problems appear to

currently outweigh the speed advantages of the electroclinic effect. However it is a relatively new phenomena so the future potential is unknown.

Chapter 8

Summary, Conclusions and Further Work

This thesis has aimed to answer some of the primary questions applicable to the use of liquid crystals for astronomy instrumentation. This chapter shall begin by summarising the results of each chapter separately, and then it continues by discussing the inter-dependance of the different liquid crystal parameters with respect to astronomical image sharpening. Finally some suggestions for further research are made.

8.1 Summary of Results.

The chapters 2 and 3 gave introductions to both liquid crystals and astronomical image sharpening. In chapter 4 it was shown that in order to correct a tilted wavefront, a realistic maximum prism angle of around 45 arcseconds is required that must have a cycle time of tens of milliseconds..

The Monolithic Prism

The basic design for a liquid crystal prism has been to use a single electrode structure along which a ramped voltage is applied. This is because it is a novel approach to addressing liquid crystals which has the main advantage of simplicity. Only 3 electrical contacts are required per prism. Section 4.3 showed, by means of a

calculation using the Huygens-Fresnel principle, that if a prism were to be made out of a number of segmented sections, then this would require at least 30 segments (and a similar number of electrical connections).

Monolithic electrode prisms were constructed to a very high degree of optical flatness, by using a mixture of industrial procedures and techniques perfected by the author.

Testing the Cell Homogeneity, Dispersion, Thickness and Voltage Characteristics.

These parameters are all ones for which measurement techniques are commonly available. However, each method has advantages and drawbacks. The common technique of measuring cell thickness requires the cell to be empty, and then to assume the cell's physical properties remain constant. In the author's experience this was not found to be so. From the point of view of image sharpening the exact cell thickness (and therefore the amount of correction provided) is not highly critical because of the very nature of the homeostasis principle behind adaptive optics, however from the point of view of making accurate measurements of, for example, the voltage characteristics the thickness is very important. The technique developed using Edser-Butler fringes provides a way of measuring cell thickness, homogeneity, dispersion, and the voltage characteristics in a way that gives applicable results. The refractive index over the whole spectrum can be measured without the use of many different spectral sources. Probably the most powerful attribute of Edser-Butler fringes is their sensitivity to changes in optical thickness. This allows an instant observational test of cell flatness (which is many times more accurate than the traditional method of observing wedge fringes) once a cell has been made, and allows very quick measurements of the voltage characteristics to be made. The technique is a quasi-imaging technique therefore the changes in optical thickness along different parts of the cell due to a ramped voltage can be seen. This thesis only contains actual results using Edser-Butler fringes, but their full usefulness can be seen in the laboratory where one is making qualitative judgements for most of the time.

The dispersion results indicate that the controllable refractive index variation

is quite wavelength dependent if the full dynamic range is utilised, however if the dynamic range is reduced then the dispersion is reduced.

Optical Quality

In section 5.3 measurements of the cell transmission and modulation transfer function were made. The cell transmission was found to be of the order of 70%. However most of this figure arises because a cell is a sandwich of different optical materials rather than because of any absorption within the liquid crystal. So this result is somewhat pessimistic and can be improved by anti-reflection coatings. The modulation transfer function was also measured, and within the bounds of experimental error there was no loss of image quality for spatial frequencies below that of the telescope diffraction limit. However even though the results indicate no apparent image degradation it would seem unlikely that the image quality after transmission by a liquid crystal cell would be as good as that of a highly polished mirror.

Dynamic Range of a Prism.

The controllable refractive index variation of BDH-E44 is about 0.26. Thus the dynamic range of a 10μm cell is 2.6μm. Equation 4.15 gives the angle of deflection, θ, of a LC prism as

$$\theta = \frac{\Delta\mu t}{W},$$

where t is the thickness and W is the length. Thus for a 10μm cell whose length is 1cm the prism angle would be 54″. However change in refractive index is not linear with voltage so in order to approximate to a linear phase wedge the usable refractive index variation is kept below 0.13. This gives a prism angle of 26″. In chapter 6 liquid crystal prism angles were measured using four different, complementary techniques. The measured prism angles were consistent with each other and with equation 4.15. The largest prism angle measured was $\sim$ 40″ for a 10μm $\times$ 7mm cell. A 7mm cell corresponds to an aperture of 54cm, which is a typical MARTINI sub-aperture size. If much smaller prisms were to be made in order to correct wavefronts of the size r_0 or less, then the amount of index variation necessary becomes much smaller for a given prism angle. This reduces dispersion and linearity problems.

Liquid Crystal Response Times.

Liquid crystal rise times are field dependent and can be made $\sim 1ms$ by applying suitably high voltages. However relaxation times are an inherent property of a liquid crystal cell and are slow (hundreds of milliseconds). This thesis has concentrated on two similar effects, the transient nematic effect and the bias effect, to improve switching times. Both utilise the fact that the liquid crystal molecules relax very quickly, at first, from a fully deformed state. Decay times of 11.5ms were measured for a 0.3μm stroke and 70ms for a 0.9μm stroke. Using a pi-cell configuration a decay time of 17ms was measured for a 0.9μm stroke.

8.2 Conclusions

All the results summarised in the last section indicate that any mode of liquid crystal operation should only utilise part of the controllable refractive index.

The dispersion effect is quite a small problem because in astronomy one is almost always concerned with using filters. Also there has been much discussion about the linearity of the wedges, this too is not such a critical parameter. It must be remembered that by correcting for wavefront tilt one is only approximating the wavefront over the particular diameter to a plane wave with some overall tilt. The actual wavefront is not a linear tilted wave. However, the problem of response times is still important and there is a definite trade-off between response times and dynamic range.

The first question to consider is what size of correction elements to use. One point to bear in mind is that some kind of wavefront sensor must be available to test the wavefront tilt over the appropriate area. In the MARTINI apparatus this is achieved with the split lens, but in the future a *Hartmann-Shack* (see e.g. TYSON[59]) array of microlenses will be used. These lenses can be made to be very small (~100's microns) but obviously they need to focus onto some kind of real-time imaging device (in MARTINI, the IPD). There must be enough room on the device to form the separate images, and very importantly there must be enough photons in each image in order to determine the centroid accurately. This limits the

brightness of the guide star used to test for the image motion and in turn limits the amount of sky-coverage[1] So it would seem reasonable that $4r_0$ correction will remain a suitable size in the visible spectrum. For a typical seeing parameter of 15cm, the $4r_0$ aperture size at the WHT conjugate focus is 7.8mm in size. A 10μm $\times$ 7.8mm cell using the transient nematic and bias effects would have a maximum prism angle of 26 arcseconds and a cycle rate of $\sim 10Hz$. By using a pi cell this rate could be improved to $\sim 50Hz$. By using a mirror backed cell to give a double passage through the cell then this would double the dynamic range to 52 arcseconds. These parameters are comparable with the necessary astronomical requirements.

A technique in image sharpening that has not yet been considered is called *co-phasing*. If simply the tilt across each sub-aperture is removed then the light from each is added incoherently to produce the final image. The size of the best image is limited by the size of the sub-apertures. If however each sub-aperture is co-phased so that the phase difference between each sub-aperture is corrected for then the light adds together coherently. The best possible image is then limited by the largest possible aperture spacing (i.e. approximately the full 4.2m aperture). In this case it is just piston that needs to be removed between apertures, however the amount is quite large. From equation 4.4 then the r.m.s wavefront error over the the full aperture will be 1.3μm for $r_0 = 15$cm. When the tilt over the sub-apertures has been corrected for then the amount of r.m.s piston required is$\sim 1\mu$m. So in order to contain a 3σ variation in both directions a piston range $\sim 6\mu$m is required. This is a very large figure and although liquid crystals should be capable of this by making thick cells, the response times would become very long. This is a problem that even mirror technology encounters. A solution to this (as mentioned in section 3.2.2 with respect to the ESO COME-ON project) is to use a two-stage correction process whereby the tilt is removed across the whole aperture using a single tip-tilt mirror and then smaller scale corrections are subsequently made. If the tilt across the whole aperture is removed then the residual mean square wavefront error is given by (see section 4.2.2)

$$\sqrt{\langle|\Delta\phi|^2\rangle} = 0.134\left(\frac{D}{r_0}\right)^{\frac{5}{3}}. \tag{8.1}$$

The r.m.s required correction for this is now only 0.5μm. However some of this will be corrected for by the $4r_0$ tilt removal so that the residual will be $\sim 0.3\mu$m. Again

[1]The amount of sky near enough to a bright enough star. In MARTINI the magnitude limit is $\sim 13^{mv}$ which gives a sky coverage of $\sim 3\%$.

taking the 3σ variation in both direction requires a piston movement of 1.2μm, or if the device is mirror backed, then 0.6μm. It would seem logical to combine the overall tip-tilt mirror with the mirror that gives a double-pass through the liquid crystal. The timescales required for co-phasing are also longer than that for sub-aperture correction because variations over the whole aperture occur at a slower rate (see section 4.2.3).

It may become desirable to correct the wavefront on a scale of r_0. In this case prisms of size 1 or 2mm are required [2]. A 1mm prism requires a stroke of only 0.15μm to give a prism angle of 30 arcseconds, and so for a 10μm cell this means there would be no dispersion or linearity problems. By utilising the transient nematic effect and the bias effect then such a cell should be operable at 40Hz and a pi-cell at much higher rates. The full 4.2m WHT aperture would require about 3000 correcting elements for complete coverage, however this number is very small in terms of current liquid crystal technology[3]

The following list indicates some pertinent points not yet discussed.

- At the present time adaptive mirror technology is much further advanced than the relevant liquid crystal technology, especially with the recent declassification of the US military research. However adaptive mirror technology is very much state-of-the-art and with the present cuts in military research it seems unlikely to develop with so much ferocity as in the past. In comparison the use of liquid crystals as optical control elements is a new field, especially with respect to astronomy. It would seem that a revolution in display technologies is taking place and this highly commercial field is driving research at a rapid rate. Thus although there are still problems at the moment no one can say what advances

[2]The smallest prism demonstrated in this thesis was 7mm in length, so by discussing 1mm prisms assumptions are being made. However it would seem likely that a 1mm prism should pose no extra problems. Results made by the author of liquid crystal fringing fields (i.e. the liquid crystal being affected by neighbouring electrode areas) for liquid crystal diffraction gratings using a variation of the Jamin interferometer (section 6.2.1) for POWELL et al.[48], indicate that fringing fields have an effect only over distances $\sim 10\mu$m. One potential problem when using very small prisms is the resistance of the ITO. High resistance ITO must be used otherwise joule heating will occur.

[3]For example Canon Inc. have made a liquid crystal television with 1280 x 1120 elements (LAGERWALL et al. [40]) in a 14inch diagonal format. Scaling this down to the size required for adaptive optics yields 80,000 elements. This technology is obviously different from that required for astronomy, but it serves to make a comparison and shows that microfabrication techniques are already far in advance of what would be needed for astronomical devices.

Advantages	Disadvantages
Low cost Low power consumption Large number of correcting elements Reliable No hysteresis A rapidly expanding technology	Not perfect Optical Quality Transmission poorer than mirror Dispersion poorer than mirror Relatively slow

Table 8.1: A summary of liquid crystal attributes.

will be made within the next decade.

- A problem with mirror technology is that the piezo-electric actuators suffer from hysteresis. This needs to be accounted for in the software controlling the supply voltages. Liquid crystals do not suffer from any noticeable hysteresis.
- Reliability. In an array of piezo-actuators it is likely that one of them will malfunction from time to time. It becomes difficult and expensive to replace one element in a highly compacted array. Liquid crystals appear to be very reliable solid state devices.

To conclude: liquid crystals provide potential for wavefront correcting elements. They provide phase controllability of the size required in astronomy, however there are some problems, particularly with the speed of operation. These capabilities and limitations are summarised in table 8.1. This thesis has suggested some solutions using existing technology, but much work needs to carried out before liquid crystals could be incorporated into an actual adaptive optics system. By this time it would seem likely that the specification of devices will have progressed. So, liquid crystals provide an attractive avenue of research for adaptive optics elements for the next generation of very large telescopes.

8.3 Further Work

The first step is to actually demonstrate that prisms are capable of operating at the speeds that have been discussed in the previous section. This will require the construction of a complex power supply to provide the appropriate voltages.

8.3.1 A Tip-Tilt Liquid Crystal Prism

All the results in this thesis have been for prisms that only deflect light in one dimension. To remove wavefront tip and tilt then a two dimensional prism arrangement is required. With the monolithic electrode structure this should be achieved in a reasonably straight forward fashion by applying a voltage ramp along each cell direction so that the resultant optical thickness distribution can be varied in two dimensions. The mathematics of the resultant of both tip and tilt is discussed in appendix E.

The voltages required at each contact then become much more complicated so it would seem reasonable to interface the power supply unit to a computer to calculate the precise voltages needed. This in turn will need more complete results of the bias voltages required so that the voltages across the active area of the cell are correct.

8.3.2 Phase Modulating Un-Polarised Light with Liquid Crystals

The nature of LC birefringence means that any electrical control of the liquid crystals extraordinary index will only affect one polarisation state of light. The obvious solution to this is to use two devices with orthogonal rubbing directions so that each will modulate different polarisation states.

The following design is for a liquid crystal modulator that would function with unpolarised light, shown in figure 8.1 The principle is to fabricate a cell with different areas having orthogonal rubbing directions, and hence orthogonal crystal axes. The device would be set up such that light is incident at an angle. The light would be transmitted through the cell with the relevant polarisation state being modulated by

the extraordinary index. The light then is transmitted through an isotropic substrate before being reflected by a mirror and back through the device. By carefully choosing the dimensions it can be arranged that the light passes through areas of the cell with orthogonal crystal axes on each pass through the liquid crystal. Therefore light polarised so that it is governed by the extraordinary index on its first pass is governed by the ordinary index on its second, and vice versa. For example a 10μm layer of liquid crystal, backed by a 50μm layer of isotropic substrate, and an angle of incidence of 45° would require a spacing of areas of orthogonal rubbing directions of 100μm. This can be achieved[4] by first rubbing the whole cell in one direction. A protective layer is then applied to the PVA and then etched away to produce the required pattern. The cell is then rubbed in the other direction. The areas of un-protected PVA are re-directed. Finally the rest of the protective layer is etched off. There are however a few disadvantages of this proposed technique. Firstly, even

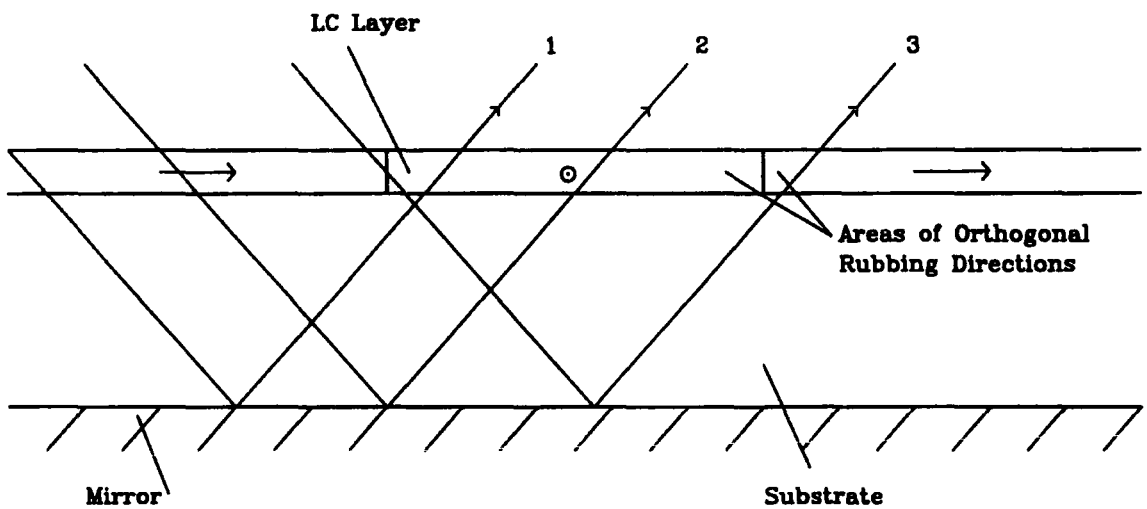

Figure 8.1: Principle of Operation of a LC Cell with unpolarised light. For clarity, the PVA and ITO layers have been omitted

though it is a double-pass device, the light is only modulated as if it had passed a single time through the cell. This is partially compensated for by the fact that the light is incident obliquely and so the path length through the liquid crystal is increased. Secondly there are some errors at the rubbing boundaries. For example in the diagram ray 3 passes through a boundary and so the two polarisation states will experience differing amounts of modulation. For the parameters above, 20% of

[4]Patented by AT&T Bell Laboratories, Holmdel, New Jersey, USA

the light would experience an average error of 50% in modulation. This value can be reduced by increasing the isotropic substrate thickness, and hence the spacing of the areas of differing rubbing direction. Another problem of the technique is that different polarisation states are phase retarded by different parts of the cell, so the technique is not so suitable for prisms devices where the refractive index is ramped, however this is no problem where simple piston control is required, for example in section 3.3.1. The design provides an interesting potential solution to an inherent problem of liquid crystals.

Appendix A

Optical Positioning of an Adaptive Optics System.

All the calculations in this thesis have assumed that the liquid crystal prisms are placed at the conjugate focus to the seeing. This is to optimise the area of the isoplanatic patch. The position of the conjugate focus determines the magnification of the telescope and hence the required correction angles.

If the image from a star is corrected, then the area around that star that is also corrected is termed the isoplanatic patch. It is a measure of the similarity between the seeing induced distortions of wavefronts coming from different sky directions. By assuming a simple seeing model, whereby all the turbulence contributing to the wavefront distortion occurs at a height h above the telescope, it can be seen from simple ray tracing (see figure 5.11) that light coming from differing angles that passes through the same part of the turbulent layer recombines as it passes through the conjugate focus. As the adaptive optics are moved away from this point then the isoplanisity decreases. Of course the atmospheric turbulence does not occur at a single height, but is an summed effect of the whole through the whole of the atmosphere, however an average height $\overline{h}$ of seeing may be defined (see RODDIER [50]) as

$$\overline{h} = \left[\frac{\int_0^\infty h^{\frac{5}{3}} C_N^2(h) dh}{\int_0^\infty C_N^2(h) dh} \right]^{\frac{3}{5}} . \tag{A.1}$$

Calculation of $\overline{h}$ then requires the vertical distribution of C_N^2. Models and measurements have been made (BARLETTI et al. [5] and HUFNAGEL [33]), however any results for $\overline{h}$ calculated therefrom are subjective and very dependant on the partic-

Telescope	focus	f/ratio	Aperture	Magnification	Average Correction Angle for $4r_0 = 15$cm
WHT	Cassegrain	f/11	4.2m	77	6.7″
"	Nasmyth	f/11	"	77	6.7″
INT	Cassegrain	f/15	2.5m	95	8.3″
JKT	Cassegrain	f/15	1.0m	239	20.9″
CFHT	Coudé	f/20	3.6m	49	4.3″
"	Cassegrain	f/8	"	124	10.8″
ESO-VLT	Nasmyth	f/15	8.0m	29	2.4″
"	Coudé	f/74	"	5	0.4″
"	Cassegrain	f/13.3	"	33	2.9″
UKLT	Cassegrain	f/7	8.0m	63	5.5″
"	"	f/15	"	29	2.5″
"	"	f/35	"	12	1.0″

WHT - William Herschel Telescope [60]
INT - Isaac Newton Telescope [60]
JKT - Jacobus Kapteyn Telescope [60]
CFHT - Canada-France-Hawaii Telescope [57]
ESO-VLT - ESO Very Large Telescope [47] (in design)
UKLT - UK Large Telescope [2] (in design)

Table A.1: Magnifications of various telescopes assuming an average height of seeing of 3.6km

ular seeing conditions. A reasonable figure for $\overline{h}$ seems to be several kilometres.

The second factor that determines the telescopes magnification is its focal length. The magnification factors of some of the important telescopes are given in table A.1 along with the average correction angle required to correct the tilt over a $4r_0$ (60cm)aperture (from equation 4.1). The magnifications are calculated from the effective focal length, the simple mirror equation, and by assuming an average height of seeing of 3.6km. It can be seen that there is quite a wide range of magnifications[1], for example the Coudé visible focus of the ESO-VLT would require very small angular corrections, whereas the JKT would require maximum deflections of over an

[1]This table is shown for comparisons only. The different foci and telescopes shown are not necessarily suited to the accommodation of an adaptive optics system

arcminute. Notice that the WHT magnification is approximately an 'average' value. It should be noted that the above argument is only relevant to angular corrections. Any 'piston' error is not altered by the telescope optics.

Appendix B

Prism Driver Circuit

Circuit diagram of the device used to provide the correct voltages to the static prism as described in chapter 6

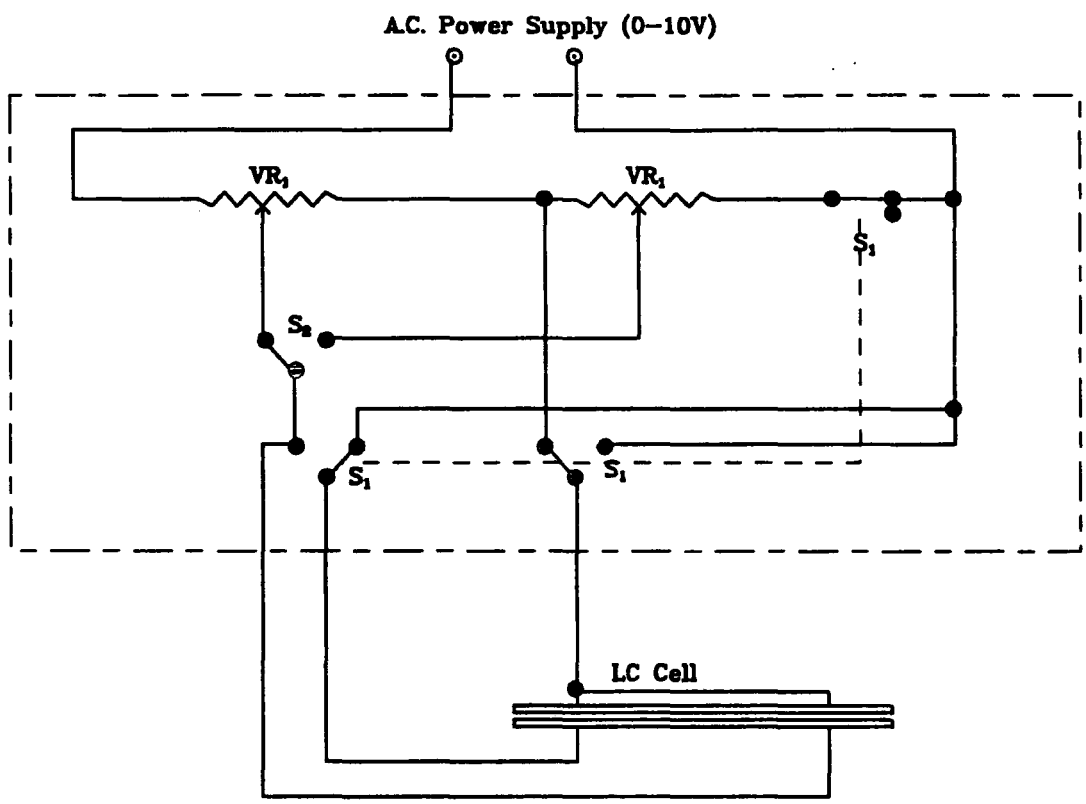

VR1 50Ω 1W wirewound
VR2 50Ω 1W wirewound
S1 triple pole double throw switch
S2 single pole double throw switch

In adition to the circuit shown, there are also connections to supply a multimeter with the voltages applied to the LC cell.

S_1 switches between *Prismatic Mode* and *Normal Mode*. In Prismatic Mode the volages are applied such that the LC cell behaves as a phase wedge and in Normal Mode no voltage ramp is applied, there is just a uniform voltage applied across the cell. In the configuration shown in the diagram the circuit is set to Prismatic Mode.

S_2 switches between negative and positive bias at the lower end of the voltage ramp. In the configuration shown a negative bias voltage is applied. If no bias is required then the wiper of the potentiometer, VR_1, is set to the far right.

The circuit is contained in a case as shown by the dash-dotted line. Connection to the LC cell is made via a 3-pin DIN socket.

Appendix C

Solid State Switching Circuit

Circuit diagram of the device used to switch between signal generators as described in chapter 7.

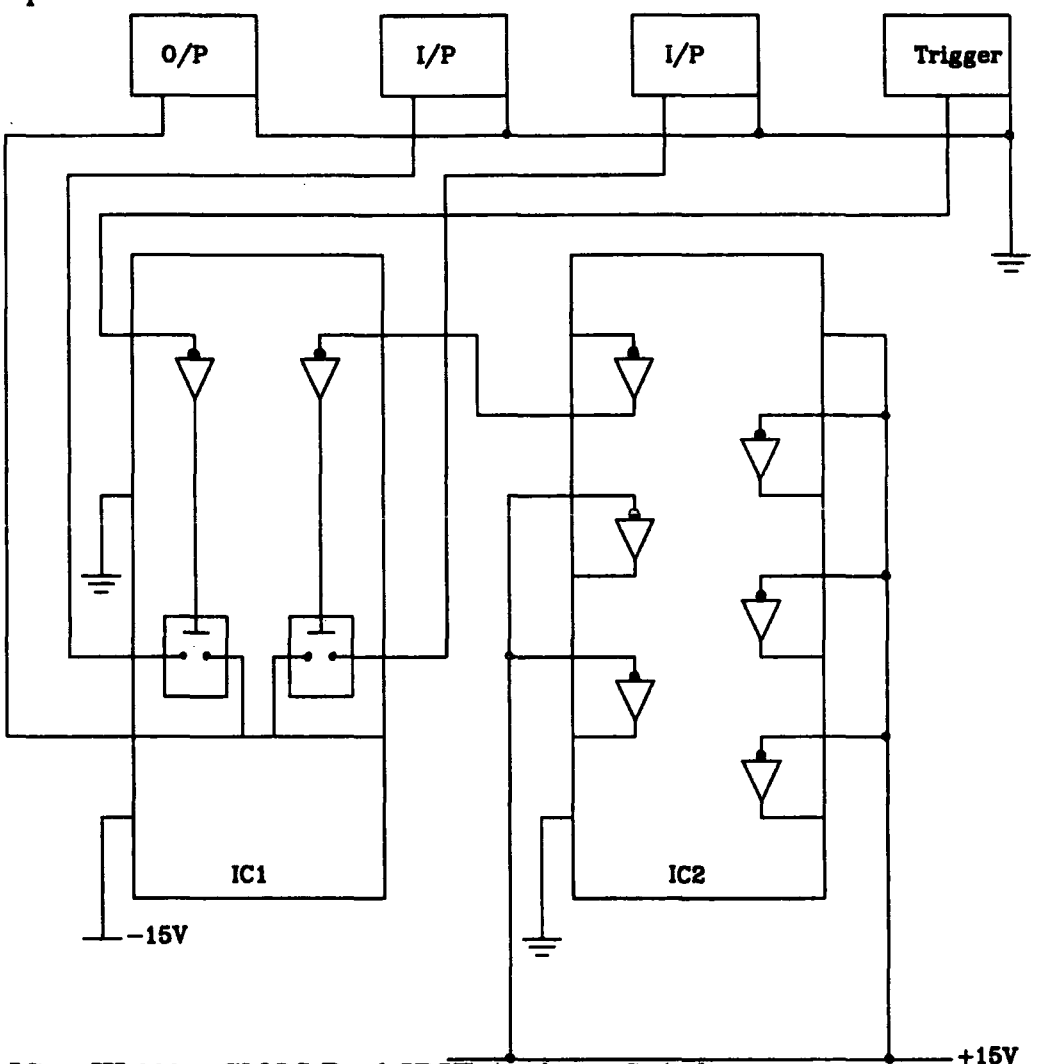

IC1 HI-200-5 CMOS Dual SPST Analogue Switch
IC2 4069 Hex-invertor

Appendix D

Triggerable Attenuator Circuit

Schematic diagram of the device used to attenuate the signal from the signal generator as described in chapter 7.

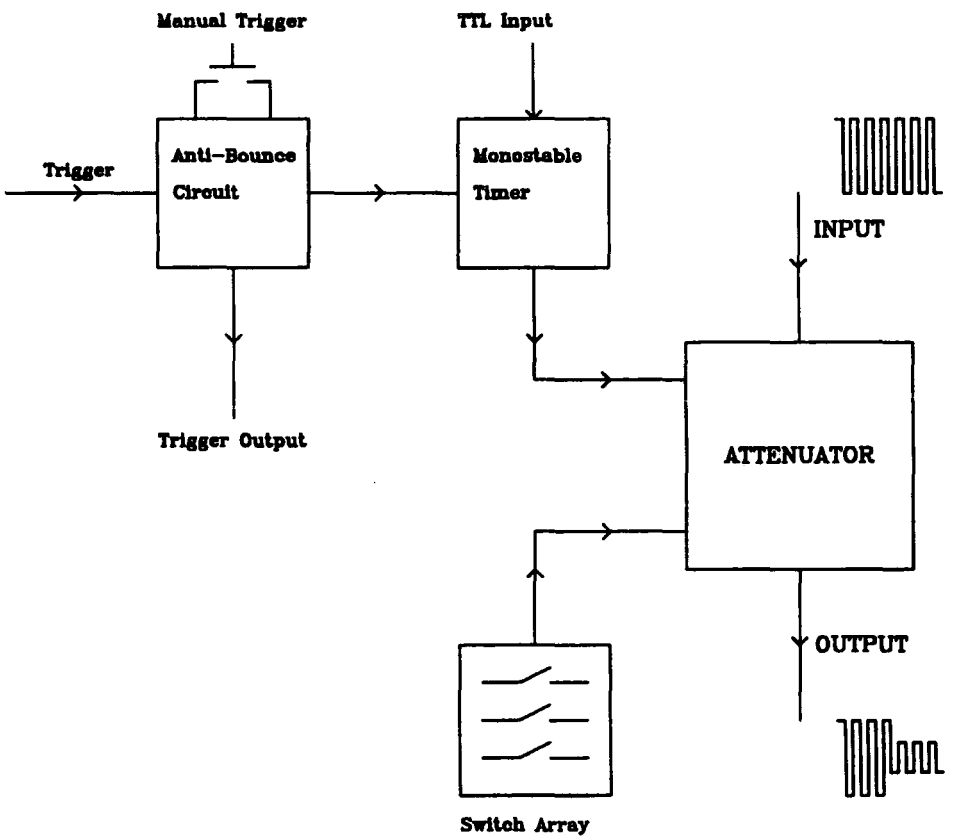

The circuit is based upon an AD7110 audio attenuator chip. The amount of

attenuation can be varied from 0 to 88 dB in discrete amounts controlled by the array of switches. The circuit is triggered from the pulse generator. After a controllable time (5 to 50ms) the timer switches the attenuator on. The circuit can be triggered manually by a push switch and an anti-bounce circuit.

Appendix E

The Resultant of Both Tip and Tilt.

The following calculation shows the resultant angle of a plane that is at arbitrary angles to both primary axes.

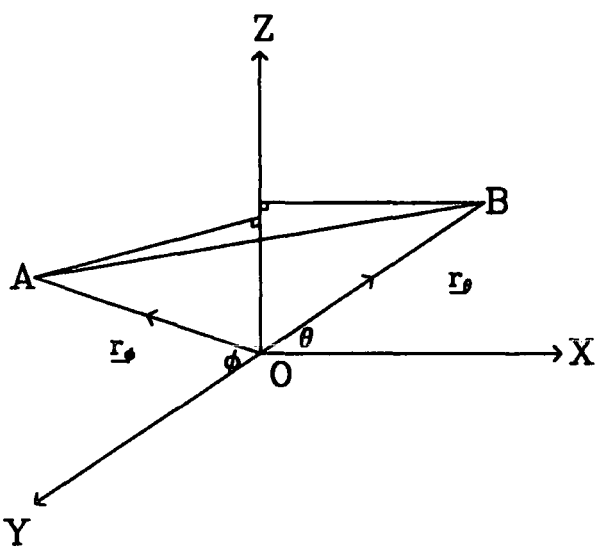

Figure E.1: A plane, P, defined by the triangle AOB, at an angle θ to the X-axis and ϕ to the Y-axis.

Consider a plane, P, that is tilted at a principle angle, ψ, to the Z=0 plane. Let the angles of tilt with the Z=0 plane in the X and Y directions be θ and ϕ, respectively. Let these angles define two unit vectors, $\underline{r}_\theta$ and $\underline{r}_\phi$ in the Y=0 and X=0 planes respectively. These are shown in the above figure. Thus P is defined

by the triangle AOB. If the three primary unit vectors are $\hat{\underline{i}}$, $\hat{\underline{j}}$, and $\hat{\underline{k}}$, then

$$\underline{r}_\theta = \cos\theta\hat{\underline{i}} + \sin\theta\hat{\underline{k}}, \tag{E.1}$$

and

$$\underline{r}_\phi = \cos\phi\hat{\underline{j}} + \sin\phi\hat{\underline{k}}. \tag{E.2}$$

Since both these vectors are contained within P then the vector product of these, $\underline{n}$ must, by definition, be a unit vector normal to P.

$$\underline{n} = \underline{r}_\theta \times \underline{r}_\phi = -\sin\theta\cos\phi\hat{\underline{i}} + \cos\theta\sin\phi\hat{\underline{j}} + \cos\theta\cos\phi\hat{\underline{k}}. \tag{E.3}$$

This vector will be at an angle, n_ψ to the Z=0 plane where

$$n_\psi = \arcsin(\underline{r}_\psi.\hat{\underline{k}}). \tag{E.4}$$

However $\psi = 90° - n_\psi$ therefore

$$\underline{\cos\psi = \cos\theta\cos\phi}. \tag{E.5}$$

The azimuthal angle, δ, of $\underline{n}$ (and hence P) is given by

$$\delta = \frac{\underline{n}.\hat{\underline{i}}}{\underline{n}.\hat{\underline{j}}} \tag{E.6}$$

or

$$\underline{\delta = \frac{\sin\theta\cos\phi}{\cos\theta\sin\phi}}. \tag{E.7}$$

Small-angled approximation.

By taking the small angled approximation, $\cos\theta = 1 - \frac{\theta^2}{2}$ and ignoring terms greater than second order then it can be shown that equation E.5 reduces to the following.

$$\underline{\psi^2 = \theta^2 + \phi^2}. \tag{E.8}$$

Bibliography

[1] G Andersson, I Dahl, P Keller, W Kuczyński, S T Lagerwall, K Sharp, and B Stebler. Submicrosecond electro-optic switching in the liquid crystal smectic a phase: The soft-mode ferroelectric effect. *Applied Physics Letters*, 51(9):640, 1987.

[2] E Atad, J W Harris, and C M Humphries. Optical design and imaging performance of the UK large telescope - part 1. Technical Report Report No. 13, Royal Observatory Edinburgh, Royal Observatory, Blackford Hill, Edinburgh EH9 3HJ, September 1990.

[3] C H Bahr and G Heppke. Optical and dielectric investigations on the electroclinic effect exhibited by a ferroelectric liquid crystal with high spontaneous polarisation. *Liquid Crystals*, 2(6):825, 1987.

[4] J E Baldwin, R C Boysen, C D Mackay, P A G Scheuer, P J Warner, R V Willstrop, and D M A Wilson. Cambridge optical aperture synthesis telescope. Technical report, Mullard Radio Astronomy and Institute of Astronomy, 1987.

[5] R Barletti, G Ceppatelli, L Paterno, A Righini, and N Speroni. *Journal of the Optical Society of America*, 66:1380, 1976.

[6] H K Bűcher, R T Klingbiel, and J P VanMeter. Frequency-addressed liquid crystal field effect. *Applied Physics Letters*, 25(4):186, 1974.

[7] L M Blinov. *Electro-Optical and Magneto-Optical Properties of Liquid Crystals*. John Wiley and Sons, 1983.

[8] D Bonaccini, G Brusa, P Salinari, P Stefanini, and V Biliotti. Adaptive optics wavefront corrector using addressable liquid crystal retarders. In *International Symposium on Optical Applied Science and Engineering (San Diego)*. SPIE, In Press 1991.

[9] P J Bos and K R Koehler/Beran. The pi-cell: A fast liquid-crystal optical switching device. *Molecular Crystals. Liquid Crystals.*, 113:329–339, 1984.

[10] D S Brown, A P Doel, C N Dunlop, J V Major, R M Myers, A Purvis, and M T Thompson. Image stabilisation - the martini project. In M H Ulrich, editor, *ESO Conference on Very Large Telescopes and their Instrumentation*, Garching - Munich, March 1988. ESO.

[11] S Chandrasekhar. *Liquid Crystals.* Cambridge University Press, 1977.

[12] W Chen, M B Feller, and Y R Shen. Investigation of anisotropic molecular orientational distributions of liquid-crystal monolayers by optical second-harmonic generation. *Physical Review Letters*, 63(24):2665, 1989.

[13] N A Clark and S T Lagerwall. Submicrosecond bistable electro-optic switching in liquid crystals. *Applied Physics Letters*, 36(11):899, 1980.

[14] N Collings, S G Latham, R C Chittick, and W A Crossland. Reconfigurable optical interconnect using an optically addressed light valve. *International Journal of Optical Computing*, 1(1):31, 1990.

[15] RSRE Liquid Crystals Division. Private Communication, July 1991.

[16] A P Doel, C N Dunlop, J V Major, R M Myers, A Purvis, and M G Thompson. Stellar image stabilization using piezo-driven active mirrors. In L D Barr, editor, *Advanced Technology Optical Telescopes IV*, page 179. SPIE, 1990.

[17] A P Doel, C N Dunlop, J V Major, R M Myers, A Purvis, and M T Thompson. A martini in the ghril room. *Gemini, Newsletter of the RGO*, number 26:20, 1989.

[18] A P Doel, C N Dunlop, J V Major, R M Myers, and R M Sharples. Martini: Sensing and control system design. In *International Symposium on Optical Applied Science and Engineering (San Diego)*. SPIE, In Press 1991.

[19] A P Doel, C N Dunlop, J V Major, R M Myers, and R M Sharples. Martini: System operation and astronomical performance. In *International Symposium on Optical Applied Science and Engineering (San Diego)*. SPIE, In Press 1991.

[20] C N Dunlop. *The Imaging Properties of Large Reflecting Astronomical Telescopes.* PhD thesis, University of Durham, 1986.

[21] C N Dunlop and J V Major. A shear interferometer for the measurement of atmospheric seeing. *Monthly Notices of the Royal Astronomical Society.*, 234:993–1003, 1988.

[22] M A Ealey. Adaptive optical components-the technology and future trends. In *International Symposium on Optical Applied Science and Engineering (San Diego).* SPIE, In Press 1991.

[23] E Edser and C P Butler. A simple method of reducing prismatic spectra. *Philosophical Magazine.*, 46:207, 1898.

[24] J L Fergason. Performance of a matrix display using surface mode. In *1980 Biennial Display Research Conference*, page 177. IEEE, 1980.

[25] J M Florence. Micro-miniature deformable mirror structures for adaptive optical systems. In *International Symposium on Optical Applied Science and Engineering (San Diego).* SPIE, In Press 1991.

[26] D L Fried. Statistics of a geometric representation of wavefront distortion. *Journal of the Optical Society of America*, 55(11):1427, 1965.

[27] D L Fried. Limiting resolution looking down through the atmosphere. *Journal of the Optical Society of America*, 56(10):1380, 1966.

[28] S Garoff and R B Meyer. Electroclinic effect at the *a-c* phase change in a chiral smectic liquid crystal. *Physical Review Letters*, 38(15):848, 1977.

[29] I S Grant and W R Philips. *Electromagnetism.* John Wiley and Sons, 1984.

[30] J W Hardy. Adaptive optics: A progress review. In *International Symposium on Optical Applied Science and Engineering (San Diego).* SPIE, In Press 1991.

[31] N H Hartshorne and A Stuart. *Crystals and the Polarising Microscope.* Edward Arnold Ltd, 4th edition, 1970.

[32] E Hecht and A Zajac. *Optics.* Addison-Wesley, 1974.

[33] R E Hufnagel. In *Digest of Technical Papers, Topical Meeting on Optical Propogation through the Atmosphere*, 1974.

[34] W G Hulburd. High-bandwidth, long stroke, segmented mirror for atmospheric compensation. In *International Symposium on Optical Applied Science and Engineering (San Diego)*. SPIE, In Press 1991.

[35] E Jakeman and E P Raynes. Electro-optic response times in liquid crystals. *Physics Letters*, 39A:69, 1972.

[36] P Kern, P Lena, G Rousset, J C Fontanella, F Merkle, and J P Gaffard. Prototype of an adaptive optical system for infrared astronomy. In M H Ulrich, editor, *ESO Conference on Very Large Telescopes and their Instrumentation*, page 657. European Southern Observatory, 1988.

[37] D Kinzer. An optical technique for measuring liquid crystal cell thickness. *Molecular Crystals. Liquid Crystals Letters*, 1(5):147, 1985.

[38] A Kolmogorov. *Turbulence – Classic Papers in Statistical Theory.* Interscience Publishers Inc., New York, 1961.

[39] G Labrunie and J Robert. Transient behaviour of the electrically controlled birefringence in a nematic liquid crystal. *Journal of Applied Physics*, 44(11):4869, 1973.

[40] S T Lagerwall, N A Clark, J Dijon, and J F Clerc. Ferroelectric liquid crystals: The development of devices. *Ferroelectrics*, 94:1205, 1989.

[41] B Margetts. Production of a segment of a fresnel lens in a liquid crystal cell. Final year undergraduate laboratory report, 1987. Department of Applied Physics and Electronics, Durham.

[42] H M Martin. Image motion as a measure of seeing quality. *Publications of the Astronomical Society of the Pacific*, 99:1360, 1987.

[43] R B Meyer, L Liébert, L Strzelecki, and P Keller. Ferroelectric liquid crystals. *Le Journal de Physique-Lettres*, 36:L–69, 1975.

[44] A A Michelson. On the application of interference methods to astronomical measurements. *Philosophical Magazine.*, 30(1), 1890. 5th Series.

[45] G W Nash, K J Harrison, and J A Nash. *Electronics Letters.*, 9:130, 1973.

[46] R J Noll. Zernike polynomials and atmospheric turbulence. *Journal of the Optical Society of America*, 66(3):207, 1976.

[47] European Southern Observatory. Proposal for the construction of the 16m very large telescope. Technical Report VLT Report No. 57, Karl Scwarzschild Straβe 2, Garching, Germany, 1987.

[48] N J Powell, R W Kelsall, G D Love, and A Purvis. Investigation of fringing fields in liquid crystal diffraction gratings. In *International Symposium on Optical Applied Science and Engineering (San Diego)*, number SPIE #1545-03. SPIE, In Press 1991.

[49] F. Reinitzer. *Monatshefte für Chemie*, 9:421, 1888.

[50] F Roddier. The effects of atmospheric turbulence in optical astronomy. In E Wolf, editor, *Progress in Optics XIX*, page 283. North-Holland, 1981.

[51] D Sandler. Laboratory results of 1500 degree-of-freedom adaptive optics system. In *International Symposium on Optical Applied Science and Engineering (San Diego)*. SPIE, In Press 1991.

[52] C M Schiller, T Horsky, D O'Mara, W Hamnett, G J Genetti, and C Warde. Charge-transfer-plate deformable membrane mirrors for adaptive optics applications. In *International Symposium on Optical Applied Science and Engineering (San Diego)*. SPIE, In Press 1991.

[53] T Shanks, N Tanvir, P Doel, C Dunlop, R Myers, J V Major, M Redfern, N Devaney, and P O'Kane. A high resolution, ground based observation of a virgo galaxy. In T Shanks, A J Banday, R S Ellis, and A W Wolfendale, editors, *Observational Tests of Inflation. Proceedings of the NATO advanced research workshop on observational tests of inflation*, page 205. Kluwer Academic Press, 1991.

[54] E G Steward. *Fourier Optics: An Introduction.* John Wiley and Sons, 1983.

[55] N Tanvir, T Shanks, J V Major, A P Doel, R M Myers, C Dunlop, M Redfern, N Devaney, and P O'Kane. The distance of a virgo cluster via image sharpening. In A Blanchard, L Celniker, M Lachièze-Ray, and J Trân Thanh Vân, editors, *Physical Cosmology: 25th Anniversary of the Cosmic Radiation Background Discovery (Blois, France)*. Editions Frontiers, 1991.

[56] N R Tanvir, J V Major, A P Doel, C N Dunlop, R M Myers, R M Redfern, P O'kane, and M N Devaney. High resolution imaging of virgo cluster galaxies i: Observational techniques and first results. *Monthly Notices of the Royal Astronomical Society*, 253(2):21p, 1991.

[57] Canada-France-Hawaii Telescope. *Observers' Manual.* Kamuela, Hawaii 96743, USA, March 1990. 4th Edition.

[58] L A Thompson and H R Ryerson. An active mirror image stabilisation instrument system (ISIS) for use on mauna kea. volume 445, page 560. SPIE, 1983.

[59] R K Tyson. *Principles of Adaptive Optics*, pages 158–161. Academic Press Ltd, 1991.

[60] S W Unger, E Brinks, R A Laing, K P Tritton, and P M Gray. *Observers' Guide.* La Palma, November 1988.

[61] A A Vasil'ev, A F Naumov, and V I Shmal'gauzen. Wavefront correction by liquid crystal devices. *Soviet Journal of Quantum Electronics.*, 4(16):421, 1986.

[62] M A Vorontsov, V A Katulin, and A F Naumov. Wavefront control by an optical-feedback interferometer. *Optics Communications*, 1.2(71):35, 1988.

[63] G Williams, N J Powell, A Purvis, and M G Clark. Electrically controllable liquid crystal fresnel lens. In *Current Developments in Optical Engineering and Commercial Optics*, page 352. SPIE volume 1168, 1989.

[64] S T Wu. Wavelength-tunable phase retardation plate. *Journal of the Optical Society of America B*, 3(1):516, 1984.

[65] S T Wu and R J Cox. Optical and electro-optic properties of cyanotolanes and cyanostilbenes: Potential infra-red liquid crystals. *Journal of Applied Physics*, 64(2):821, 1988.

[66] S T Wu, U Efron, and L D Hess. Birefringence measurements of liquid crystals. *Applied Optics*, 23(21):3911, 1984.

[67] S T Wu, U Efron, and T Y Hsu. Near-infrared-to-visible image conversion using a si liquid crystal light valve. *Optics Letters*, 1(13):13, 1988.

[68] S T Wu, A M Lackner, and U Efron. Optimal operation temperature of liquid crystal modulators. ***Applied Optics***, 26(16):3441, 1987.

[69] S T Wu and C S Wu. Small angle relaxation of highly deformed nematic liquid crystals. ***Applied Optics***, 53(19):1794, 1988.

Acknowledgements

I would like to mention here, as a small token of thanks, a few of the people who have helped me in different ways to nurture this thesis.

Firstly my supervisor, John Major, whose time, experience, and geniality is much appreciated.

The other members of the MARTINI group; Peter Doel, Colin Dunlop, and Richard Myers.

My colleagues in the SEAS; Norman Powell, Alan Purvis, and Geoff Williams.

The Technical Staff, both in the Physics Department and in the SEAS. Especially John Gibson for his help in the clean room, Tom Jackson and the Electronics Workshop, Dennis Jobling and the Student Workshop. Experimental work becomes impossible without them.

My colleagues in the 'real' world; Mike Wiltshire at GEC, and Maurice Stanley at RSRE.

Members of the Physics Deptartment academic staff, especially; Desmond Evans for searching questions, George Rochester for Edser-Butler fringes, Richard Stephenson and Arnold Wolfendale for my initial interest.

My friends within the Department; Alfonso, Dominic, Esperanza, Nial, Rafael, Stephen and Tony.

All my different friends without the Department.

My parents, for their support and encouragement.